

T.C.
THE SAKARYA UNIVERSITY
THE GRADUATE SCHOOL

88174

**BIOMECHANICAL ANALYSIS AND
MATHEMATICAL MODELING OF THE HUMAN
ESOPHAGEAL FUNCTION**

Ph.D. THESIS

Ethem Toklu, Ms.

**DR. FÜKSİM KURBAN
DOÇ. DR. M. N. KURBAN**

Department of Graduate School : MECHANICAL ENG.

Sub-department of Graduate School : ENERGY

October 1998

T.C.
SAKARYA ÜNİVERSİTESİ
FEN BİLİMLERİ ENSTİTÜSÜ

İNSAN YEMEK BORUSUNUN BİOMEKANİK ANALİZİ
VE MATEMATİKSEL MODELLENMESİ

DOKTORA TEZİ

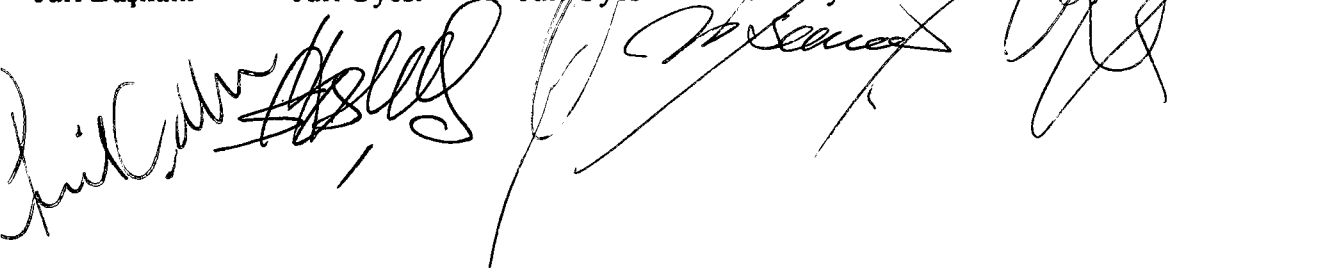
Mak.Y.Müh. Ethem Toklu

Enstitü Anabilim Dalı : MAKİNA MÜH.

Enstitü Bilim Dalı : ENERJİ

Bu tez 08/04/1999 tarihinde aşağıdaki jüri tarafından Oybirliği/Oyçokluğu ile kabul edilmiştir.

Prof.Dr.	Prof.Dr.	Doç.Dr.	Doç.Dr.	Doç.Dr.
İsmail ÇALLI	Salim ÖZÇELEBİ	Mesut GÜR	H.İbrahim SARAC	H.Rıza GÜVEN
Jüri Başkanı	Jüri Üyesi	Jüri Üyesi	Jüri Üyesi	Jüri Üyesi



ACKNOWLEDGEMENTS

I am extremely indebted to my advisor, Prof. Dr. Ismail Calli. Over the past 6 years, he has been at times a teacher, a mentor, and a friend. I am also indebted to my advisor Prof. Dr. James G. Brasseur in Department of Mechanical Engineering at the Pennsylvania State University, USA. Any modest research skills which I have developed are due in large part to their teaching. I look forward to a new aspect of our relationship in collaborations in years come.

A very special thank you goes out to Mr. Yılmaz Kanbak, Dr. Muammer Kantarcı, Mr. Mehmet Eskiyapan, Mr. Mehmet Umutlu and Mr. Salim Dursun. Financial support for this work was provided by them. I also express my deepest gratitude to Mr. Burhan Satar, Dr. H. İbrahim Saraç, Dr. Nedim Sözbir and Dr. H. Rıza Güven.

There are many who have passed through the laboratory group of Dr. Brasseur who have been both good friends and helpful colleagues. Those who have left include Dr. Meijing Li, Dr. Mark Nicosia and Dr. Charles Carrano. Those still in the lab group include Dr. Keshavamurthy Indereshkumar and Mr. Anupam Pal.

To my family, Dad, Gülşen, Temel, Ayşe, Fatma and Pamuk, thank you for being there through it all – it means more than words can express. To my wife, Ebru, and my son, Tunahan, you never let me forget that I could do it. Your support means everything.

Finally, this past year did not see the passing of my dear mom, Emine Toklu. I dedicate this thesis to her memory.

TABLE OF CONTENTS

NOMENCLATURE	v
LIST OF FIGURES	vi
ABSTRACT.....	xiii
OZET	xiv
CHAPTER 1. INTRODUCTION	1
1.1. Anatomy of the Esophagus.....	2
1.2. Physiology of the Esophagus	6
1.2.1. Normal Esophageal Motility	9
1.2.2. Esophageal Motility Disorder	12
1.2.3. Active and Passive Tension of Esophageal Muscle	15
CHAPTER 2. BIOLOGICAL DATA ANALYSIS	19
2.1. Method.....	22
2.1.2. Biological Protocol and Manometry	22
2.1.2. Data Analysis	24
2.2. Results	27
2.2.1. Subpressure Wave and Segment in the Esophagus	27
2.2.2. Locations and Lengths of Subpressure Waves and Segments	29
2.2.3. Pressure Amplitude of Subpressure Waves and Segments	31
2.2.4. Spatial and Temporal Duration of Subpressure Waves and Segments.....	31
2.2.5. Wave Speeds	35
2.2.6. Pressure Through.....	35
2.3. Discussion	38

CHAPTER 3. NUMERICAL MODEL.....	44
3.1. Introduction and Literature Review	44
3.2. Lubrication Theory Approximations.....	48
3.3. Laplace Equation	51
3.4. Combination of Lubrication Theory with Laplace Equation	53
3.5. Numerical Solution.....	54
3.6. Analysis of Tension in the Muscle Wall	59
3.7. Comparison of Numerical Solution with Analytic Solution	63
3.8. Effect of the Tube Occlusion on the Pressure Field	66
3.8.1. Effects of the Number of Grid Points of the Tube Length.....	70
3.9. Peristaltic Pumping Performance	72
3.10. Comparison of Single Peristaltic Waves with Train Waves	74
3.10.1. Particle Trajectory and Reflux	74
3.10.2. Net Loss Refluxed Fluid From the Tube Inlet	79
3.10.3. Pumping Performance in Single Wave Peristaltic Transport....	84
<hr/>	
CHAPTER 4. PREDICTION OF THE WALL GEOMETRY	85
4.1. Numerical Method.....	89
4.2. Results	90
CHAPTER 5. CONCLUSIONS	102
REFERENCES	104
VITA	112

NOMENCLATURE

ε	tube occlusion
λ	wavelength
L	tube length
T	tension
P	pressure
H	wall geometry
t	time
x	axial direction
c	wave speed
a	average wave radius
μ	viscosity
τ	wall thickness
Q	volume flow rate
r	radial direction
u	axial velocity
v	radial velocity
A_0	resting state cross-section area

LIST OF FIGURES

- Figure 1.1. A schematic illustration of the esophagus in relation to the pharynx above and the stomach below. The primary afferent and efferent innervation are through the vagus nerve. The epiglottis serves to close off the trachea during swallowing, so that bolus fluid is directed into the esophagus rather than the lungs.....3
- Figure 1.2. A typical cross-section of the gut, showing the layered structure of the wall. Reproduced from Guyton [23]. The structure of the esophagus is essentially the same.....5
-
- Figure 1.3. Concurrent videofluoroscopic and manometric data for normal swallow (from Kahrilas [30]).....7
- Figure 1.4. Superimposition of a schematic diagram of normal esophageal bolus transport with radiographic images of barium swallow [7].....10
- Figure 1.5. Tracings from the video images on the right depict the distribution of the barium bolus at the times indicated by arrows on the manometric record. In this example, a single swallow transported the majority of barium through the peristaltic contraction was evident at the 8 s mark in the aortic arch region. The peristaltic amplitude associated with this escape phenomenon was 13 mmHg, inscribed from the second most oral recording site [28].....13
- Figure 2.1. Pressure wave in raw manometric data. Recorded manometric data at each port is shown on time vs. pressure plot (thin lines). Space between each port is 1.5 cm. Thick line show converted data23

Figure 2.2. Trajectory of appearance of subpressure waves and segments in the axial direction along the esophagus. P_1 , P_2 , P_3 and P_4 corresponding of subpressure waves. A, B and C represent segment. Arrows show directions of subpressure waves. These figures can be seen as animation, if plots are followed in time order.....25

Figure 2.3. Subpressure waves and segments of a instant swallowing are shown on; (a) distance vs. pressure, (b) time vs. pressure, (c) time vs. distance plots along the esophagus28

Figure 2.4. Locations and axial duration of subpressure waves and segments along the esophagus. Thin and thick solid lines show subpressure waves and segments, respectively. Dots represent centers of subpressure waves and segments. Error bars represent \pm SD.....30

Figure 2.5. Average pressure distributions of each subpressure waves and segments and their locations along the esophagus and \pm SD32

Figure 2.6. Length and duration of subpressure waves. Δx and Δt corresponding of spatial and temporal duration, respectively. Numbers in the bracket show swallowing numbers, which is used in this analysis.....33

Figure 2.7. Length and duration of segments. Δx and Δt corresponding of spatial and temporal duration, respectively. Numbers in the bracket show swallowing number, which is used in this analysis.....34

Figure 2.8. Comparison of speeds of primary and subpressure waves36

Figure 2.9. Pressure distribution of a swallowing on the contour plot and primary and subpressure waves on it37

Figure 2.10. Pressure troughs along the esophagus. Circle and square represent first and second pressure trough location, respectively.....39

Figure 3.1. A single contraction wave of peristaltic transport is illustrated. The fluid bolus is transported from left to right by contraction waves along the tube. The contraction wave speed, wavelength, tube length and tube occlusion are defined respectively as c , λ , L and ε . The fluid viscosity and average bolus radius within one wavelength are μ and a , respectively.....49

Figure 3.2. A force balance across an esophageal cross-section. P , T , P_0 , R and τ represent intraluminal pressure, tension in muscle wall, thoracic cavity pressure, radius of tube and muscle thickness, respectively52

Figure 3.3. Calculating region and oblique coordinates, which are employed in the numerical analysis.....55

Figure 3.4. Tension distributions along the tube at six time instants in one wave period with one wave in the tube ($L/\lambda = 1$). Here, (a) $t=0$ s; (b) 0.4 s; (c) 0.8 s; (d) 1.2 s; (e) 1.6 s; (f) 2 s. The solid lines are tension distributions along the tube, and dotted lines are the corresponding sinusoidal wall shapes. In the calculation, $\varepsilon/a = 0.0523$, $Re=0.00457$60

Figure 3.5. As figure 3.4 but different ε . Here, (a) $t=0$ s; (b) 0.4 s; (c) 0.8 s; (d) 1.2 s; (e) 1.6 s; (f) 2 s. The solid lines are tension distributions along the tube, and dotted lines are the corresponding sinusoidal wall shapes. In the calculation, $\varepsilon/a = 0.523$, $Re=0.00457$ 62

Figure 3.6. Comparison the pressures between the analytic and numerical solutions. Here, (a) $t=0$ s; (b) 0.4 s; (c) 0.8 s; (d) 1.2 s; (e) 1.6 s; (f) 2 s. The solid lines are pressure distributions from numerical solution, dashed lines are pressure distributions from analytic solution of [32], and dotted lines are the corresponding sinusoidal wall shapes. In the calculation, $\varepsilon/a = 0.0523$, $Re=0.00457$ 64

Figure 3.7. Same as figure 3.6, but different ε/a . Here, (a) $t=0$ s; (b) 0.4 s; (c) 0.8 s; (d) 1.2 s; (e) 1.6 s; (f) 2 s. The solid lines are pressure distributions from numerical solution, dashed lines are pressure distributions from analytic solution of [32], and dotted lines are the corresponding sinusoidal wall shapes. In the calculation, $\varepsilon/a = 0.103$, $Re=0.00473$65

Figure 3.8. Maximum pressure in the flow domain (in the occlusion region) from numerical model as a function of the tube occlusion. As $\varepsilon \rightarrow 0$, the pressure in the occlusion region increases without bound.....67

Figure 3.9. An infinite series of periodic sine waves, produced by the lateral motions of the wall. (a) The totally occluded tube transports the trapped fluid within the peristaltic wave. (b) Incomplete occlusion allows some fluid to leak proximally into trailing waves.....68

Figure 3.10. Fluid motions with incomplete occlusion. The observer is moving to the right with the traveling peristaltic waves. A region of fluid trapped relative to the moving wave is shown, surrounded by fluid that leaks proximally into the trailing wave.....69

Figure 3.11. Error is plotted as a function of grid size. For same grid size pressure is calculated from our numerical method and analytic solution of lubrication theory approximation.....71

Figure 3.12. A single contraction wave which has ‘tear drop’ shape. Similar as in the figure 3.1, the fluid bolus is transported from left to right against a pressure difference by peristaltic contraction wave along the tube75

Figure 3.13. Trajectories of fluid particles for different cases of peristaltic transport: (a) a single sinusoidal wave ($L/\lambda = 5$); (b) train of sinusoidal waves with integral $L/\lambda = 5$; (c) train of sinusoidal waves with non-integral $L/\lambda = 4.76$. In all calculations a non-dimensional adverse pressure

difference of 18.85 was applied across the tube. Initially the fluid particles are located at $x = 12$ and 18 cm. $\varepsilon/a = 0.354$ in all cases76

Figure 3.14. Distributions of the distance that fluid particles travel relative to their initial positions for the four cases of figure 3.13. The abscissa is the distance a particle has traveled, non-dimensionalized with the wavelength, after the three wave periods. The distributions are normalized to unity. In all cases, a non-dimensional adverse pressure difference of 18.85 was applied across the tube ends, and the trajectories of 451 particles are calculated. At the initial time, the 451 particles are distributed at 41 uniformly spaced cross sections, in each of which 11 particles are evenly placed from the wall to centre of the tube. The hatched bars correspond to refluxed particles. Single wave peristaltic transport leads to substantially greater reflux than train wave peristaltic transport. $\varepsilon/a = 0.354$ in all cases.....78

Figure 3.15. Pressure-volume flow rate characteristics of single wave peristaltic transport with different relative tube occlusion ε/a and different tube-to-wave lengths L/λ . The average volume flow rate at the tube inlet \bar{Q}_{inlet} is plotted against pressure difference $\Delta P = P_L - P_0$ in groups for different ε/a , where L/λ is varied within each group from 3 to 2 in the direction indicated by the arrow. A negative value of volume flow rate \bar{Q}_{inlet} implies fluid reflux from the tube inlet.....80

Figure 3.16. Average volume flow rate at the tube inlet \bar{Q}_{inlet} as a function of tube occlusion ε/a for fixed favourable pressure difference ΔP . A negative value of volume flow rate \bar{Q}_{inlet} implies fluid reflux at the inlet. At fixed ΔP a critical occlusion ε_c exists at which the amount of refluxed fluid from the inlet to the tube reaches a maximum. This critical occlusion shifts to smaller ε/a as the favourable pressure difference increases ...82

Figure 3.17. Pressure-volume flow rate characteristics of single wave peristaltic transport with different relative tube occlusions ε/a and different tube-to-wave lengths L/λ . The average volume flow rate at the tube outlet \bar{Q}_{outlet} is plotted against pressure difference $\Delta P = P_i - P_0$ in groups for different ε/a , where L/λ is varied within each group from 3 to 2 in the direction indicated by the arrow83

Figure 4.1. Raw radiographic image plotted along with the spatial distribution of intraluminal pressure. Pressure distribution is shown with the solid line. The scale is shown in the right corner of the image. Horizontal dotted line represents bolus tail and corresponding intraluminal pressure86

Figure 4.2. Schematic of the axial motion of tantalum markers attached to the feline esophageal wall in response to secondary peristalsis [14].....88

Figure 4.3. Comparison of predicted bolus shape with analytic bolus shape for different time steps. Solid and dotted lines represent predicted and analytic bolus shape, respectively. Here, $\varepsilon/a = 0.1$, $c=3$ cm/s and $\lambda = L = 6$ cm91

Figure 4.4. Variation of bolus volume, which is obtained from calculations as seen in figure 4.3, is shown in time. Dotted and solid lines represent calculated and analytic bolus volume92

Figure 4.5. Similar to figure 4.3, comparison of predicted bolus shape with analytic bolus shape for different time steps. Solid and dotted lines represent predicted and analytic bolus shape, respectively. Here, $\varepsilon/a = 0.08$, $c=3$ cm/s and $\lambda = L = 6$ cm93

Figure 4.6. Similar to figure 4.4, variation of bolus volume, which is obtained from calculations as seen in figure 4.5, is shown in time. Dotted and solid lines represent calculated and analytic bolus volume.....94

Figure 4.7. Similar to figure 4.3, comparison of predicted bolus shape with analytic bolus shape for different time steps. Solid and dotted lines represent predicted and analytic bolus shape, respectively. Here, $\varepsilon/a = 0.06$, $c=3$ cm/s and $\lambda = L = 6$ cm.....95

Figure 4.8. Similar to figure 4.4, variation of bolus volume, which is obtained from calculations as seen in figure 4.7, is shown in time. Dotted and solid lines represent calculated and analytic bolus volume.....96

Figure 4.9. Similar to figure 4.3, comparison of predicted bolus shape with analytic bolus shape for different time steps. Solid and dotted lines represent predicted and analytic bolus shape, respectively. Here, $\varepsilon/a = 0.04$, $c=3$ cm/s and $\lambda = L = 6$ cm.....97

Figure 4.10. Similar to figure 4.4, variation of bolus volume, which is obtained from calculations as seen in figure 4.9, is shown in time. Dotted and solid lines represent calculated and analytic bolus volume.....98

Figure 4.11. Similar to figure 4.3, comparison of predicted bolus shape with analytic bolus shape for different time steps. Solid and dotted lines represent predicted and analytic bolus shape, respectively. Here, $\varepsilon/a = 0.02$, $c=3$ cm/s and $\lambda = L = 6$ cm.....99

Figure 4.12. Similar to figure 4.4, variation of bolus volume, which is obtained from calculations as seen in figure 4.11, is shown in time. Dotted and solid lines represent calculated and analytic bolus volume.....100

ABSTRACT

In this thesis we applied basic principles and numerical models to study the mechanical function of the human esophagus during normal swallowing. The primary aim is to characterize and understand the mechanics of the human esophagus. To reach this goal, three interconnected study have been carried out: (1) analysis of biological data to quantify the relationship among bolus motion, motions of anatomical features and normal swallowing, (2) a fluid and solid mechanics study to find out relationship between flow and tension in the muscle wall of the esophagus of normal swallowing, (3) to predict wall geometry from tension in the muscle wall.

~~Biological data analysis is performed from the recorded manometrical data, which is collected during swallowing. We find out several functions of the human esophagus from this analysis. To interpret only manometrical data without radiographic images have lots of difficulties. Limited information can be from manometry.~~

We attempted to combine fluid and solid mechanics. There is not enough study about combination of fluid and solid mechanics in the literature. We developed a mathematical model for this purpose. This model gave us ability to calculate tension in the muscle wall directly from wall geometry.

In the last part of this study, we attempt to predict wall geometry during swallowing. We predicted wall geometry from tension. This study gives us opportunity to interpret and understand in detail esophageal functions in the absence of radiography.

ÖZET

Bu tezde, temel prensipleri ve nümerik yöntemleri, insan yemek borusunun normal yutma boyunca mekanik fonksiyonlarını araştırmak için uyguladık. Asil amacımız, insan yemek borusunu karakterize etmek ve anlamaktır. Bu amaca ulaşmak için 3 ayrı birbirleriyle bağlantılı çalışma yaptık; (1) biyolojik data analizi, normal yutma boyunca kaydedilen manometrik datadan lokma hareketini, yemek borusunun duvarlarının hareketini ve normal yutmayı inceledik, (2) normal yutma boyunca yemek borusunun içindeki akışla kaslardaki gerilme arasında bir ilişki aramak için akışkanlar ve katı mekaniğini birleştirdik, (3) kaslardaki gerilmelerden yemek borusunun duvarlarının aldığı şekli hesapladık.

Akışkanlar ve katı mekaniğini birleştirmeyi denedik. Bu konuda yeterli çalışma literatürde bulunmamaktadır. Bu amaç için bir matematik model geliştirdik. Bu model bize yemek borusu duvarlarındaki (kaslardaki) gerilmeyi hesaplama imkanı vermektedir.

Son kısımda kaslardaki gerilmelerden yola çıkarak yemek borusunun yutma boyunca aldığı şekli hesapladık. Bu yolla, radyolojik resmin olmamasına rağmen sadece manometrik dataları kullanarak yemek borusunun fonksiyonlarını yorumlama ve daha iyi anlama fırsatını elde ettik.

CHAPTER 1. INTRODUCTION

Swallowing is the transport of an ingested "food bolus" through the esophagus from the mouth to the stomach by peristaltic contractions. Swallowing can be initiated voluntarily, but thereafter it is almost entirely under reflex control. The swallowing reflex is a rigidly ordered sequence of events that propels food from the mouth to the stomach. At the same time it inhibits respiration and prevents the entrance of food into the trachea. The afferent limb of the swallowing reflex begins with touch receptors, most notably those near the opening of the pharynx.

The swallowing process can be divided into three phases: oral, pharyngeal, and esophageal. The oral phase of swallowing is initiated by separating a bolus of food from the mass in the mouth with tip of the tongue. The bolus to be swallowed is moved upward and backward in the pressing first the tip of the tongue and later the more posterior portions of the tongue as well against the hard palate. This forces the bolus in to the pharynx, where it stimulates the tactile receptors that initiate the swallowing reflex.

The pharyngeal phase of swallowing involves the following sequence of events, which occur in less than 1 second: (a) The soft palate is pulled upward, and the palatopharyngeal folds move inward toward one another. This prevents reflux of food into the nasopharynx and provides a narrow passage through which food moves into the pharynx. (b) The vocal cords are pulled together. The larynx is moved upward against the epiglottis. These actions prevent food from entering the trachea. (c) The upper esophageal sphincter (UES) relaxes to receive the bolus food. Then the pharyngeal superior constrictor muscles contract strongly to force the bolus deeply into the pharynx. (d) A peristaltic wave is initiated with contraction of the pharyngeal superior constrictor muscles, and moves toward the esophagus. This forces the bolus of food through the relaxed UES.

The esophageal phase of swallowing is controlled mainly by the swallowing center. After the bolus of food passes the UES, the sphincter reflexly constricts. A peristaltic wave then begins just below the UES and traverses the entire esophagus in about 10 second. This initial wave of peristalsis, called primary peristalsis, is controlled by the swallowing center. The peristaltic wave travels down the esophagus at 3 to 5 cm/s. When the bolus reaches the lower esophageal sphincter (LES), intrabolus pressure is increased by muscle contractions until it equals the pressure in the stomach. The LES then opens and the bolus is forced into the stomach.

1.1 Anatomy of the Esophagus

The esophagus lies posterior to the trachea in the neck, and passes along the dorsal wall of the mediastinum in the thoracic cavity. The human esophagus has a length of approximately 20-22 cm and diameter of about 2 cm. Figure 1.1 shows the longitudinal anatomy of the upper portion of the gastrointestinal tract. Also illustrated in this figure are the vagus nerve, which carries sensory (afferent) and motor (efferent) signals to and from the brain, and the trachea which runs next to the esophagus in the throat. The epiglottis, which serves in "airway protection," ensures that swallowed material enters the gastrointestinal system rather than the lungs.

The proportion of each muscle type is species-dependent but, in humans, the proximal 5 % including the UES, is striated, the middle 35 – 40 % is mixed with an increasing proportion of smooth muscle as one moves distally, and the distal 50 – 60 % is entirely smooth muscle. The bundles of the outer, longitudinal muscle arise from the cricoid cartilage receiving slips from the cricopharyngeus and pass dorsolaterally to fuse posteriorly approximately 3 cm below the cricoid cartilage. This arrangement results in a posterior triangular area - Laimer's triangle - which is devoid of longitudinal muscle. Distal to Laimer's triangle the longitudinal muscles form a continuous sheaths of uniform thickness about the esophagus.

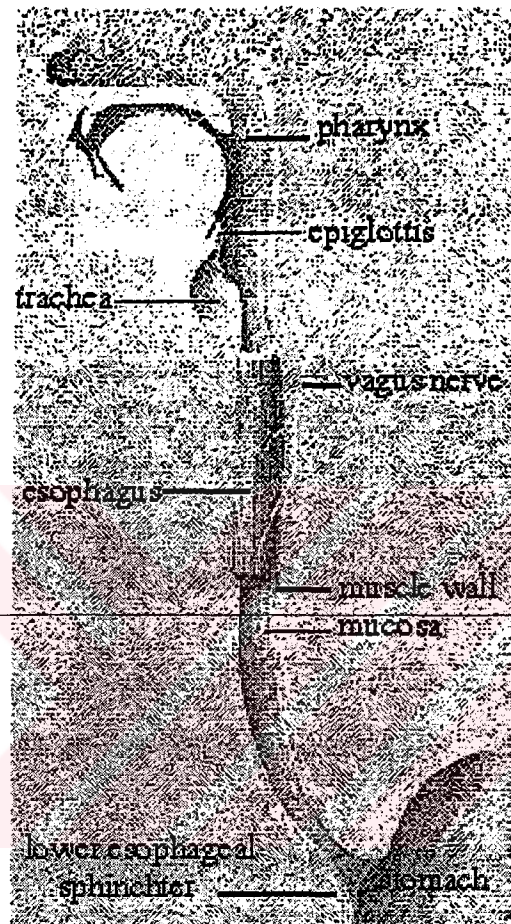


Figure 3.1. A schematic illustration of the esophagus in relation to the pharynx above and the stomach below. The primary afferent and efferent innervation are through the vagus nerve. The epiglottis serves to close off the trachea during swallowing, so that bolus fluid is directed into the esophagus rather than the lungs.

Both the striated and smooth muscle portions of the esophagus contain a nerve network, known as the myenteric plexus, situated between the longitudinal and circular muscle layers. In the smooth muscle portion, these enteric neurons are generally considered the relay neurons between the vagus and the smooth muscle; function in the striated muscle esophagus is obscure. A second nerve network, the submucosal or Meissner's plexus, is situated between the muscularis mucosa and the circular muscle layer. Except during swallowing, normal muscular tone keeps the lumen closed, and the mucosa and the submucosa are thrown into large folds. The muscularis mucosae consist of an irregular layer of smooth muscles medial to the mucous esophageal glands of the submucosa. The muscularis externa has inner circular and outer longitudinal layers. The ganglia of the myenteric plexus are more numerous in the smooth muscle region than in the striated muscle region of the esophagus but, throughout, they are far less dense and smaller than in other region of gut. The submucous plexus of the esophagus is exceedingly sparse; a few ganglion cells are present in the human esophagus. Figure 1.2 (from Guyton [23]) illustrates a typical cross-section of the gut and esophagus.

The extrinsic innervation of esophagus is via the vagus nerve. Fibers innervating the striated muscle are axons of lower motor neurons with cell bodies situated in nucleus ambiguus, whereas innervation of the smooth muscle esophagus is provided by the dorsal motor nucleus of the vagus. Efferent nerve fibers reach the cervical esophagus by the pharyngoesophageal nerve, and histologic studies show that vagal afferents snapse directly on striated muscle neuromuscular junctions. The vagus nerves also provide sensory innervation in the cervical esophagus. This is via the SLN with cell bodies in the nodose ganglion, whereas in the remainder of the esophagus sensory fibers travel via the recurrent laryngeal nerve or, in the most distal esophagus, via the esophageal branches of the vagus. Histologic studies demonstrate many free nerve endings in the mucosa, submucosa and muscular layers. Additionally, a few encapsulated structures resembling spindles have been described in humans. These vagal afferents are strongly stimulated by esophageal distension [30].

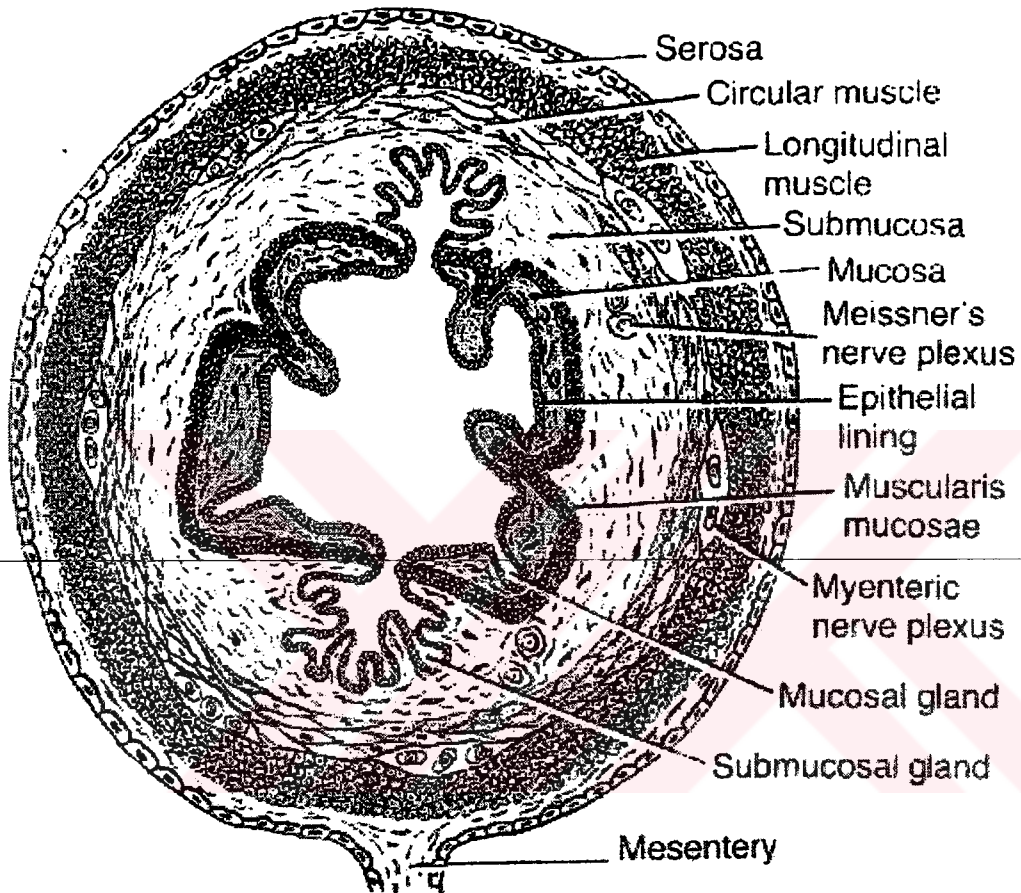


Figure 3.2. A typical cross-section of the gut, showing the layered structure of the wall. Reproduced from Guyton [23]. The structure of the esophagus is essentially the same.

The circular muscle ring that functions as the lower esophageal sphincter (LES) angles obliquely upward from the lesser to greater curvature of the stomach and is contiguous with the circular muscle of the esophageal muscle of the esophageal body. The maximal thickness of the LES occurs at the greater curvature of the stomach. Towards the stomach, the LES is split into two segments: one forms short transverse muscle clasps around the esophagus, and the other forms long oblique loops in the stomach (gastric sling fibers). The LES is normally situated within the esophageal hiatus of the diaphragm which, in its most common configuration, is formed entirely by fibers of the right diaphragmatic crus [29].

1.2. Physiology of Esophagus

The basic function of esophagus is to provide a coordinated pathway for swallowed material. After food is swallowed, the esophagus functions as a conduit to move the food from the pharynx to the stomach. It is important to prevent air from entering at the upper end of the esophagus and to keep corrosive gastric contents from refluxing back into the esophagus at its lower end. Reflux is particularly problematic because the pressure in the thoracic esophagus is close to intrathoracic pressure, which is less than atmospheric pressure and thus less than intraabdominal pressure.

Esophageal peristalsis becomes evident shortly after the pharyngeal contraction traverses the UES. The peristaltic contraction moves from the proximal striated muscle to the distal smooth muscle of the esophagus at a speed of 2-4 cm/s. The longitudinal muscle of the esophagus also contracts at the onset of peristalsis. The net effect is a transient shortening of the structure by 2-2.5 cm [14, 19]. The mechanical correlate of peristalsis is a stripping wave that milks the esophagus clean, from its proximal to its distal end (figure 1.3).

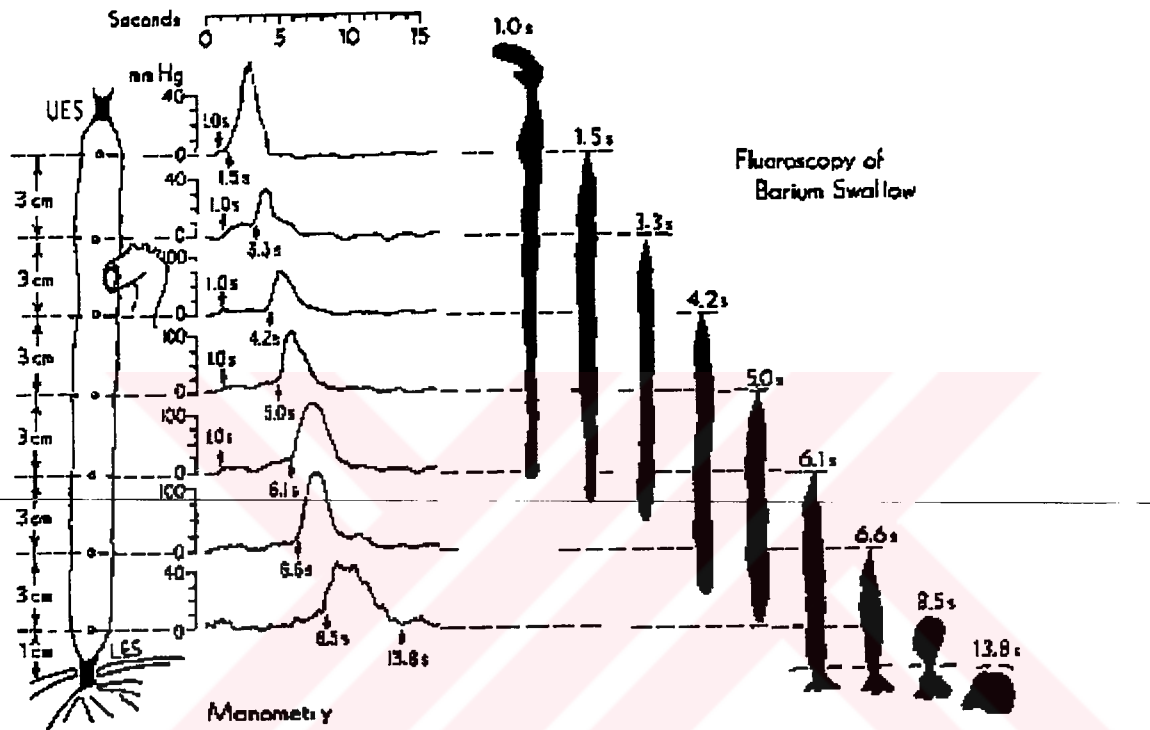


Figure 1.3. Concurrent videofluoroscopic and manometric data for normal swallow (from Kahrilas [30]).

Another property of the peristaltic mechanism is deglutitive inhibition. A second swallow, initiated while the earlier peristaltic contraction is still progressing in the striated muscle esophagus, causes rapid and complete inhibition of the contraction induced by the first swallow (voluntary swallowing). If the first swallow has reached the smooth muscle esophagus, it may proceed distally for a few seconds after the second swallow (esophageal distention), but its peristaltic amplitude diminishes progressively until it disappears. Inhibition of basal LES tone induced by swallowing occurs concurrently with the deglutitive inhibition that traverses the smooth muscle esophagus. The LES relaxation commences well before onset of the peristaltic contraction in the proximal esophagus [29].

Distinct physiologic control mechanisms govern the striated and smooth esophageal musculatures. The striated-muscle esophagus receives exclusively excitatory vagal innervation, and the peristaltic contraction of this segment results from the sequential activation of motor units in a craniocaudal sequence. There is convincing evidence that the organization of peristalsis in the striated-muscle esophagus is subject to control from within the swallowing center of the medulla in much the same way as the oropharyngeal musculature [29].

Vagal control of the smooth-muscle esophagus is more complex than that of the striated-muscle esophagus. Vagal fibers synapse on neurons of the myenteric plexus rather than directly at neuromuscular junctions, and vagal stimulation can either excite or inhibit the esophageal musculature, depending on which myenteric plexus neurons are activated. Furthermore, although facilitated by vagal fibers, the myenteric plexus neurons are able to organize peristalsis themselves, as indicated by the absence of vagal activity during secondary peristalsis. A second population of vagal efferents is activated with a short latency and probably represents central mediation of deglutitive inhibition. Thus, the activity of neurons in the dorsal motor nucleus of the vagus reflects several properties of primary peristalsis in the smooth-muscle esophagus, including deglutitive inhibition and the speed and vigor of peristaltic contractions.

The esophagus has an intramural nerve network, the myenteric plexus, located between the longitudinal and circular muscles that can generate peristaltic contractions. Although the relationship between the morphology and function of the nerve plexuses has yet to be determined, it is apparent that there are two main types of effector neurons within the esophageal myenteric plexus [30]. Excitatory neurons mediate contraction of both longitudinal and circular muscle layers via cholinergic receptors. Inhibitory neurons predominantly affect the circular muscle layer via nitric oxide neurons. Cholinergic excitation of the excitatory neurons is nicotinic as well. Both types of neurons innervate the entire smooth-muscle esophagus, including the LES. The process that mediates LES relaxation is identical to the process that mediates the inhibitory front along the esophagus; indeed, the smooth muscle of the sphincter should be viewed as identical to the adjacent circular muscle, except that it maintains a tonic contraction at rest via a myogenic mechanism.

1.2.1 Normal esophageal motility

The esophagus is stripped clean of all bolus fluid by the contraction wave in normal swallowing. When the bolus fluid completely passes through the UES and UES closes, esophageal peristalsis begins. Then the bolus is propelled downwards towards the stomach by a combination of gravitational forces and peristalsis. The effect of gravity on bolus motion depends on the viscosity of the bolus. Liquids travel faster than the peristaltic wave when the subject is in the upright position. In fact, when water is swallowed, it reaches the LES a few seconds earlier than the peristaltic wave [61]. As a consequence, to study peristaltic transport of low viscosity fluid, it is common to place the subject in a supine position. However, the viscosity of normal boluses is high and the effect of gravity is not significant. Figure 1.3 is a good example to normal swallowing.

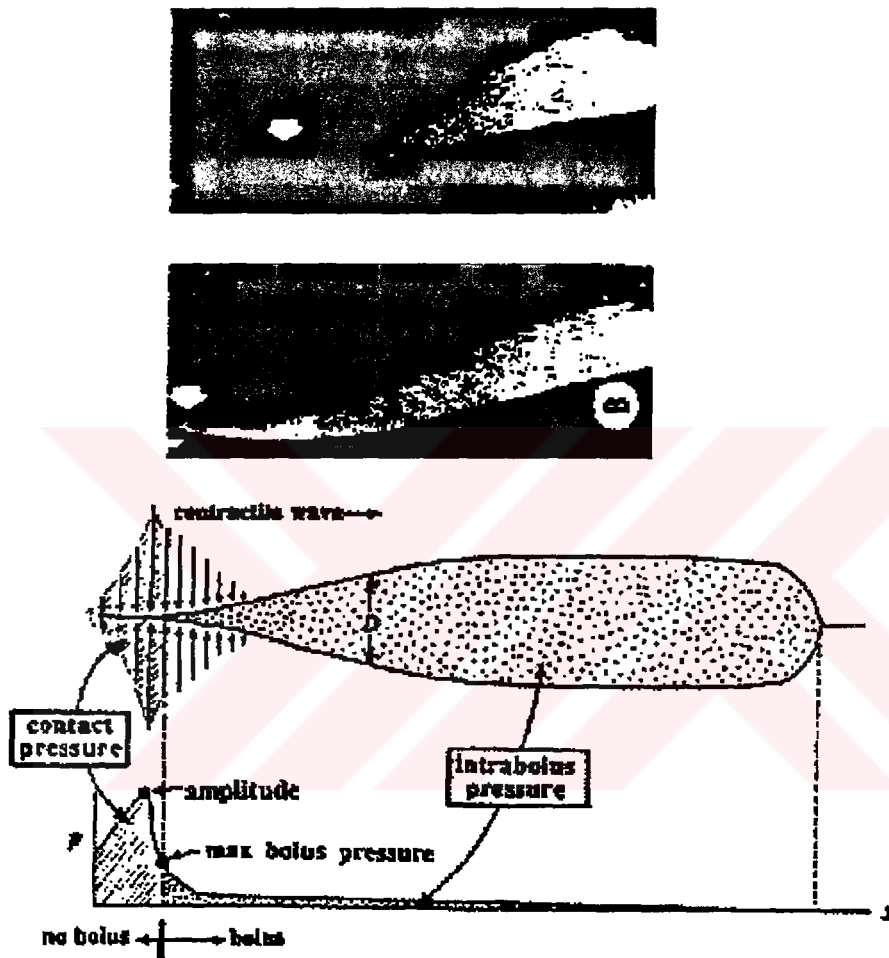


Figure 1.4. Superimposition of a schematic diagram of normal esophageal bolus transport with radiographic images of barium swallow [7].

The arrival of the tail at a manometric port precedes the contraction wave so that the peristaltic wave keeps the bolus ahead of it at all instances. The relationship between the manometrically recorded contractile wave and movement of the bolus at a fixed time is shown in figure 1.4. As the main body of the bolus sweeps past a measurement port, manometric pressure will initially increase gradually. Then, as the tail and contraction zone pass over the manometric port, a rapid rise in pressure to a large maximal value will occur, followed by a decrease in intraluminal pressure on the proximal side of the pressure peak. As shown in figure 1.3, a gradual increase in pressure within the main body of the bolus followed by a rapid increase near the tail is typical in manometric measurements of esophageal bolus transport. The place where bolus fluid ends (the bolus/no-bolus transition point) is somewhere on the rapid rise in pressure, before the peak amplitude; from that point on, the manometer records purely contractile pressure [7]. Maximum bolus pressure P_{max} is much less than contractile pressure P_{amp} in the normal swallowing. P_{amp} and P_{max} are biologically independent. Mechanically contractile pressure does not affect bolus motion directly. P_{max} must be less than P_{amp} to prevent retrograde leakage of bolus fluid through the contraction zone. The speed of the bolus can be correlated to the speed of the maximum peak in pressure. The wave can take about 10 seconds to reach the LES. The wave in the striated muscle region is moved slower than in the smooth muscle region.

Motility studies have shown that the speed and force of the esophageal contractions are also dependent on the size and viscosity of the bolus. Increasing the size of the bolus reduces its velocity and increases the contraction forces. Similarly, increasing the bolus viscosity increases the force of the contractions and reduces the velocity of the bolus [62]. The temperature of the bolus also affects peristalsis. Dooley et al. [16] have shown that warm boluses increase the speed of the contraction wave while cold boluses slow down the peristaltic wave.

1.2.2 Esophageal motility disorders

Normally the esophagus is successful in transporting all of the bolus into the stomach without any pain or discomfort felt by the subject. However, there are number of conditions which can cause the esophagus to perform poorly. These disorders are classified as either primary or secondary. In primary motility disorders the esophagus is the major organ involved, whereas in secondary disorders, organs within the body cavity affect the esophagus. In either case, the esophagus loses its ability to function normally and the subject experiences pain while swallowing.

Any extrinsic or intrinsic changes to esophageal wall can potentially cause it to dysfunction. Intrinsic changes to the wall shape are caused by inflammation of the wall due to the prescience of tumors or ulcers on the inner lining. Extrinsic structural changes are be caused when other organs in the body cavity press against the esophagus. A common example is the aorta pressing against the esophagus in the aortic arch region. In either case, the esophagus loses its ability to distend fully and a stricture created. The degree of dysphagia caused is proportional to the severity of the constriction caused by the stricture and also its size. Typically strictures caused by the aorta pressing against the esophagus are "functional" because they do not severely occlude the esophagus. Severe constrictions, caused by lesions and ring formations, usually lead to dysphagia. Figure 1.5 shows concurrent manometric and videofluoroscopic data of a case study in which bolus fluid is retained as the peristaltic contraction wave passes through the intraluminal segment adjacent to the aortic arch [28]. The accepted explanation for bolus retention is that the contraction wave propagates through the aortic arch region in this excessively weakened state allowing the lumen to open and bolus fluid to leak in a retrograde direction. The contraction wave then strengthens and seals the lumen, once again distal to the aortic arch segment. Once sealed by the advancing peristaltic wave, bolus fluid is again transported toward the stomach, leaving behind the bolus fluid retained in the aortic arch region [15]. Chronic retention of bolus fluid in the aortic arch region is an indication of esophageal dysfunction.

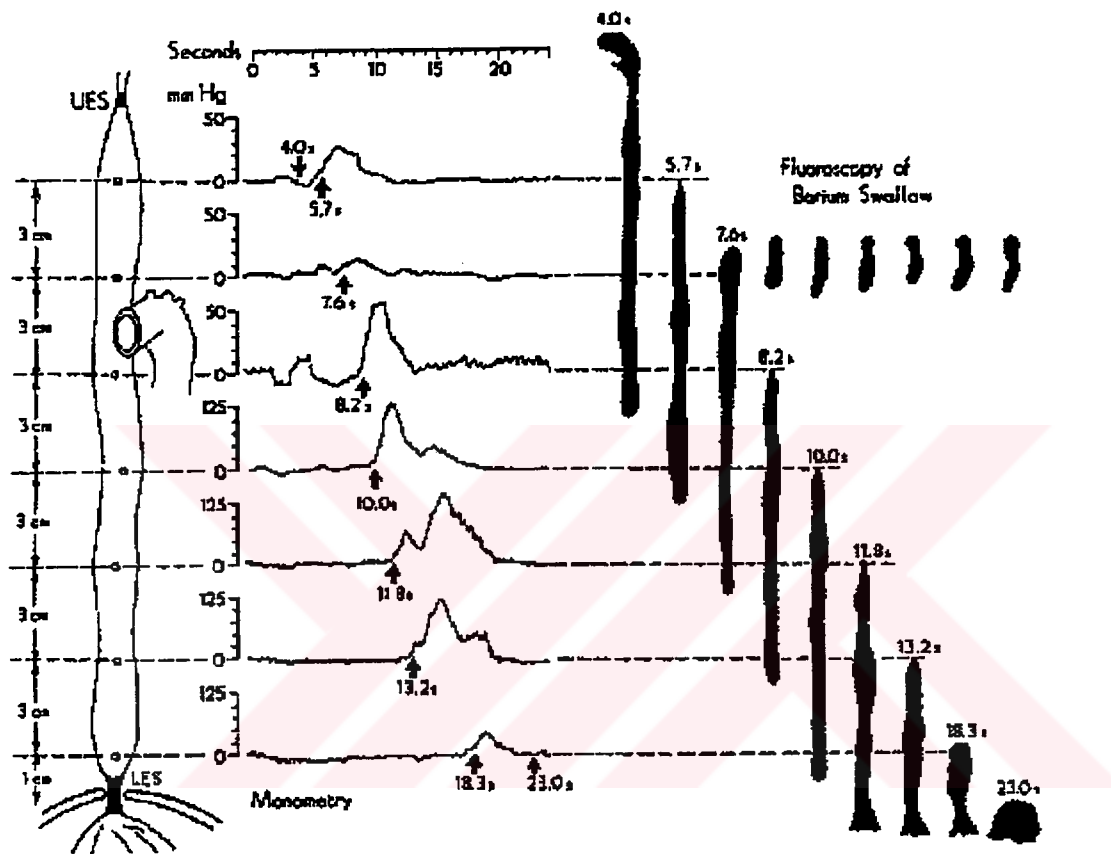


Figure 1.5. Tracings from the video images on the right depict the distribution of the barium bolus at the times indicated by arrows on the manometric record. In this example, a single swallow transported the majority of barium through the peristaltic contraction was evident at the 8 s mark in the aortic arch region. The peristaltic amplitude associated with this escape phenomenon was 13 mmHg, inscribed from the second most orad recording site [28].

Lesions, like ulcers, tumors and abscesses, on the esophageal wall are a common cause for inflammation of esophageal walls. They can affect the entire length of the esophagus but are usually found in the distal end of the esophagus. 'Lye' strictures [39] are formed when corrosive agents like caustics are swallowed. Corrosive materials are capable of destroying the mucosal layer in the esophagus and in the process of healing fibrotic tissue forms on the wall. The esophageal wall thickens and narrows the lumen to form a stricture. Similarly 'peptic' strictures are formed when there is persistent vomiting and ulcers develop on the esophageal wall [39]. Tumors are also types of lesion which protrude into the lumen and impart a rounded smooth bulge to the esophageal wall. Both benign and malignant tumors have been found in all parts of the esophagus. Some other conditions like achalasia, observed when a portion of the esophagus fails to relax, and generalized muscular hypertrophy are known to effect the esophageal wall intramurally so that the esophageal wall is greatly thickened and the lumen becomes narrowed [60].

In all cases of lesions, the strictures are not rigid obstructions within the esophagus. They allow partial distension of the esophageal only when sufficient pressure is exerted on the esophageal wall. The constricted wall offers definite resistance to the advancing bolus and in severe cases may even block the esophagus. All patients with strictures of any kind complain about dysphagia and present themselves in poor nutritional health. Endoscopic observation has shown a conical narrowing of the esophagus which gives the stricture the shape of an hourglass [54].

Severe constrictions in the esophagus are also caused by ring structures. The ring is a membranous structure in the shape of an annulus. It is usually found very close to the lower esophageal sphincter which makes differentiating them difficult. The ring is distinguishable only because it remains fixed and does not change its locations. On the other hand, the sphincter undergoes transient contractions as the bolus fluid passes by. The ring is a passive structure observed only when the lumen proximal and distal to it is distended more than its maximal diameter. An 'annular indentation' located about 4-5 cm from the lower esophageal sphincter. The thickness of the ring is about 2-4 mm and its inner radius can vary from 10-20 mm [17].

Since the lower esophageal ring is so close to the lower esophageal sphincter, there is a lot of speculation about whether it is caused by the thickening of the epithelium in the esophagus or whether it is caused by a herniation of the diaphragm into the thoracic cavity. Eckardt et al. [18] used potential difference measurements and manometric data in patients exhibiting mucosal rings and concluded that the rings are due to thickening of longitudinal and circular muscles in the esophagus.

Most patients with lower esophageal ring complain of violent pain when trying to swallow solid food because the food cannot pass and produces a complete obstruction at the site of the ring. The passage of fluid also slows down tremendously near the ring. Severity of dysphagia is dependent on the diameter of the ring and the size of bolus swallowed. Schatzki et al. [49] has reported that ring diameters of 20 millimeters or more seldom cause dysphagia. However if the diameter is less than 13 millimeters then almost always there is dysphagia.

1.2.3 Active and passive tension of esophageal muscle

The role of circular muscle in esophageal peristalsis has been stressed, whereas the longitudinal musculature has been neglected. The circular and longitudinal esophageal musculature, however, act in concert during bolus transport. Sequential circular--muscle contraction serve to push the bolus toward the stomach. Longitudinal peristaltic contraction causes the esophagus to engulf the bolus; to shorten, thereby decreasing the length of bolus travel; to pull the bolus toward the stomach; and contributes to the LES opening mechanism [15].

Manometrically measured intraluminal pressure and wall muscle tension, acting on the bolus, are directly related. The source of the intrabolus pressure is active compressive tension within the circular muscle of the esophageal wall, plus any passive elastic tension that would exist in the absence of active muscle squeeze [7]. To define more precisely "active" and "passive," one must understand some basic principles of smooth muscle physiology. There is considerable heterogeneity among smooth muscles from different organs [42] and because esophageal smooth muscle is rarely studied, much of the following discussion necessarily extrapolates from

studies using smooth muscles from other organs (vascular, tracheal or other gastrointestinal smooth muscle).

Although terminology applied to striated muscle physiology is often used to describe smooth muscle, there are important differences between the two muscle types. One such difference is the specification of a "resting" state. Because striated muscle contraction follows from the removal of inhibition (i.e., the exposure of active sites along the actin filament by the movement of the tropomyosin filament [55]), there is an unambiguously defined resting state characterized by the absence of neural stimulation. Striated muscle tension can therefore be unambiguously separated into active and passive components.

Although control of smooth muscle contraction is not fully understood, the mechanisms involved are more complex than in striated muscle. Smooth muscle contraction is controlled through chemical modification (phosphorylation / dephosphorylation) of certain regulatory proteins attached to the myosin head. Phosphorylation increases the affinity of the myosin head for the actin filament, leading to the contraction cycle. Because different inhibitory mechanisms may lead to different inhibited states (i.e., different levels of decreased phosphorylation), an unambiguously defined "passive" state cannot be defined in smooth muscle.

Furthermore, quantifying a "zero-stress" state of passive tension for a particular preparation (striated or smooth muscle) is not straightforward. When soft biological tissue is near its resting length, relatively small tensile changes can lead to large tissue deformations [3]. Because there is no unambiguous way to relate the in vitro muscle strip length with in vivo dimensions, the in vivo resting state is unknown and the in vitro data cannot be used to parameterize the model without guessing the resting state. Given the sensitivity between elongation and stress, however, the model becomes very sensitive to the guess. Even more importantly, the neuromuscular physiology of a denervated excised segment of esophageal smooth muscle is fundamentally different from a fully innervated esophagus in vivo.

Given the fundamental differences between the in vivo and in vitro esophagus, the in vivo physiological system guides the parameterization of "passive" tension. Because a peristaltic contraction wave is preceded by a wave of inhibition in the circular muscle, and because local contraction of longitudinal muscle is correlated spatially with the peristaltic contraction wave, the "passive" tensile state is defined as that inhibited state which exists along the distal-most portion of the liquid bolus. The muscle tension within the esophageal wall at the bolus head, in this state of inhibition, is labeled T_p . Although there are certain chemical and electrical events associated with this state (the release of an inhibitory neurotransmitter and the resulting membrane hyperpolarization, respectively), T_p reflects the physiological base state which we shall define as "passive". Total tension is then given by

$$T = T_a + T_p. \quad (1.1)$$

Where, T_a is "active" or "contractile" muscle tension.

CHAPTER 2. BIOLOGICAL DATA ANALYSIS

In this chapter, we wanted to understand in detail the spatial structure of circular muscle contraction along the esophagus in relationship to the movement of bolus fluid locally in different esophageal segment and find out the differences in this relationship between dry and bolus swallowing.

The local structure of peristaltic muscle contraction is investigated along the esophagus, which transports a bolus. The change in local structure of contraction is characterized as the peristaltic waves pass through the transition zone (pressure trough region) from the upper to the lower esophagus. We searched for structure in the contraction characteristics that are intrinsic to an individual's esophagus, especially local region of segmental contraction.

Manometry and videofluoroscopy are the two primary tools used to study esophageal motility, both in clinical and research setting. These two modalities provide fundamentally different information concerning bolus transport. Intraluminal manometry, which measures pressure at several fixed locations along the esophagus as a function of time, provides quantitative information regarding the forces applied to an ingested bolus by the esophageal musculature. Intraluminal manometric pressure can be recorded using the conventional infused-catheter system, intraluminal strain gauges and conventional pull-through techniques. High fidelity instrumentation, valid recording condition must be provided to obtain accurate measurement. Accurate determined intraluminal pressure values is enable identification of individuals with hypotensive or hypertensive peristalsis. The contraction wave is seen as a positive pressure on manometry which traverses the entire length of the esophageal body. On the other hand, videofluoroscopy records the geometry and motion of the esophageal wall in response to these forces. The peristaltic contraction wave imparts an inverted V configuration to the tail of the

barium bolus on videofluoroscopy. A precise relationship exist between the tail of barium bolus as observed radiographically and the manometric tracing of the peristaltic wave (see figure 1.4). Studies which track the barium bolus tail by cine during simultaneous manometric recording of intraluminal esophageal pressure demonstrate that passage of the bolus tail past a pressure sensor corresponds precisely to the upstroke of the peristaltic pressure complex recorded by the sensor [15].

The manometric evaluation of esophageal motility has focused on the peristaltic pressure waveform that results from the aborad sequence of esophageal muscle contraction and relaxation [47]. Ren et al. has obtained concurrent esophageal videofluoroscopic and intraluminal manometric recordings in supine normal volunteers using different bolus volumes and viscosities and abdominal compression. It was found that intrabolus pressure has increased with bolus volume, viscosities, and abdominal compression. Esophageal diameter has increased with larger bolus volumes. Intrabolus pressure was highest in the bolus tail and is affected significantly by factor resisting bolus transport and, as such, has the potential to be an important indicator of the presence of the abnormal resistive forces [47].

Brasseur et al. has studied interpretation of manometric data with and without concurrent radiographic image. An interpretation of manometric recording in terms of motions of the swallowing apparatus and the muscle activity leading to those motions is of obvious importance for clinical analysis and for basic motility research [7]. An appreciation of the mechanics of the swallowing process and bolus transport is necessary for proper interpretation of manometric intraluminal pressure measurements in terms of the temporal changes in lumen geometry.

Interpretation of manometric signals has been sought for situations in which peristalsis is weak, or absent, failure of the closure segment occurs, or muscle contractions exist with or without peristaltic contractions. In the absence of bolus motion, the existence of isobaric pressure waves might suggest localized muscle contractions in one or more locations along a fluid bolus, or they might suggest that a segment of the esophagus is contracting as a unit. If peristaltic contraction exist

which progresses distally while, at the same time, nonspecific muscle contractions occur along the esophageal wall, one would assume that a bolus is being transported distally past the manometric port. However, the nonspecific muscle contractions are of sufficient strength to mask the gradual increase in intraluminal pressure typical of normal bolus transport, and make it impossible to estimate the time at which the bolus head passes any manometric port. Therefore, the origin of these nonspecific pressure waves is uncertain. However, after the peak in the manometric signal passes a given manometric port, one might argue that the bolus has likely passed that port and therefore the luminal segment above that port is devoid of bolus fluid [7].

To better understand spatial relationships of peristaltic contraction, topographic plots have been constructed from conventional esophageal manometric waves. Using a computerized gridding and plotting system, it has been seen that typical postdeglutitive waves are spatially interconnected. This technique has been used to make observations about esophageal motility in normal subjects that had not been made using conventional methods [11]. Ray and Staiano have also constructed topographic plots from esophageal manometric tracings in asymptomatic volunteers and symptomatic patients with high amplitude peristaltic contraction waves to identify segmental contraction differences between two groups. Three amplitude troughs dividing the peristaltic contraction into four sequential segments have been noticed in volunteers. Only the first and third troughs had been identified in the other group [12].

Manometric pressure has been analyzed in the axial direction in order to describe the peristaltic pressure wave as it propagates through the esophagus in the direction of the bolus and to determine what sampling interval along the esophageal length is required for accurate representation. The appearance of the contraction wave as it propagates in the axial direction has importance because of the interface of this wave with the bolus and additional appeal for understanding the coordination of underlying neuromuscular events responsible for transit [13].

Esophageal bolus transport is inherently a mechanical process. However, there has not been enough study to apply basic principles of mechanics and dynamic modeling to determining the esophageal function. The primary mechanical variable used to quantify bolus transport is peak intraluminal pressure or pressure amplitude. The aortic arch region demarcates the transition from the striated to smooth muscle dominated regions of the esophagus. The accepted explanation for the reduction in pressure amplitude through this region is the smooth transition of a single peristaltic wave as it passes from the upper to the lower esophagus. Although the physiology and histology of striated and smooth muscle are known to be very different, and although characteristics of peristaltic transport change significantly between the two segments, the transition is regarded as a relatively smooth one [5]. The transition between striated and smooth muscle in cases of bolus retention must be associated with a spatially "double peaked" pressure characteristics along the esophageal lumen which manometrically gives the impression of decrease in peristaltic wave speed [33]. These decreases in pressure amplitude and wave speed are actually a consequence of two separate contractile waves, one in the upper esophagus, above the transition zone, and one in lower esophagus, below the transition zone. The manometrically observed decrease in amplitude and wave speed are reflections of the deceleration and decrease in amplitude of the upper wave while, at the same time, a lower wave forms somewhat distally. The transition from distinct upper to lower peristaltic waves creates a double--peaked pressure characteristic along the lumen over a short period of time [5].

The studies from past to date have aimed to understand esophageal bolus transport, neural control of esophagus and behaviors of esophageal muscles. However, they could not be completely understood. Manometry and videofluoroscopy do not provide all information about esophageal function. Therefore it is very difficult to determine all features of esophagus in detail using these tools. And locations of contractile activity cannot be determined in the bolus surface using only manometry [7]. The manometric measurement does not provide any information without concurrent radiographic data on where muscle wall compression is applied to the bolus. The bolus/no-bolus transition point cannot be determined from manometric measurement alone [7].

We aimed in this analysis: (1) to understand manometric pressure variation in detail in entire esophagus, (2) to find out peristaltic pressure waves and segments, (3) better interpretation of manometry.

2.1 Method

2.1.1 Biological protocol and manometry

Manometric and videofluoroscopic data were obtained at the Medical College of Wisconsin. By inserting a catheter into the esophagus via the nasal cavity, intraluminal manometric pressure has obtained. The water perfused catheter which has 4 mm outer diameter and 10 ports spaced 1.5 cm with proximal port has placed as first port at the UES. A tantalum marker placed adjacent to each recording orifice showed its location on videofluorocopy. Videofluoroscopy was recorded at 30 frame/s with a videocassette recorder. A modified dual timer encoded time in hundredths of a second on each video frame while sending a pulse signal at 1 s intervals to a channel on the polygraph tracing. Pressure data is often available along the entire length of the esophagus. Lead markers are incorporated in the tube to facilitate radiologic identification of the ports. Manometry gives the time history of pressure at each port during the swallowing sequence. While the measuring port is within the bolus, intrabolus pressure is recorded. After the bolus fluid passes the port, the esophageal wall completely covers the port and pressures measured are a direct indications of the force of muscle contraction per unit area of the esophagus.

Barium, water and dry swallowings are obtained on manometry and videofluoroscopy. Standard low and high viscosity barium preparation [made by mixing powdered E--Z--EM barium with Knott's Berry Farm strawberry syrup] was swallowed by subjects during videofluoromanometry. Water was also swallowed. Dry swallowing was obtained only doing swallowing motion without bolus. Bolus volume is 5, 10, 15 or 20 ml for barium and water swallowing.

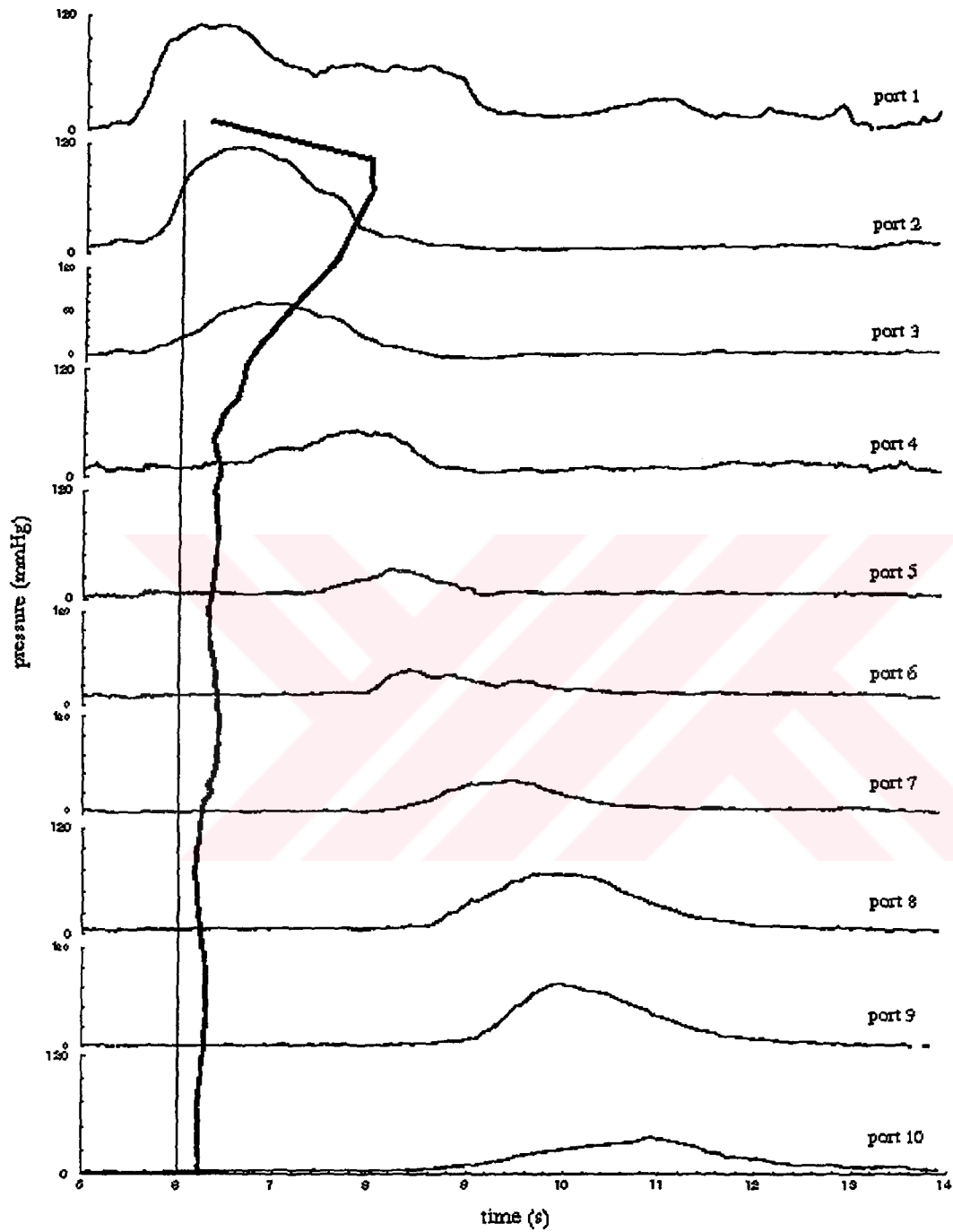


Figure 2.1. Pressure wave in raw manometric data. Recorded manometric data at each port is shown on time vs. pressure plot (thin lines). Space between each port is 1.5 cm. Thick line show converted data.

Manometric data can be recorded for barium, water and dry swallowing. But videofluoroscopy can be recorded only for barium swallowing. Because barium preparation is visible on video screen and others are invisible.

Manometric data consist of temporal variations in pressure at fixed axial locations. We require the spatial distribution of intraluminal pressure at fixed instants in time. The methodology of Li et al [33] was used to transform the raw manometric data into the full-space time pressure distribution. The method makes use of the observation that the peristaltic wave changes little when viewed from a reference frame moving along with the peak in pressure. First, the raw data are transformed to this coordinate system and spline interpolations are applied to estimate the pressure between ports. The interpolated data are then transformed back to the original coordinates.

2.1.2 Data analysis

We analyzed intraluminal esophageal pressure data in detail for 77 swallowing in 4 subjects. Of the 77 swallows, 13 were dry and 64 were wet with 5 and 10 ml boluses of barium and water. The spatial variations in intraluminal pressure along the esophagus were plotted at closely spaced fixed instants in time. Using these plots, pressure distribution at a fixed time is obtained in esophagus. Every time step can be obtained with same technique. Characteristics of pressure wave, transition zone etc. can be determined along the esophagus for every time step. Figure 2.1 shows temporal distribution of the pressure, which is recorded manometrically, and spatial distribution, which is converted using raw data of intraluminal pressure. Thin lines represent variation of pressure in time at each port location. Thick line corresponds of variation of pressure along the esophagus at a fixed time. Existence of pressure waves can be seen on both plots. But pressure data in spatial distribution, which is converted from raw data, is more detailed than temporal distribution, which is raw data.

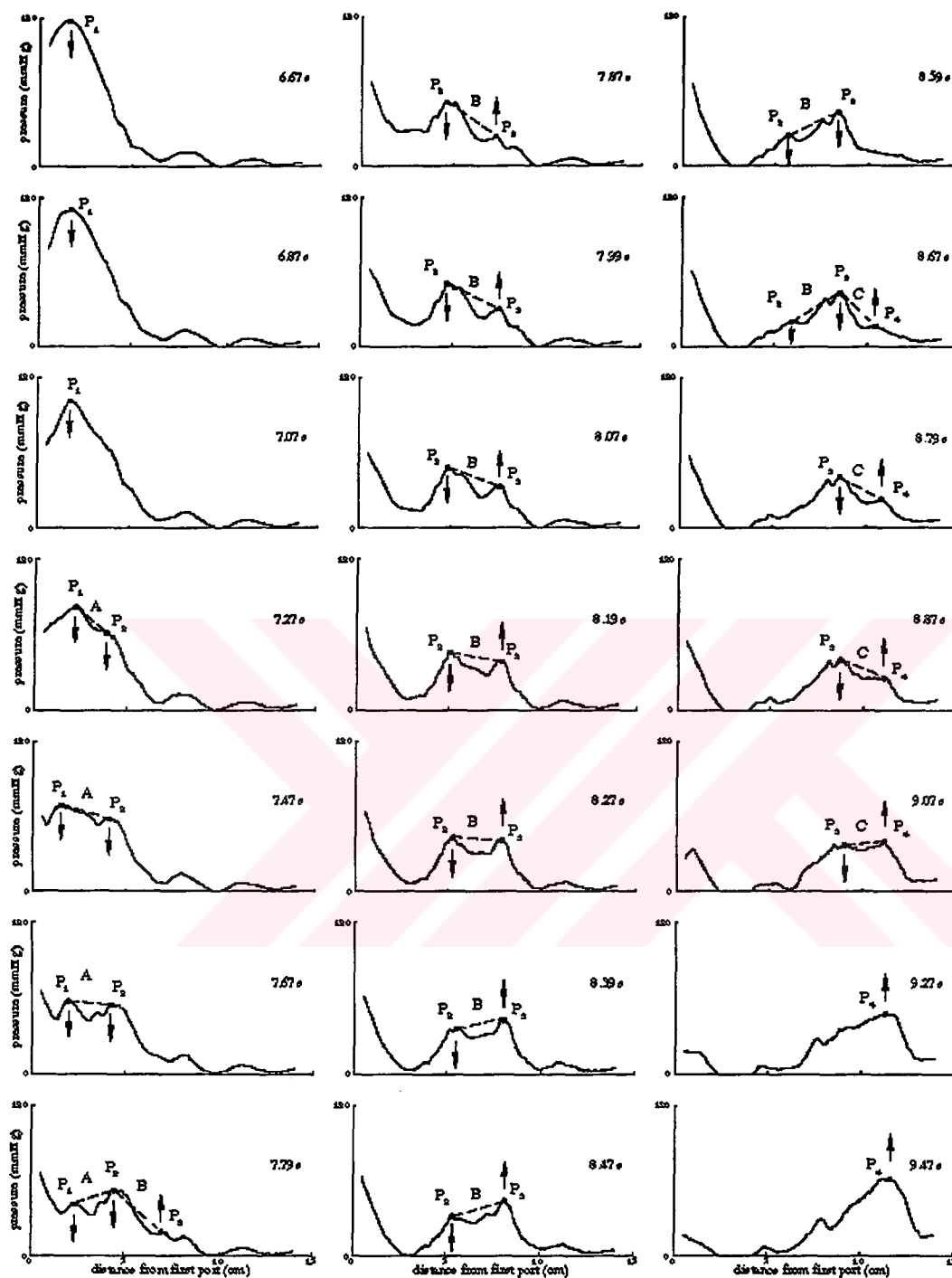


Figure 2.2. Trajectory of appearance of subpressure waves and segments in the axial direction along the esophagus. P₁, P₂, P₃ and P₄ corresponding of subpressure waves. A, B and C represent segment. Arrows show directions of subpressure waves. These figures can be seen as animation, if plots are followed in time order.

The temporal evolution of these spatial pressure distributions were then animated on the computer to reveal details by which the axial distribution in pressure (and indirectly, muscle tone) evolved in time. Figure 2.2 shows an instant animation of a swallowing. Animation method is applied all swallowing of subjects. Intraluminal pressure vs. distance (beginning of the axes is first port location) along the esophagus.

Along the animation, manometric pressure waves are propagated in the axial direction in the esophagus. It is noticed that several subpressure waves appear during a single swallowing. P_1 , P_2 , P_3 and P_4 represent subpressure waves. A, B and C represent segment. Subpressure wave is a small pressure wave, which occurs in a small region of esophagus. Amplitude of peak pressure begins to increase and then decrease in time. Finally it stops increasing or decreasing. From beginning to the ending of variation of peak pressure is defined as beginning and end of subpressure wave. Segment is a transition between two subpressure waves. These subpressure waves are interconnected each other by segmental contractions along the esophagus. The appearance of the subpressure waves and segments in a swallowing of one subject, which has 4 subpressure waves and 3 segments, is seen in the 2.2 during swallowing. Each subpressure wave appears in different locations of the esophagus and traces each other in time.

In order to determine subpressure wave and segment in detail; maximum peak pressure value, its time and location are collected in the every subpressure waves. Similarly, average pressure value, its time and location are collected in the every segment. Namely, to obtain subpressure waves and segments, pressure amplitude and location of every subpressure wave and segment collected for every time step during every single swallowing. Pressure amplitude is a peak pressure of subpressure waves and corresponds P_1 , P_2 , P_3 and P_4 in figure 2.2.

Maximum peak pressure and its location of subpressure waves is determined using collected peak pressure. Average value of pressure, length and temporal duration of subpressure waves and segments calculated.

2.2 Results

2.2.1 Subpressure wave and segment in the esophagus

Contractile waves, which govern esophageal bolus transport, are reported in previous studies. Brasseur and Dodds have studied bolus/no-bolus transition point and two distinct contractile waves [7]. Clouse et al. has found several contractile waves in their topographic plots studies and propagating pressure wave [11, 12, 13]. Our results correlate their findings and also our studies more detailed.

The animation method of analyzing and viewing data from standard esophageal manometry provided better information about esophageal peristalsis. From the animated axial intraluminal pressure distributions the existence of "subpressure waves" riding over and between peristaltic pressure waves observed in every swallow.

Findings of detailed analysis of animation are that there are 4 subpressures and 3 segments in one subject, 3 subpressure waves and 2 segments in 3 subjects. Pressure, time and location of a single swallow, which have 4 subpressure waves and 3 segments, are shown in figure 2.3.

The first subpressure wave began with a low amplitude (~30 mmHg) in the proximal esophagus, smoothly increased a high amplitude (~120 mmHg) and disappeared after decreased a low amplitude (~25 mmHg). Before first subpressure wave completely disappeared, second subpressure wave began with high amplitude and finished similar first subpressure wave. Third and fourth subpressure waves occurred as first subpressure wave. First and second subpressure waves occur in the striated muscle region while third and fourth subpressure waves in the smooth muscle region for a subject which has 4 subpressure wave. However, first subpressure wave appears in the striated muscle region while second and third subpressure waves in the smooth muscle region for other 3 subjects which have 3 subpressure wave.

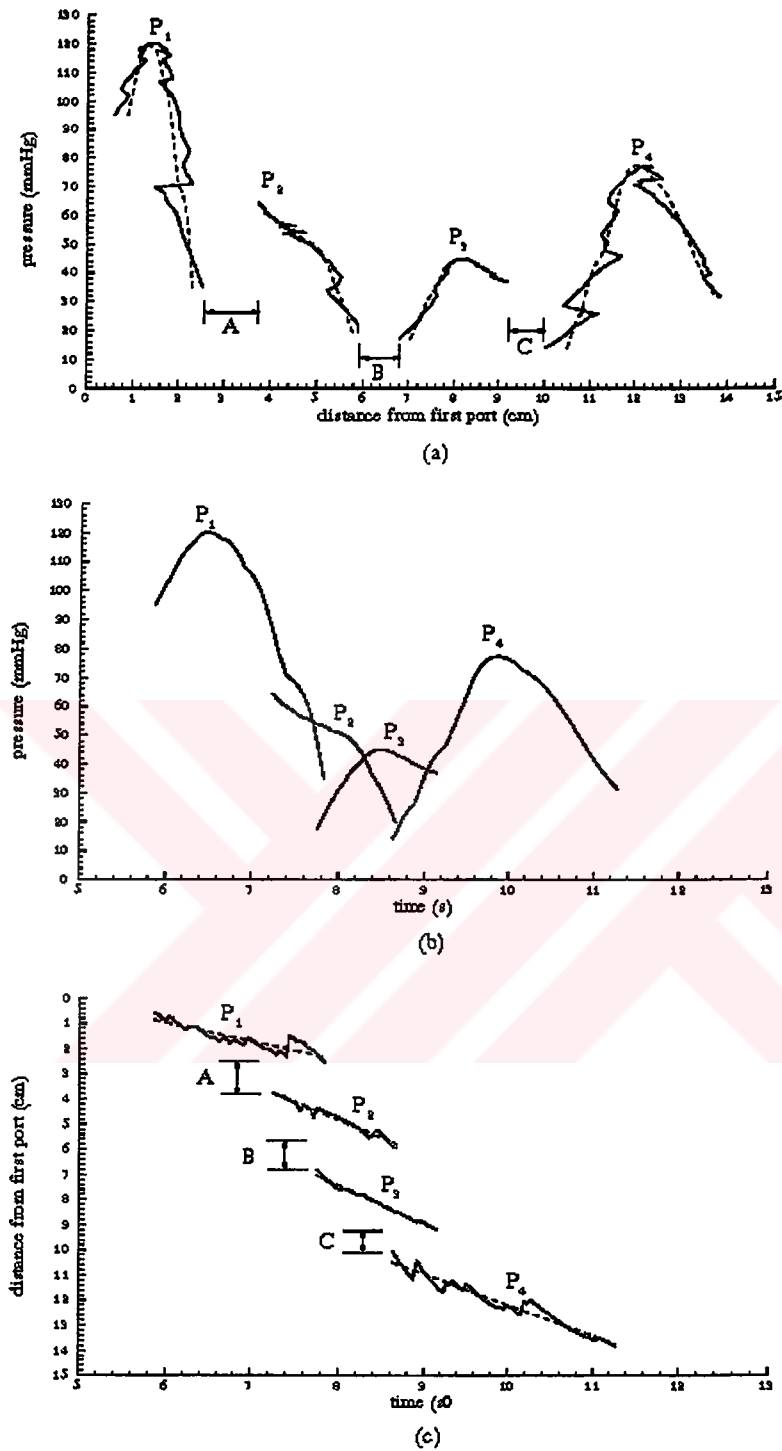


Figure 2.3. Subpressure waves and segments of a instant swallowing are shown on; (a) distance vs. pressure, (b) time vs. pressure, (c) time vs. distance plots along the esophagus.

2.2.2 Locations and lengths of subpressure waves and segments

Locations and axial lengths of subpressure waves and segments are determined along the esophagus by applying statistical method and shown in figure 2.4. In the figure, thin and thick lines represent subpressure waves and segments with \pm SD, respectively. Range of axial length (duration) of subpressure waves and segments are 1.1-3.8 cm and 2-4 cm along the esophagus, respectively. In general, first and last subpressure waves appear 0.5-3.2 cm and 10.5-14 cm of esophagus. However, second and third subpressure waves appear between 4-5.8 cm and 7-9.2 cm on one subject which has 4 subpressure wave, while second subpressure wave appear between 4-9 cm on other subjects. Consider, total length of esophagus is approximately 21-22 cm. Our manometric data covers first 15 cm. We do not have data for other part of esophagus. Investigators are reported existing of contraction waves in the LES region.

According to results of this study, appearance of subpressure waves and segments are well organized along the esophagus. They do not occur randomly. Furthermore, subpressure waves and segments appear approximately in the same place in the esophagus for every swallowing of each subject.

Appearance of subpressure waves and segments in the same location along the esophagus independent on types of swallowing (barium, water and dry) and bolus volume. Although there is not bolus in dry swallowing, dry swallowing shows same characteristics as bolus (barium and water) swallowing. Explanation of this situation will be considered in discussion section.

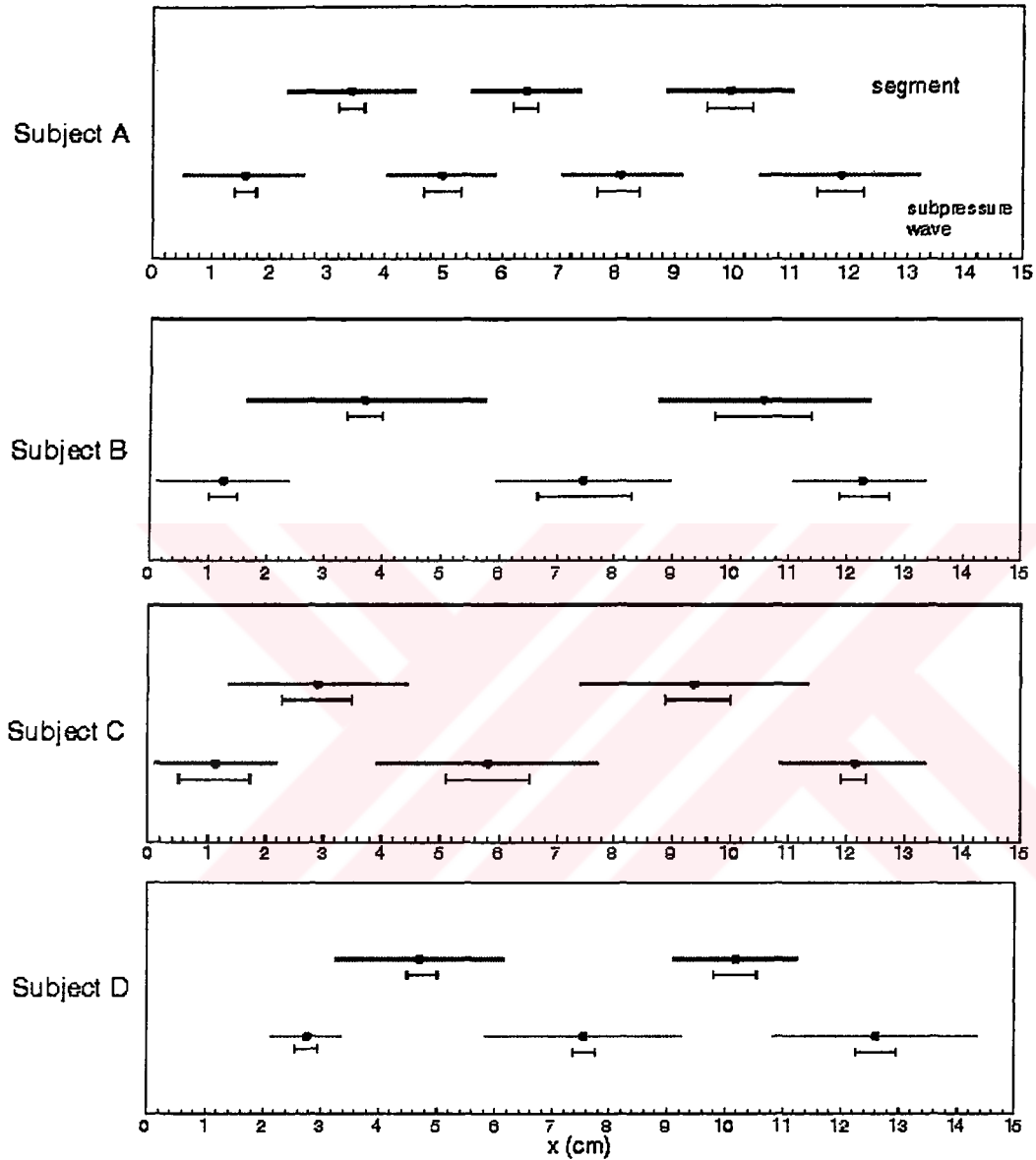


Figure 2.4. Locations and axial duration of subpressure waves and segments along the esophagus. Thin and thick solid lines show subpressure waves and segments, respectively. Dots represent centers of subpressure waves and segments. Error bars represent \pm SD.

2.2.3 Pressure amplitude of subpressure waves and segments

Average pressure amplitude of subpressure waves and segments are determined by applying statistical method on collected data. Average pressure distribution of 4 subjects along the esophagus is shown in figure 2.5. Solid and dashed lines represent subpressure waves and segments, respectively. Error bars shows standard deviation. To provide better comparison between cases, labels are kept same for all subjects in the figure.

Average pressure is high in first subpressure waves of subjects A, B and C (110, 90 and 100 mmHg respectively). But first subpressure wave of subject D is lower (55 mmHg). Last subpressure waves of subject A, B and C lower than first subpressure waves, but this is opposite for subject D. Second subpressure waves of 4 subjects are lower than last subpressure waves. Segment is basically low pressure region and its average amplitude is between 30-50 mmHg.

We did not consider location and shape of bolus, because of we studied only interpretation of manometric data in this chapter. However, pressure, which is talked about here, corresponds bolus/no-bolus transition point, bolus tail region and contractile zone behind the bolus tail. This pressure is produced behind the bolus tail by muscle contraction. Although dry swallowing does not have bolus, pressure is still produced in the esophagus.

2.2.4 Spatial and temporal duration of subpressure waves and segments

Spatial and temporal duration of subpressure waves are shown in figure 2.6. Δx and Δt are corresponding of spatial and temporal duration, respectively. Spatial duration of subpressure waves are between 2.5-3.5 cm and temporal duration is between 2-3 s in the esophagus. The number of swallows used for average is given in the bracket and error bars show the standard deviation. 1, 2, 3 and 4 represent subpressure waves in order.

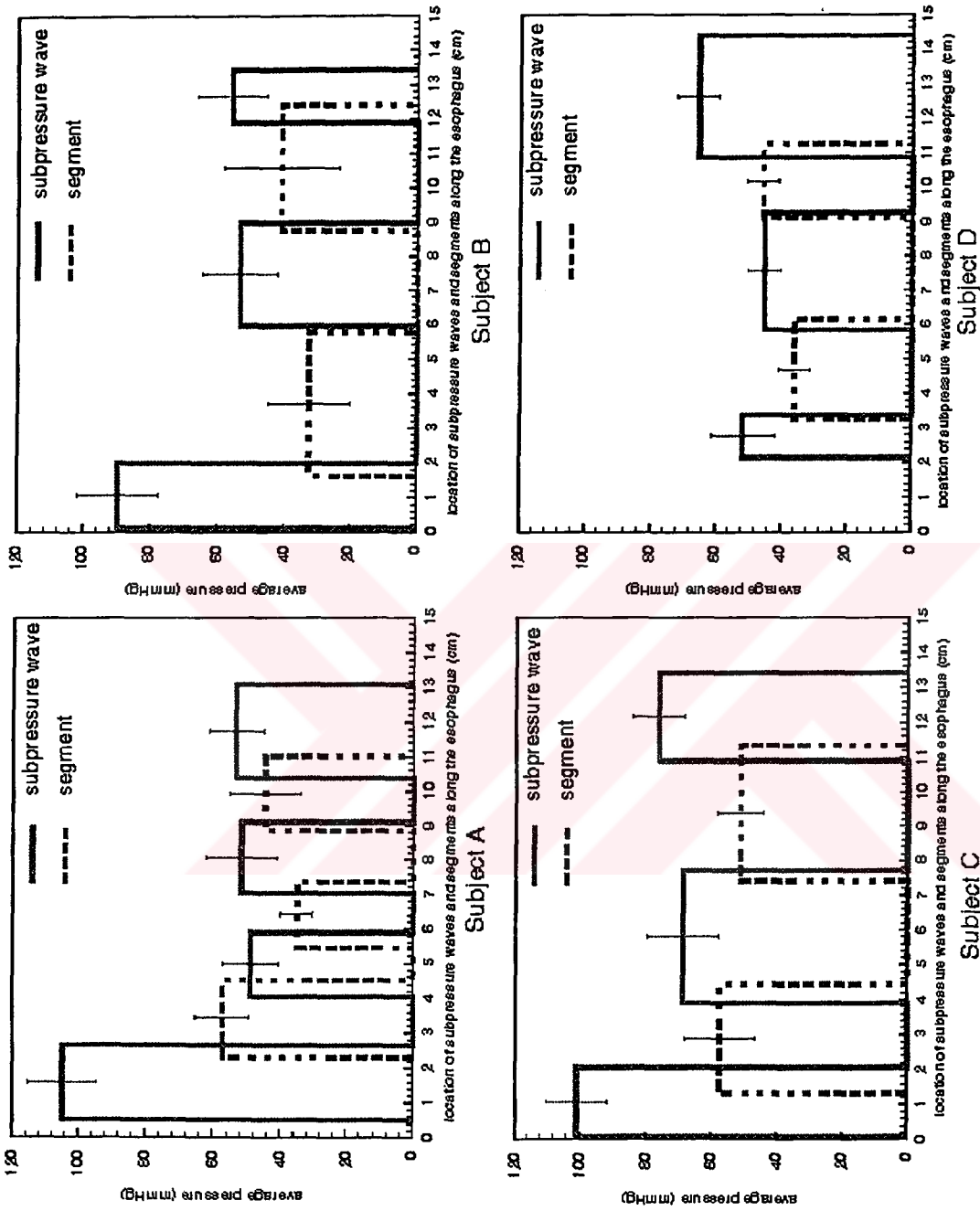


Figure 2.5. Average pressure distributions of each subpressure waves and segments and their locations along the esophagus and \pm SD.

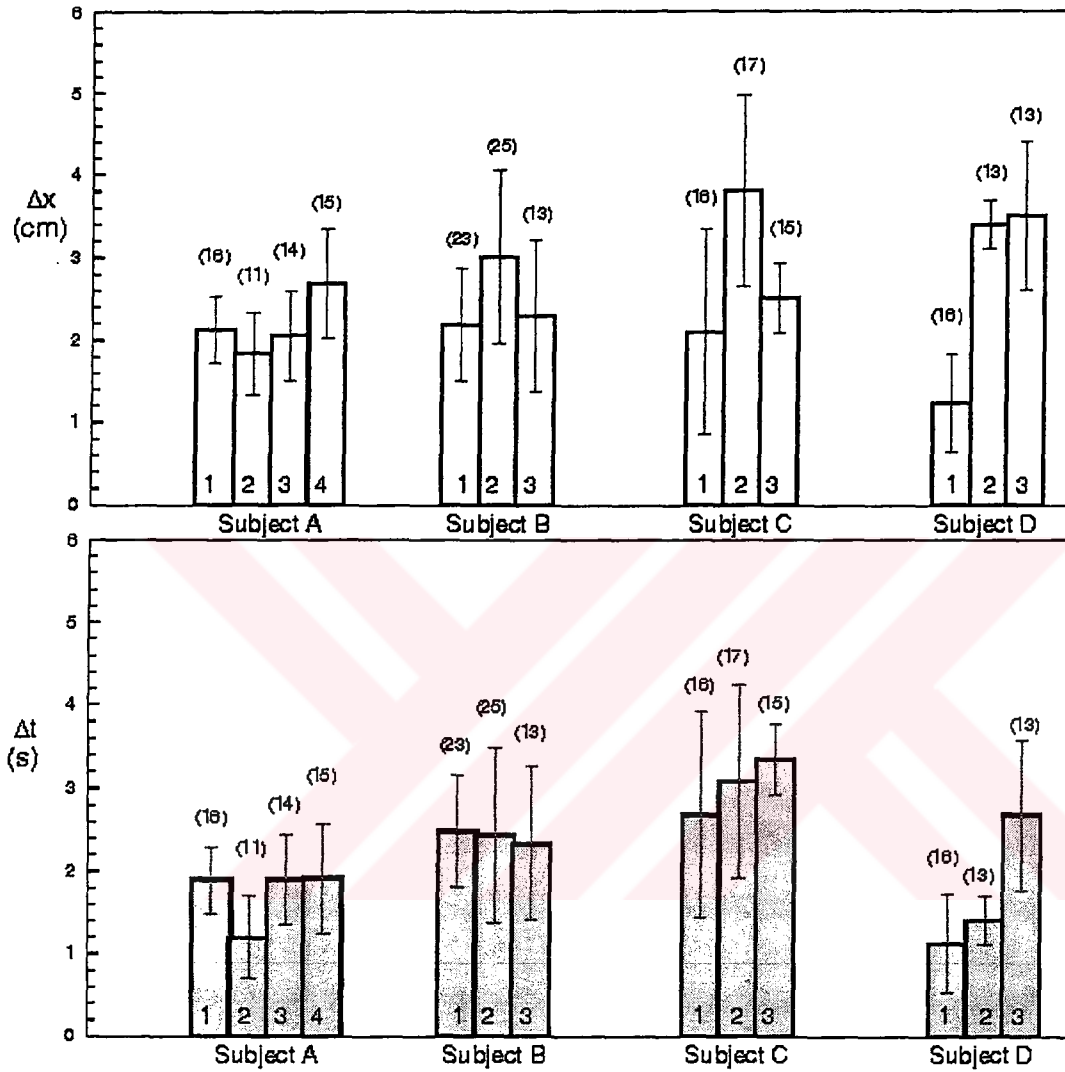


Figure 2.6. Length and duration of subpressure waves. Δx and Δt corresponding of spatial and temporal duration, respectively. Numbers in the bracket show swallowing numbers, which is used in this analysis.

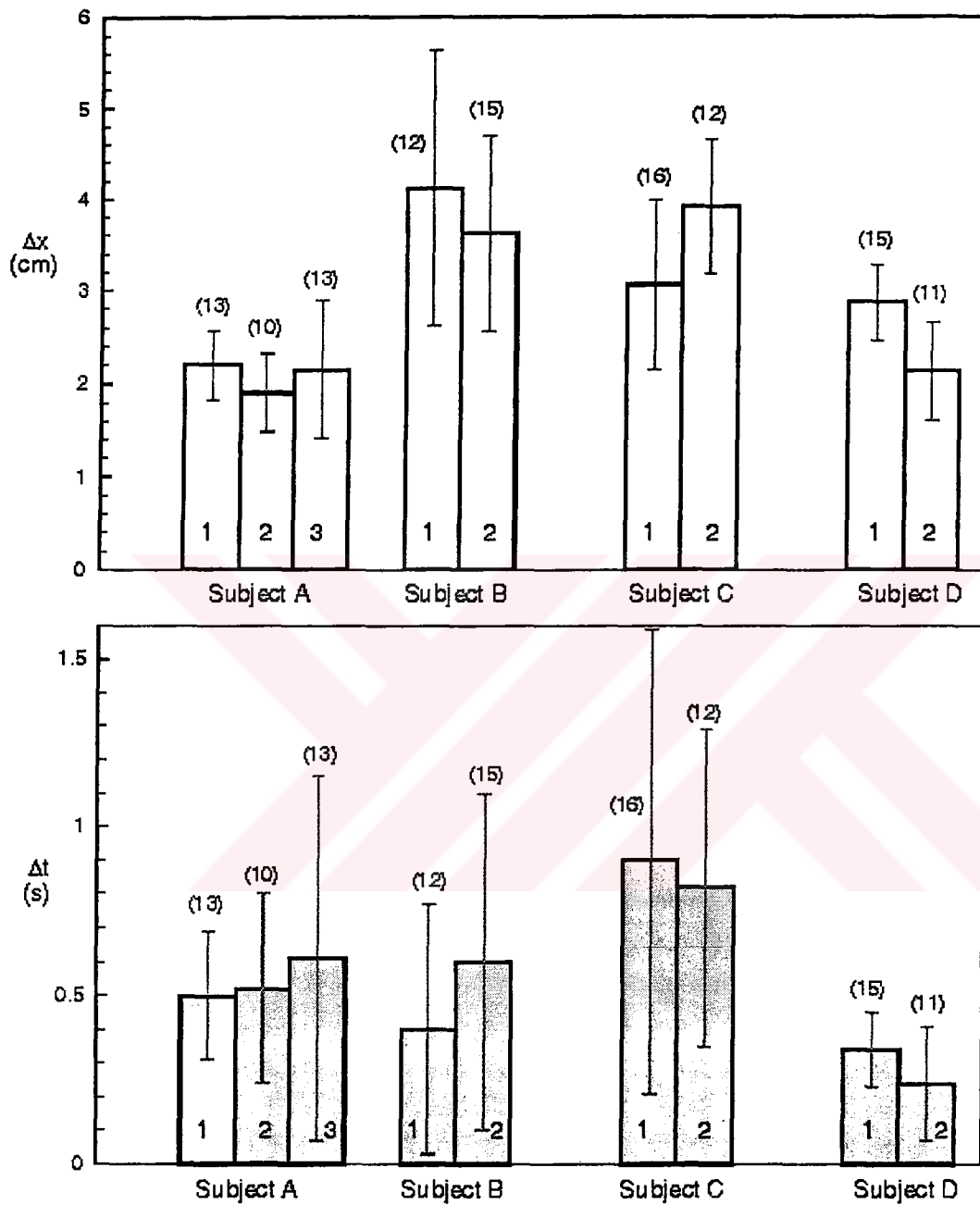


Figure 2.7. Length and duration of segments. Δx and Δt corresponding of spatial and temporal duration, respectively. Numbers in the bracket show swallowing number, which is used in this analysis.

Spatial and temporal duration of segment are shown in figure 2.7. Δx and Δt are corresponding of spatial and temporal duration, respectively. Spatial duration of segments is between 2-3 cm and temporal durations are between 0.5-0.8 s in the esophagus. The number of swallows used for average is given in the bracket and error bars show the standard deviation. 1, 2, 3 and 4 represent subpressure waves in order.

2.2.5 Wave speeds

Average primary and subpressure wave speeds are calculated for all swallowing of each subject and shown in figure 2.8. Primary wave speed is between 2-3 cm/s. And subpressure wave speed is between 1-2 cm/s. Error bars show \pm standard deviation.

Pressure distribution of a single swallowing along the esophagus and subpressure waves of this swallowing are shown together on a contour plot in figure 2.9. Contour plot shows pressure distribution from beginning to end of a swallowing along the esophagus. In this figure, dashed line, solid lines and dotted line corresponding of primary wave, subpressure waves and linearized form of primary and subpressure waves, respectively.

2.2.6 Pressure trough

Dodds [15] has obtained a pressure trough at the level of aortic arch during peristalsis. Clouse et al. [11] has confirmed in their studies, and additionally they have reported existence of second pressure trough in the distal esophagus. Findings of our analysis confirm their results. On the other word, we found two pressure troughs along the esophagus on each swallowing of 4 subject. Location of pressure trough does not change swallow to swallow on each subject. Pressure troughs appear approximately same at location in the esophagus for all swallowing of a subject. Pressure troughs are independent on sort of swallowing (barium, water and dry) and bolus volume. Figure 2.10 shows location of pressure trough of 4 subject.

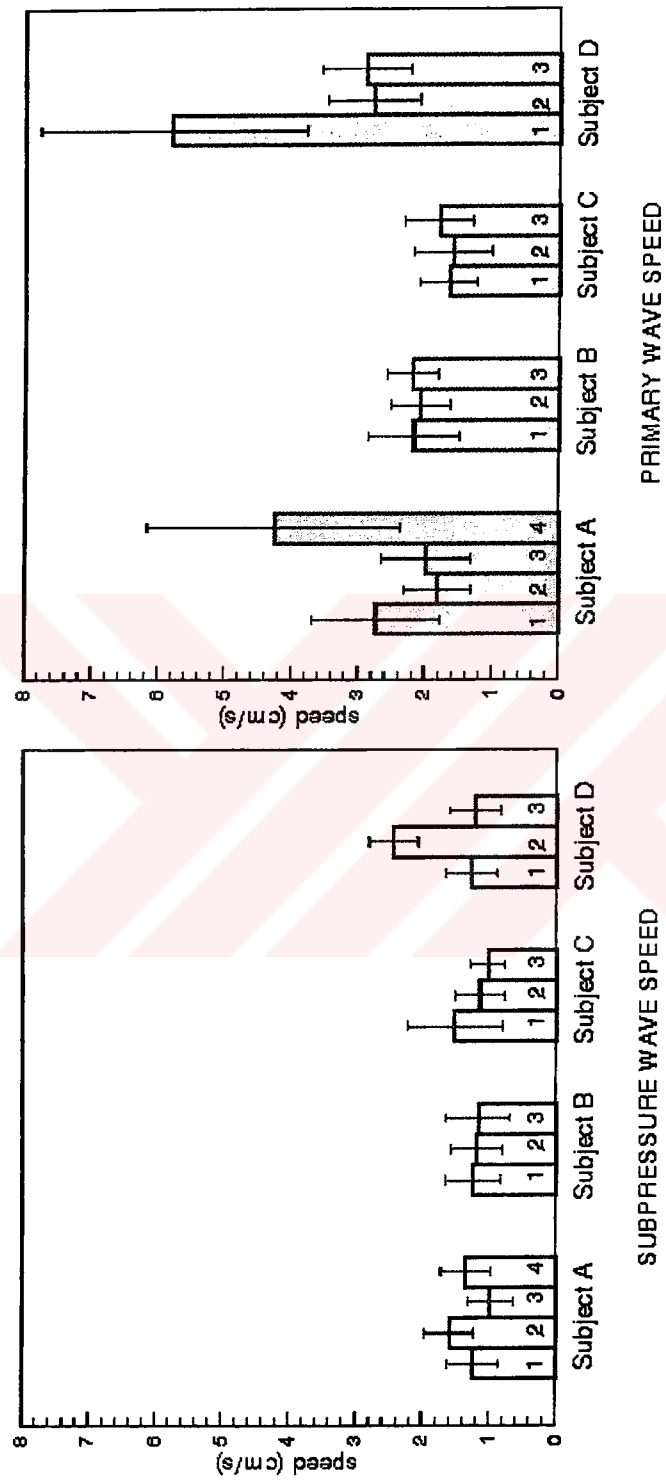


Figure 2.8. Comparison of speeds of primary and subpressure waves.

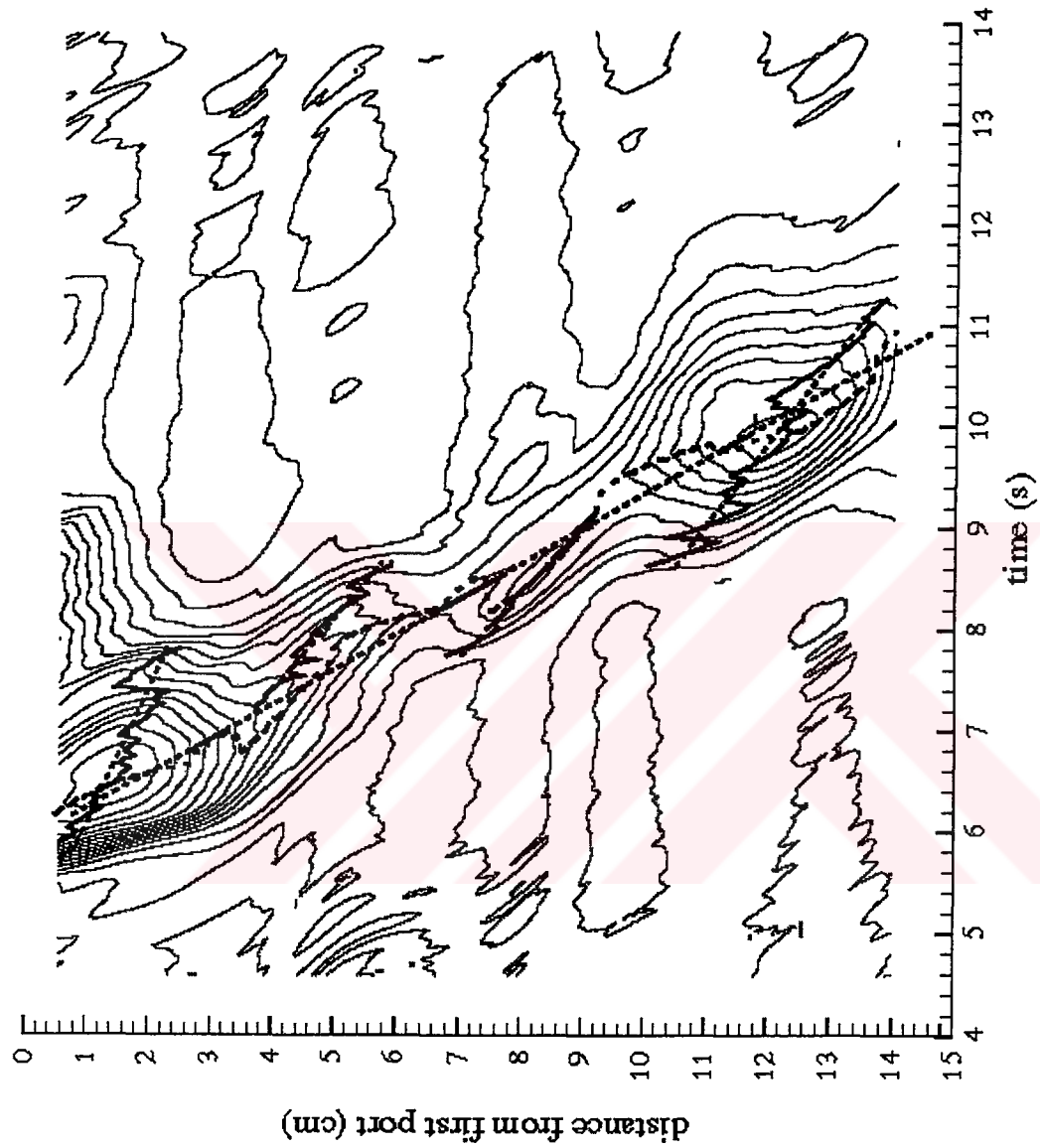


Figure 2.9. Pressure distribution of a swallowing on the contour plot and primary and subpressure waves on it.

2.3 Discussion

Interpretation of intraluminal manometric data alone in human esophagus during swallowing is the purpose for understanding features of esophagus and phase of swallowing without radiographic images. However, analysis of in vivo data is difficult for several reasons including noisy data and uncertainty in material parameter. To confidently draw conclusions concerning the physiology of peristaltic transport from manometric data analysis it is necessary to understand behavior of the esophageal parameters.

Conventional manometric analysis has relied on examination of the pressure measurements over time at discreet sites within the esophagus. Although this approach provides essential data concerning occlusive contraction events produced by the muscle fibers (primary circular) at the site, the ability to infer a relationship of these events to bolus movement is limited.

The intraluminal pressure wave propagates in the axial direction during esophageal peristalsis. The wave covers approximately 74% of the esophageal length at one time, and the front proceeds with two distinct periods of acceleration and deceleration through the striated and smooth muscle regions of esophagus, respectively. The wave characteristically has three sequential components; one in the proximal, striated muscle region and two in the remainder of the esophageal body [13]. We demonstrate the appearance of subpressure waves and segments during esophageal peristalsis as they propagate in the axial direction. The subpressure waves and segments are broad, covering as much as entire esophageal length in time. First subpressure waves (first and second on subject A) appear in the proximal esophageal (striated muscle) region, second and third subpressure waves (third and fourth on subject A) appear in the distal esophageal (smooth muscle) region.

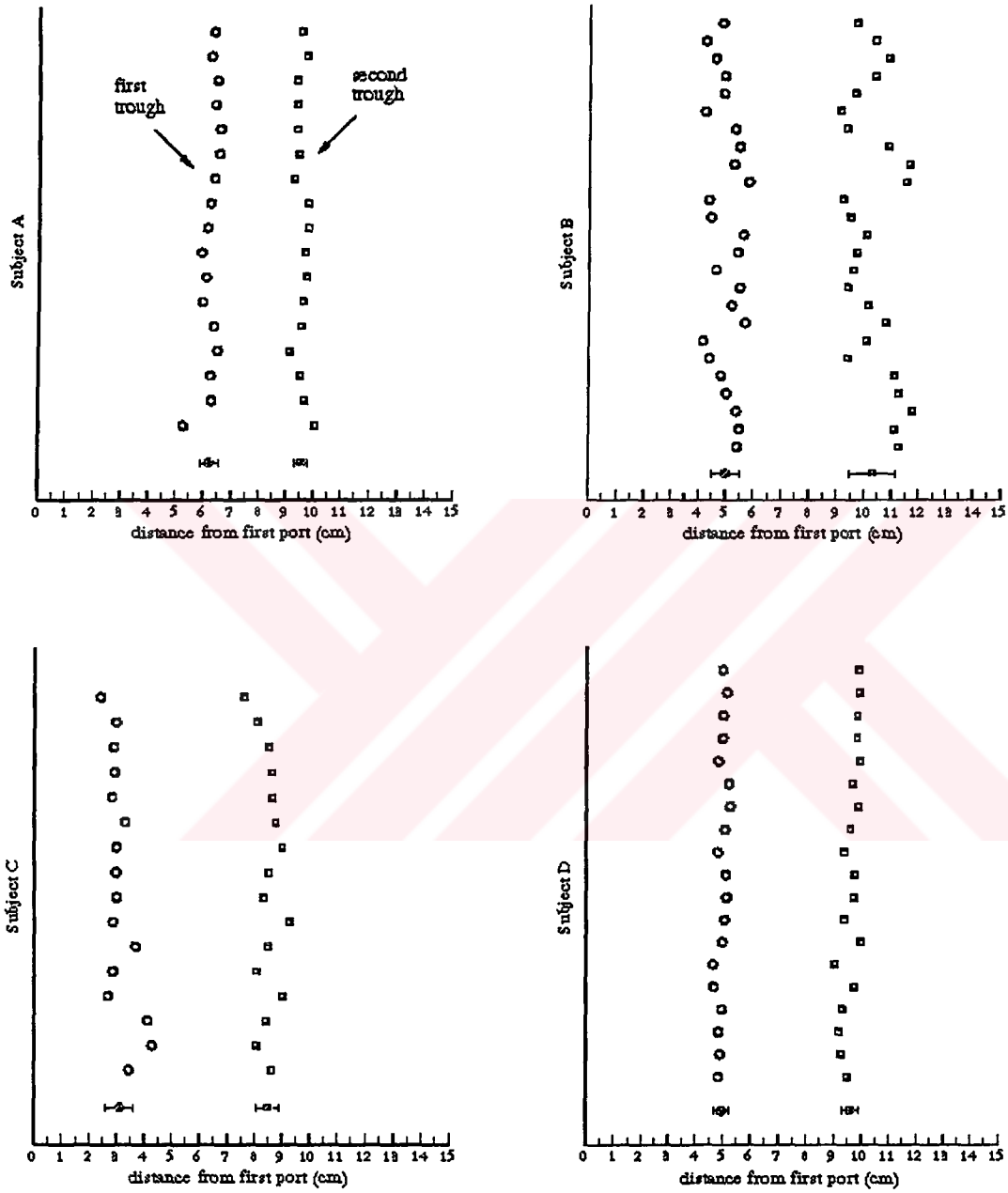


Figure 2.10. Pressure troughs along the esophagus. Circle and square represent first and second pressure trough location, respectively.

An anatomic explanation for separation of the esophagus into several contraction regions (subpressure waves, segments) is less easily available. Physiological studies of esophageal peristalsis in the opossum have shown both cholinergic and noncholinergic intramural neurons are present in the distal esophagus, and both likely participate in peristalsis. A gradient of influence by these neurons on smooth muscle control is present so that cholinergic influence is greatest in the more proximal segments of this region, and noncholinergic influence is greatest more distally. A similar gradient may be present in humans, as atropine affects speed of peristalsis, contraction amplitude, and contraction duration in the proximal segment of the smooth muscle esophagus. At present it is unknown whether this gradient is related to changing proportions of cholinergic and noncholinergic neurons or to a gradient of neurotransmitters within the same nerve terminals [11].

The existence of pressure trough at level of the aortic arc during peristalsis is determined in the previous studies [12, 15]. Pressure trough separates proximal esophageal contraction from the distal region. A second trough of less depth has observed to divide the distal esophageal body into two esophageal contractions [11]. Our findings about pressure trough correlate previous studies. We observed pressure troughs at aortic arch region and distal esophagus, too. Furthermore, our results show that location of each pressure trough is approximately same on all swallowing of each subject along the esophagus. Pressure trough at aortic arch region is deeper than other. An anatomic explanation for the first pressure trough is generally accepted. Esophageal circular muscle is entirely striated muscle for only the first 4% of esophageal length. A mixture of striated and smooth muscle fibers is found over the next third of esophagus, and the transition midpoint occurs at 4.7 ± 0.6 cm below cricopharyngeus [37]. This transition corresponds almost precisely to the location of the first trough in our subjects. A similar anatomic explanation for the second trough is lacking. A plausible explanation is that two distinct contraction units are present in the smooth muscle esophagus. These units may reflect transition from cholinergic to noncholinergic neurons, as has been demonstrated in the opossum, or other unrecognized neural variation in the control of peristalsis, as intimated by a gradient in neuron density through this region [12].

The pressure configuration in the subpressure wave and segment are mechanically independent, yet only the latter is relevant to bolus transport [47, 5]. Nevertheless, examining the entire contractile segment may provide information not directly related to bolus movement that is useful in understanding motility and motor disorder. For example, the analysis shows that subpressure waves and segments approximately appear in the same location along the esophagus. Esophageal contraction is realized as regional and these regions consist of subpressure waves and segments along the esophagus. These contracting segments can be affected by pharmacologic manipulation. Consequently, studying the contracting regions may provide information concerning the physiologic basis for esophageal peristalsis. Likewise, the contraction region may have contribution to symptoms (e.g. chest pain) that is independent of bolus transport [13].

During esophageal peristaltic transport, esophageal manometric recording sites record from two distinct pressure domains. First from within the intraluminal esophageal bolus and then the pressure distribution from within the segment of esophageal closure caused by the circular peristaltic contraction wave that seals the esophageal lumen proximal to the bolus and pushes the bolus aborally toward the stomach. Alterations in intrabolus pressure do not alter pressures within the peristaltic closure segment and, conversely, the pressure wave within the closure segment is not reflected into the esophageal bolus [46]. We focused only manometry, therefore this study does not include bolus geometry. Although we surveyed all pressure domains, because of subpressure waves and segments sit generally behind the bolus tail, we observed second pressure domains, which is mentioned above. Average pressure distribution of subpressure waves and segments for all subjects along the esophagus are shown in figure 2.4. High pressure amplitude generally exists 0-2.5 cm of esophagus. A modest decreasing follows along the esophagus and again increases, but not as high as before.

Spatial and temporal duration of subpressure waves and segments of all subject is shown in figure 2.6 and 2.7. Subpressure waves occur in 2-3 s and 2.5-3.5 cm and segments occur in 0.5-0.8 s and 2-3 cm along the esophagus. Segments are a transition period between subpressure waves.

Primary and subpressure wave speeds are illustrated in figure 2.8. Primary wave covers entire esophagus and subpressure wave covers its length. Velocity of peristalsis has been measured with different methods. We applied least square method to calculate both primary and subpressure wave speeds.

Dodds [15] has reported that the precise study conditions during manometry will affect the pressure values obtained. For example, peristaltic amplitudes are partially determined by manometric assembly diameter and swallowing modality. Consequently, these conditions should always be specified and preferably standardized. The incidence of a normal peristaltic sequence is significantly lower following a dry swallow compared to wet swallow. Further, peristalsis associated with a wet swallow is associated with greater peristaltic wave amplitude and slower wave speed than peristalsis elicited by a dry swallow [15]. We analyzed wet (barium and water) and dry swallowing in this study. Our findings show that there is not a significant difference between peristaltic sequence of dry and wet swallowing. Dry swallowing shows almost same characteristics as wet swallow. Subpressure waves and segments exist in dry swallow without exception.

Primary and subpressure waves are shown on the contour plot (figure 2.9). This figure gives detail information about pressure distribution along the esophagus, primary wave and subpressure waves. In summary, esophageal peristalsis occurs as a series of interconnected segmental contraction. The location of segmental regions appear to be stereotyped to an individual's esophagus; there are subpressure waves and segments along the esophagus and each subpressure wave and segment located approximately same place for different swallowings within a subject. Segmental contraction in the upper half of the esophagus appear to be of two types; (a) cover the upper and lower contraction waves, (b) cover the transition zone. Subpressure wave sits on side of transition zone (segment straddles the transition zone). This

observation appears to be independent of muscle type, suggesting pre-programmed neuromuscular control of peristalsis embedded either within the CNS or the enteric nervous system within the esophageal wall.



CHAPTER 3. NUMERICAL MODEL

3.1 Introduction and Literature Review

Peristalsis is a mechanism for pumping fluid in a tube by means of a moving contractile ring around the tube, which pushes the material onward. This is analogous to constricting a distensible tube with one's fingers and moving the occlusion forward along the tube. The peristaltic wave generated along the flexible walls of the tube provides an efficient transport of fluids in living organisms and in industrial pumping. It is an inherent property of many syncytial smooth muscle tubes, since stimulation at any point causes a contractile ring around the tube. Peristalsis generates propulsive and mixing fluid movements. The peristaltic propulsive movement is observed in the gastrointestinal tract, the transport of a food bolus through the esophagus, the ureter and other ducts throughout the body. Peristalsis is a mechanism used in blood pumps and is commercially applied in the transport of materials which must be kept uncontaminated or which are corrosive and must be separated from the pump machinery. Two interesting phenomena associated with peristaltic flows are fluid trapping and material reflux. The former describes the development and downstream transport of free eddies, called fluid boluses. The latter refers to the net upstream convection of fluid particles against the traveling boundary waves. From the fluid mechanics point of view, these phenomena demonstrate the complexity, but also motivate the fundamental study of peristaltic flow [43].

Even though peristalsis is a well-known pumping phenomenon observed in biological systems for many decades, the first attempt to study the fluid mechanics of peristaltic transport was by Latham [31]. Burns and Parkes [9] have developed a mathematical model for homogeneous fluids in a channel idealized under the assumption of inertia free motion due to an infinite train of peristalsis waves. Peristaltic pumping assumed trains of periodic sinusoidal waves in infinitely long

two-dimensional channels or axisymmetric tubes by Shapiro [50], Fung and Yih [21], Yih and Fung [63], Shapiro, Jaffrin and Weinberg [51]. These models, which were applied primarily to characterize the basic fluid mechanics of the pumping process, turn out two classes. First, the model developed by Fung and Yih which is restricted to small peristaltic wave amplitudes but has no restrictions on Reynolds number. Second, the lubrication theory model introduced by Shapiro et al [51] in which effects of fluid inertia and wall curvature are neglected but no restrictions are placed on wave amplitude. The effect of inertia and streamline curvature on peristaltic motion was investigated for a two dimensional channel by Jaffrin [27] and for axisymmetric tubes by Manton [36]. The effect of the intensity of the Poiseuille flow on the peristaltic motion was studied by Mitra and Prasad [38]. Liron [34] examined the efficiency of peristaltic pumping. The lubrication theory model is applicable globally in the limit of totally occluding peristaltic waves and is found to be a reasonably accurate approximation of global pumping characteristics at a small Reynolds number and wall curvature [27, 57, 58]. For many biological system, especially for peristaltic transport through the esophagus and small bowels, the fluid bolus is sufficiently viscous, and the peristaltic wavelength sufficiently long, to justify application of the lubrication theory approximation [32].

The classical lubrication theory model of peristaltic pumping has been extended by several authors to include effects of non-Newtonian fluids [52, 53, 4] and different cross-sectional shapes [26, 45]. Studies of pressure within the ureter showed that the pressure signature within the fluid bolus near the contraction region is very sensitive to wall shape [35, 7]. Roos and Lykoudis [48] studied the effects of an inserted catheter on the fluid mechanics of urethral peristaltic transport. To explore the effects of a mucous layer in the gastrointestinal tracts, Brasseur et al. [6] studied the effects of a peripheral layer of different viscosity adjacent to the tube wall during peristalsis. Numerical calculations [59, 8, 56, 57, 58] which have appeared in the literature mainly as extensions to the two dimensional wall models, have been used primarily to explore basic fluid mechanics issues rather than to describe a physiological flow.

The classical lubrication theory model of peristaltic transport has generalized to allow for arbitrary wave shape, arbitrary wavenumber and finite tube length by Li and Brasseur [32]. They studied basic fluid mechanical issues of the non-steady effects associated with finite tube lengths and the inherent difference between single and multiple wave transport, and the application of the generalized model to the simulation and biological study of esophageal bolus transport. Pressure and shear stress were also considered in addition to volume flow rate and pressure difference between the end of the tube.

Besides these investigations, Rath [44] studied the interaction of the elastic wall and the fluid. Rath developed a theoretical model for peristaltic flow through circular cylindrical tubes with elastic walls. The model consisted of an elastic pipe connecting with two fluids filled rigid vessels. The peristaltic motion has produced by an external peristaltic pressure along the axis of tube. It has assumed that the walls of the pipe are sufficiently thin, so that the circumferential stress has taken to be constant over the wall thickness. It has assumed that the flow is laminar. The nonlinear partial differential equations had been solved numerically. Carew and Pedley [10] developed a model for coupled problem of wall deformation and fluid flow for peristaltic pumping in ureter. The model has based on thin shell and lubrication theories, and driven by a propagating wave of smooth muscle activation. It made use of the available experimental data on the mechanical properties of smooth muscle and accounted for the soft material between the muscle layer and vessel lumen. The main input was the activation wave of muscular contraction. Equations for the time-dependent problem in tubes of arbitrary length have derived and applied to the particular case of periodic activation waves in an infinite tube. Predictions on phase-lag in wall constriction with respect to peak activation wave, lumen occlusion due to thickening lumen material with contracting smooth muscle, and the general bolus shape have observed as in qualitative agreement. Some modifications to the mechanical, elastic, and hydrodynamic properties of ureter that has made peristalsis less efficient, due for example disease, were identified. In particular, the flow rate–pressure rise relationship was linear for weak to moderate

activation waves, but as the lumen was squeezed shut, it was seen to be nonlinear in a way that was increase pumping efficiency [10].

Useful mathematical models of organ level muscle mechanics have been developed for the cardiovascular system and limited portions of the gastrointestinal tract. Several early investigators developed models to analyze average stresses within the in vivo myocardium based on experimental measurement of pressure versus volume and cineradiography in both human and animal studies. The first models used a thin wall static force balance in simple geometries (the Laplace equation) but were subsequently generalized to include thick wall approximations for spherical and ellipsoidal cavities. Eventually, more sophisticated models using classical elasticity theory and numerical methods emerged [40].

Previous investigators have estimated total muscle tension within the human esophageal wall by combining the Laplace equation with in vivo measurements of intraluminal pressure. Biancani et al. [2] measured maximum intraluminal pressure at fixed axial locations during a swallow of luminal radius by using different size manometric catheters. “Resting” luminal radius and wall thickness were estimated from human cadavers and conservation of volume was used to estimate thickness in the “deformed” state (i.e., as the collapsed esophageal lumen was stretched by different sized catheters). They found that at each axial location, maximal intraluminal pressure and wall tension increased with increasing catheter diameter. Orvar et al. [41] measured esophageal pressure versus radius characteristics using an impedance planimeter by distending the esophageal wall using a balloon filled to known volume. The equilibrium intraluminal pressure was measured and used to estimate circumferential wall tension and esophageal compliance.

In this chapter, lubrication theory and Laplace equation are combined, and a model is developed between esophageal geometry and muscle tension. The Laplace equation is often applied to relate wall tension to transmural pressure differences. This equation is simplified for our model. Our first objective is to calculate pressure from lubrication theory and tension from combined equation by applying numerical method. Our second objective is to predict esophageal wall geometry from known

pressure and tension, and we will explain its method and results in next chapter. Once complete, however, we have a numerical system from which an algorithm can be designed to predict esophageal wall geometry from manometric data obtained from the esophagus during normal and abnormal transport of fluid boluses.

3.2 Lubrication Theory Approximations

We analyze the lubrication theory using well-known solution for an infinitely long elastic walled tube whose walls are moving sinusoidally in the transverse direction, creating peristaltic wave speed. Application of the lubrication theory approximations to the non-steady problem requires that the flow dynamics be dominated by a single peristalsis driven timescale and highly disparate single axial vs. radial lengthscales, and that the flow be driven by frictional force. Consider the schematic illustration of peristaltic transport in figure 3.1, which illustrates a single wave moving along a finite tube. The lubrication theory approximation is applied to peristaltic transport driven by arbitrarily shaped deformations of the tube wall with pressure boundary conditions at the tube ends. Axisymmetric flow in a tube of circular cross-section is assumed with a single-phase Newtonian incompressible fluid of uniform viscosity μ . The characteristic velocity of the incompressible peristaltic wave is c , the wavelength of the peristaltic wave is λ , the length of tube is L and minimum tube radius, or “tube occlusion”, is ε . The shape of the tube wall is given by $H(x,t)$. Each material point on wall moves only radially with velocity $\partial H(x,t)/\partial t$. The problem is formulated in the “laboratory frame”, whereby the observer is fixed relative to the tube ends as peristaltic waves move past [32].

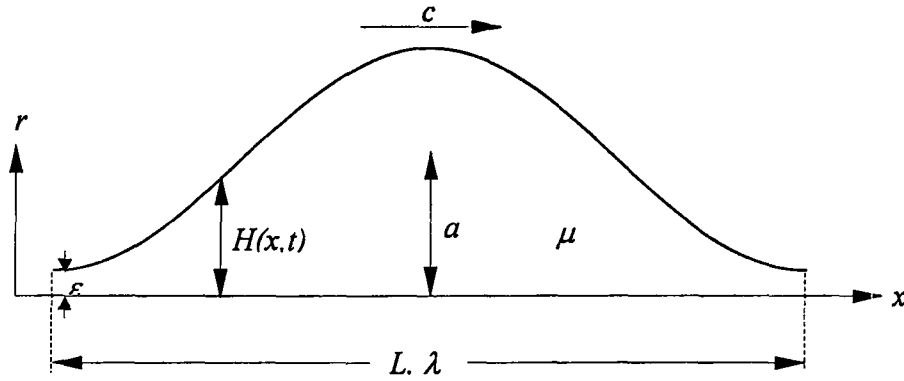


Figure 3.1. A single contraction wave of peristaltic transport is illustrated. The fluid bolus is transported from left to right by contraction waves along the tube. The contraction wave speed, wavelength, tube length and tube occlusion are defined respectively as c , λ , L and ε . The fluid viscosity and average bolus radius within one wavelength are μ and a , respectively.

To apply lubrication theory to general non-steady problem, the dominant axial scale λ is assumed to be large relative to the dominant radial scale, a , where a is taken to be the average radius of the bolus. In peristaltically driven flows the appropriate timescale is the wave period, λ/c , and k is a wave number and given by $k = a/\lambda$. In the general non-steady case, λ , a and c are average values over time. Correspondingly, the only appropriate Reynolds number is given by

$$Re = \frac{\rho c a}{\mu} \left(\frac{a}{\lambda} \right) \quad (3.1)$$

To simplify the problem, the lubrication theory approximations of infinitesimally small wall curvature ($k \rightarrow 0$) and Reynolds number ($Re \rightarrow 0$) are introduced. The approximations assume that inertial effects are negligible and that the dominant axial scale is much larger than the dominant radial scale.

In this limit, we can write the equation of conservation of momentum in an axisymmetric coordinate system moving with the wave shape at speed c as follows:

$$\frac{\partial p}{\partial x} = \frac{\mu}{r} \frac{\partial}{\partial r} \left(r \frac{\partial u}{\partial r} \right) \quad (3.2)$$

$$\frac{\partial p}{\partial r} = 0 \text{ or } p = p(x) \quad (3.3)$$

The continuity equation is given by

$$\frac{1}{r} \frac{\partial(rv)}{\partial r} + \frac{\partial u}{\partial x} = 0 \quad (3.4)$$

where u and v are the axial and radial velocity components, respectively. Boundary conditions are:

$$r = 0 \rightarrow \frac{\partial u}{\partial r} = 0, v = 0 \quad (3.5)$$

$$r = H \rightarrow u = 0, v = \frac{\partial H}{\partial t} \quad (3.6)$$

The lubrication theory approximations lead to local Poiseuille flow at every cross-section which communicates with its neighbouring sections through continuity. The limits $k \rightarrow 0$ and $Re \rightarrow 0$ provide reasonably good global approximations even when the curvature and the Reynolds number are finite but small [27, 57, 58].

Since the pressure is only function of x , equation (3.2) can be directly integrated twice using the boundary conditions. We obtain the axial velocity field as follow:

$$u = \frac{1}{4\mu} \frac{\partial p}{\partial x} (r^2 - H^2) \quad (3.7)$$

Radial velocity field is obtained as follow by substituting (3.7) into (3.4) and integrating twice:

$$v = \frac{r}{4\mu} \left[H \frac{\partial H}{\partial x} \frac{\partial p}{\partial x} - \frac{\partial^2 p}{\partial x^2} \left(\frac{1}{4} r^2 - \frac{1}{2} H^2 \right) \right]. \quad (3.8)$$

Equation (3.7) gives the axial velocity of the fluid in the moving system in terms of the local pressure gradient. Evaluating equation (3.8) at the wall produces a relationship between the motion of the tube and the axial pressure gradient $\partial p/\partial x$:

$$\frac{H^3}{16\mu} \frac{\partial^2 p}{\partial x^2} + \frac{H^2}{4\mu} \frac{\partial H}{\partial x} \frac{\partial p}{\partial x} = \frac{\partial H}{\partial t} \quad (3.9)$$

Analytic solution of equation (3.9) has obtained for single and train wave in finite length tube by Li and Brasseur [32].

3.3 Laplace Equation

Laplace equation (force balance) is applied across an esophageal cross-section to relate intraluminal pressure, thoracic cavity pressure, tension in muscle wall, wall geometry and wall thickness. Figure 3.2 illustrates a force balance across an esophageal cross-section.

Force balance across the esophageal wall is

$$P = \frac{T\tau + P_0(R + \tau)}{R}.$$

Substitute H instead of R into equation. For simplicity, we assumed $P_0=0$ and equation is decreased to:

$$P = \frac{T\tau}{H}. \quad (3.10)$$

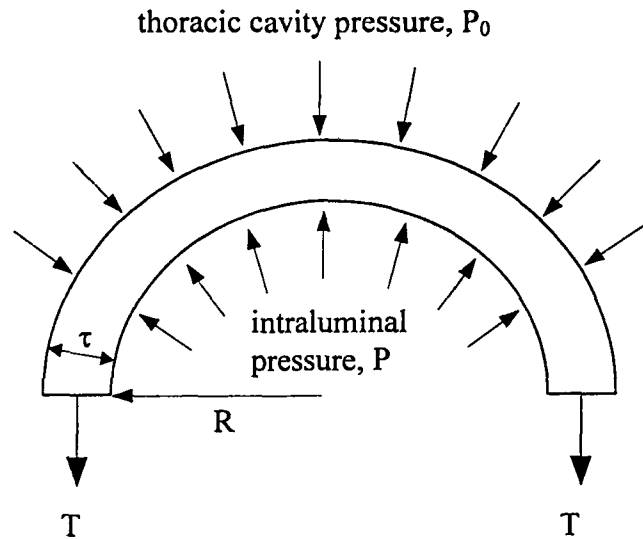


Figure 3.2. A force balance across an esophageal cross-section. P , T , P_0 , R and τ represent intraluminal pressure, tension in muscle wall, thoracic cavity pressure, radius of tube and muscle thickness, respectively.

From conservation of volume relationship between wall thickness and tube radius is

$$\pi(R + \tau)^2 - \pi R^2 = \text{constant}$$

$A_0 = \tau_0 R_0$ is cross-section area of undeformed state of esophagus. Because of

$\frac{\tau}{R} \ll 1$, equation (3.11) becomes as

$$\tau = \frac{A_0}{R}$$

Substitute H instead of R in the equation, then

$$\tau = \frac{A_0}{H} \quad (3.11)$$

By substituting equation (3.11) into equation (3.10), final form of force balance is obtained as:

$$P = \frac{A_0 T}{H^2} \quad (3.12)$$

Here, T is essentially the average tension $\langle T \rangle$ (force/area) within the muscle. Equation (3.12) shows that, for same H , increased muscle thickness produces higher intraluminal pressure, and therefore, higher contractile force.

3.4 Combination of Lubrication Theory with Laplace Equation

Lubrication theory approximation gives a relationship between intraluminal pressure and wall geometry. Our simplified Laplace equation gives a relationship between intraluminal pressure, tension in wall, wall geometry and wall thickness. To obtain a direct relationship between tension in wall and wall geometry, we combined equation (3.9) with equation (3.12).

First derivative of equation (3.12) in x direction is

$$\frac{\partial P}{\partial x} = \frac{A_0}{H^2} \frac{\partial T}{\partial x} - \frac{2A_0 T}{H^3} \frac{\partial H}{\partial x}. \quad (3.13)$$

Second derivative of equation (3.12) or first derivative of equation (3.13) in x direction is

$$\frac{\partial^2 P}{\partial x^2} = \frac{-2A_0 T}{H^3} \frac{\partial^2 H}{\partial x^2} + \frac{6A_0 T}{H^4} \left(\frac{\partial H}{\partial x} \right)^2 - \frac{4A_0}{H^3} \frac{\partial H}{\partial x} \frac{\partial T}{\partial x} + \frac{A_0}{H^2} \frac{\partial^2 T}{\partial x^2}. \quad (3.14)$$

First and second derivatives of P according with x direction are obtained from Laplace equation. By substituting equation (3.13) and (3.14) into equation (3.9), relationship between tension and wall geometry in absence of pressure is obtained as follow:

$$-\frac{A_0}{8} \frac{\partial^2 H}{\partial x^2} T + \frac{A_0 H}{16} \frac{\partial^2 T}{\partial x^2} - \frac{A_0}{8H} \left(\frac{\partial H}{\partial x} \right)^2 T = \mu \frac{\partial H}{\partial t} \quad (3.15)$$

There is not enough study in literature for interaction between flow in tube and tube wall. In living organs, it is important to understand interaction between flow and wall geometry mechanically and physiologically. Equation (3.15) provides interaction for sinusoidal wall geometry. Tension can be calculated from known wall geometry. Wall geometry can also be calculated from known tension. Numerical solution is given in next sections.

In this section, the shape of the tube is sinusoidal, described by

$$H(x, t) = \varepsilon + 0.5\alpha \left(1 - \cos 2\pi \left(\frac{x - ct}{\lambda} \right) \right). \quad (3.16)$$

Here, α is the wave amplitude and $\alpha = 2(a - \varepsilon)$. Li and Brasseur [Li&Brasseur93] have considered integral numbers of train waves propagating with constant speed through a tube of finite length with fixed equal pressure at the inlet and the outlet of the tube. In our case, integral number is constant and $\frac{L}{\lambda} = 1$.

3.5 Numerical Solution

Equation (3.15) is solved numerically by using a finite-difference technique on the peristaltic flow induced by an infinite train of sinusoidal waves in a axisymmetric channel. Simple and appropriate oblique lattice coordinates are introduced and equation (3.15) represented by the difference equation. For proper comparison with analytic solution of equation (3.9) which is obtained by Li and Brasseur [32], the

magnitudes of wave amplitude, wavelength and Reynolds number are chosen same with their study.

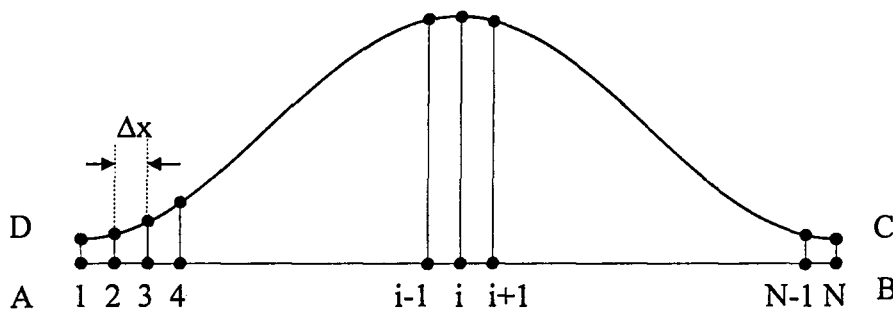


Figure 3.3. Calculating region and oblique coordinates, which are employed in the numerical analysis.

The flow induced by an infinite train of peristaltic waves is expected to be the same as the periodic flow that appears at the central part of the finite calculating region, where no influences of the boundary conditions at the leading and trailing end section are found. We consider the finite region $ABCD$ in the wave frames, as shown in figure 3.3. The domain of AB is divided into smaller intervals separated by N nodes with spacing Δx . Δt represents time intervals. Following finite difference schemes are used to discrete derivative terms.

For first order derivative, second order forward difference method is applied in axial direction.

$$\frac{\partial H}{\partial x} = \frac{H'_{i+1} - H'_{i-1}}{2\Delta x} \quad (3.17)$$

First order forward difference method is applied for time induced term.

$$\frac{\partial H}{\partial t} = \frac{H_i^{j+1} - H_i^j}{\Delta t} \quad (3.18)$$

Higher order finite difference approximation is applied to second order derivatives to obtain accurate solution.

$$\frac{\partial^2 T}{\partial x^2} = \frac{1}{12\Delta x^2} (-T_{i+2}^j + 16T_{i+1}^j - 30T_i^j + 16T_{i-1}^j - T_{i-2}^j) \quad (3.19)$$

Substituting finite difference approximation of differential terms in equation (3.15), finite difference scheme can be written as

$$\begin{aligned} & -\frac{A_0}{192\Delta x^2} H_i^j T_{i-2}^j + \frac{A_0}{12\Delta x^2} H_i^j T_{i-1}^j \\ & + \frac{A_0}{96\Delta x^2} \left(H_{i-2}^j - 16H_{i-1}^j + 15H_i^j - 16H_{i+1}^j + H_{i+2}^j - \frac{(H_{i+1}^j - H_{i-1}^j)^2}{3H_i^j} \right) T_i^j \\ & + \frac{A_0}{12\Delta x^2} H_i^j T_{i+1}^j - \frac{A_0}{192\Delta x^2} H_i^j T_{i+2}^j = \mu \frac{H_i^{j+1} - H_i^j}{\Delta t} \end{aligned} \quad (3.20)$$

In the present calculations, the integral number of meshes are chosen as $i = 1, 2, 3, \dots, N$ and $j = 1, 2, 3, \dots, M$. From numerical results, it is ascertained that the sensitivities of numerical solutions to the variations of N and M are always very small. This fact indicates that the numerical results are independent of the local Reynolds number of the mesh size. Therefore, the truncation error and the artificial viscosity do not appear for this range of N and M . In the case of the calculation to be compared with the Li and Brasseur's results, and accuracy will be discussed later.

A linear equation system is obtained from equation (3.20). Simply, equation (3.20) can be rewritten as

$$d_i^j T_{i-2}^j + e_i^j T_{i-1}^j + f_i^j T_i^j + g_i^j T_{i+1}^j + h_i^j T_{i+2}^j = w_i^j. \quad (3.21)$$

Where, d, e, f, g and h represent coefficients and their values are as follow:

$$d_i^j = -\frac{A_0}{192\Delta x^2} H_i^j$$

$$e_i^j = \frac{A_0}{12\Delta x^2} H_i^j$$

$$f_i^j = \frac{A_0}{96\Delta x^2} \left(H_{i-2}^j - 16H_{i-1}^j + 15H_i^j - 16H_{i+1}^j + H_{i+2}^j - \frac{(H_{i+1}^j - H_{i-1}^j)^2}{3H_i^j} \right)$$

$$g_i^j = \frac{A_0}{12\Delta x^2} H_i^j$$

$$h_i^j = -\frac{A_0}{192\Delta x^2} H_i^j$$

$$w_i^j = \mu \frac{H_i^{j+1} - H_i^j}{\Delta t}$$

We need boundary conditions to obtain tension, T , from equation (3.20). Boundary conditions are given in following section. The studies of Rath concentrated on the relationship between intraluminal pressure and thin wall geometry. We relate wall geometry directly with tension. Here, tension represent average tension as pointed out before. All analyses of peristaltic transport are based on a model in which the shape of the peristaltic wave is assumed. Physiologically, peristaltic contractions arise from active tensile forces originating within the tube wall. Not all commonly assumed sin-wave shapes are compatible with physiologically realizable contractile forces. The commonly assumed sin-wave shape is associated with active compression at the proximal end of the wave, but active extension at the distal end of the wave; active extension can not occur in the physiological system. This issue was discussed in Li and Brasseur [32] study.

Because of the peristaltic wave is periodic, boundary conditions are written as follow:

$$\begin{aligned}
H_{i-2}^j &= H_{N-2}^j \text{ at } i = 1 \\
T_{i-2}^j &= T_{N-2}^j \text{ at } i = 1 \\
H_{i-1}^j &= H_{N-1}^j \text{ at } i = 1 \\
T_{i-1}^j &= T_{N-1}^j \text{ at } i = 1 \\
H_{i-2}^j &= H_{N-1}^j \text{ at } i = 2 \\
T_{i-2}^j &= T_{N-1}^j \text{ at } i = 2 \\
H_{i+2}^j &= H_2^j \text{ at } i = N - 1 \\
T_{i+2}^j &= T_2^j \text{ at } i = N - 1 \\
H_{i+1}^j &= H_2^j \text{ at } i = N \\
T_{i+1}^j &= T_2^j \text{ at } i = N \\
H_{i+2}^j &= H_3^j \text{ at } i = N \\
T_{i+2}^j &= T_3^j \text{ at } i = N \\
H_i^{j+1} &= H_i^2 \text{ at } j = M
\end{aligned} \tag{3.22}$$

We introduced viscosity as $\mu = l \frac{N}{m^2}$. A linear equation system is obtained from equation (3.20) and solved using boundary conditions. $N \times N$ square coefficients matrix appears from linear system and finding inverse of coefficients matrix, tension T , is calculated directly. We can apply our numerical method to single wave and train wave. Both of them give excellent solution. We can also solve non-integral numbers of waves problem using this technique.

To compare our results with Li and Brasseur [32], we calculated pressure from tension using Laplace equation.

3.6 Analysis of Tension in the Muscle Wall

Numerical calculations are performed for an axisymmetric tube. The flow in the region of finite tube obtained by the analysis in previous section involves the periodic flow in the tube. Smooth muscle possesses passive elastic properties that come into play only when the muscles react to a stimulus. When a muscle length changes, the tension generated depends on both the length of the muscle fiber and its speed of contraction and lengthening [10]. To quantitatively analyze the function of an internal organ, one must understand its properties in both resting and active states. In the case of the esophagus, where the bolus in the organ moves in response to the contraction of the esophageal wall, a complete analysis of the peristalsis requires a combination of fluid mechanics, solid mechanics and physiology of the contraction of the esophagus. Yin and Fung [64] studied the passive and length-tension properties of the dog ureter. For the length-tension relationship in active contraction, Zupkas and Fung [65] have reported that the maximum level of active tension was found to develop at a stretch level at which the resting tension exceeds the active tension.

ε/a and L/λ are varied by altering the tube occlusion and the length of the tube relative to the wave. Figure 3.4 shows tension variations at six specially chosen times during one wave period with one waves existing in the tube ($L/\lambda = 1$). In this figure, the solid lines are the tension distributions along the tubes and the dashed lines are the corresponding wall shapes. In the calculation the initial location of the peristaltic wave is chosen with the point of minimum radius positioned at the inlet of the tube. All variables are dimensional. Note from figure 3.4 that within each peristaltic wave there exist two peaks in the tension distribution with a gradual tension ramp in between. The transition from a large negative peak to a large positive peak takes place at the point of minimum radius within the contraction zones. To the right of this point the tube wall is moving radially inward ($\partial H/\partial t < 0$), creating a large gradient in tension there.

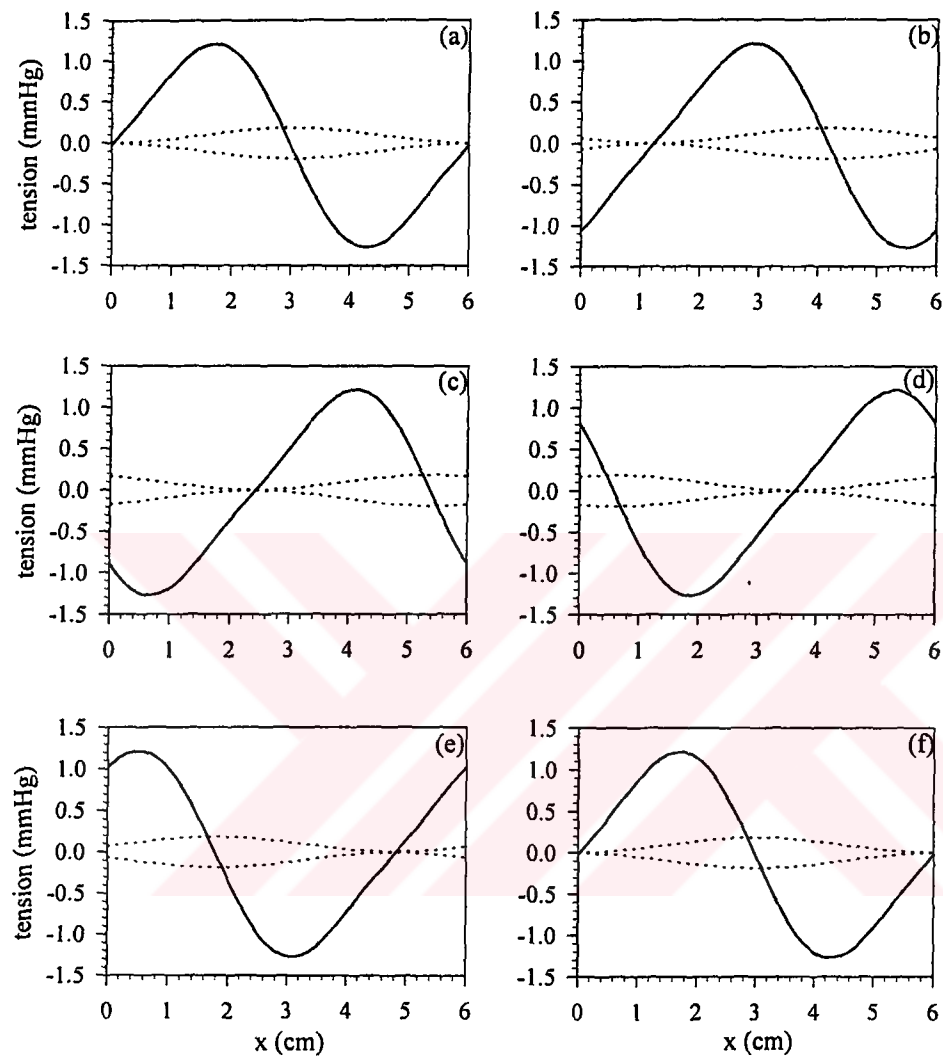


Figure 3.4. Tension distributions along the tube at six time instants in one wave period with one wave in the tube ($L/\lambda = 1$). Here, (a) $t=0$ s; (b) 0.4 s; (c) 0.8 s; (d) 1.2 s; (e) 1.6 s; (f) 2 s. The solid lines are tension distributions along the tube, and dotted lines are the corresponding sinusoidal wall shapes. In the calculation, $\varepsilon/a = 0.0523$, $Re=0.00457$.

In the esophagus, for example, this radially inward motion of the tube wall is produced by the contraction of circular muscles within the esophageal wall. To the left of the point of maximal occlusion the tube wall is moving radially outward leading to a corresponding drop in tension. Note that at the point of maximal occlusion the axial tension gradient is positive and the local instantaneous flow is to the left. In all other regions of tube, however, the axially tension gradient is negative and the local instantaneous flow is to the right – in the direction of the peristaltic wave. When averaged over one wave period, the net effect is transport in the direction of peristaltic wave motion.

It is typical for highly occluded peristaltic pumps to have large tension gradient near the points of maximal occlusion, but a relatively small tension gradient within the main body of the peristaltic wave. Less highly occluded pumps show a similar tension distribution but lower peak tensions, lower tension gradients in the contraction zones, and a larger tension gradient within the main body of the peristaltic wave relative to that within the contraction zone. Figure 3.5 shows the time-varying tension distribution for a larger ε/a of peristaltic wave in the tube, where all other variables are the same as in figure 3.4 except ε . Note that the spatial and temporal distributions of tension magnitudes in these two cases are different. Larger ε causes significant decrease on tension magnitude.

Although the mechanical and pharmacological properties of the different organs do differ [1, 20, 22], some features found in esophagus can be observed in other smooth muscle organs. Hellstrand [24] has reported that in quick releases of portal vein segment, a peak plateau of velocity of contraction was observed late in the rising portion of the contraction cycle. An explanation of this phenomena in a framework such as Huxley's sliding element theory is lacking as the mechanics of contraction in smooth muscle is not clearly understood. A lack of understanding of the mechanisms for contraction in the esophagus does not forbid defining the organ function from interpreting in vivo observations in terms of in vitro experiments, or vice versa [65].

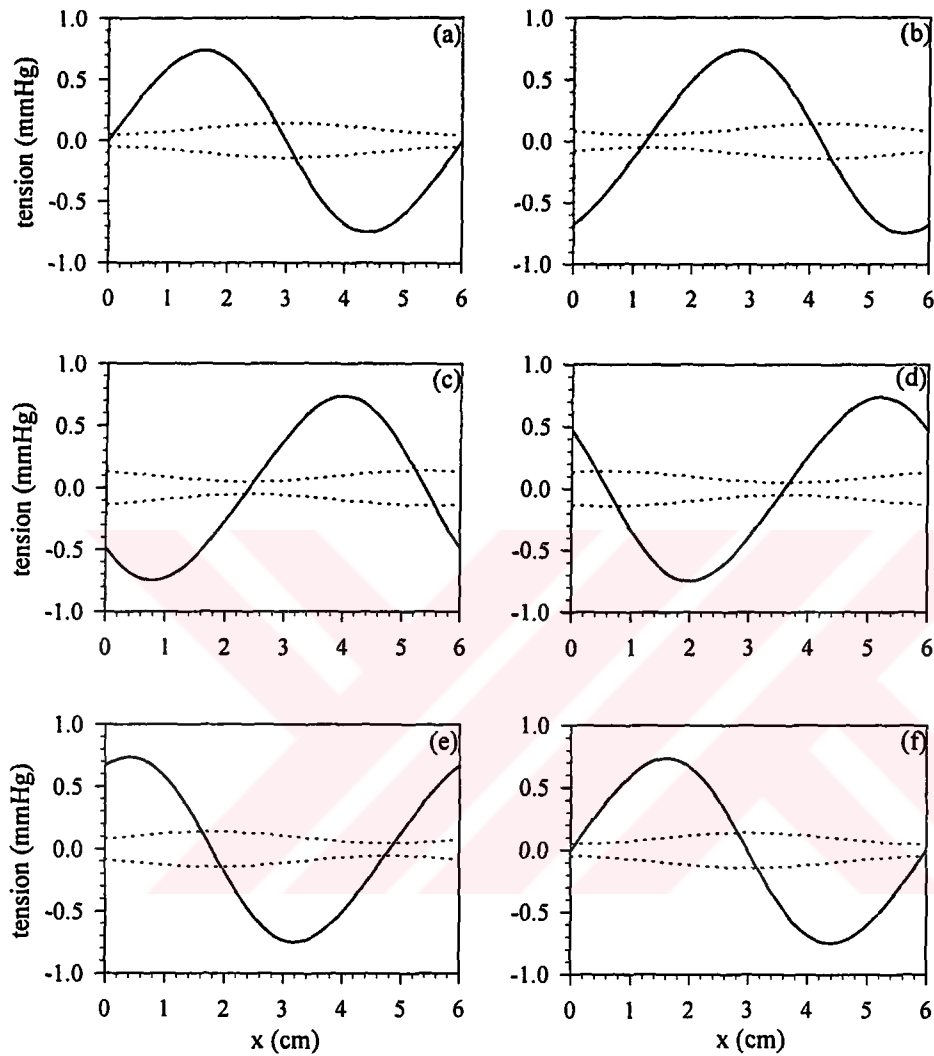


Figure 3.5. As figure 3.4 but different ϵ . Here, (a) $t=0$ s; (b) 0.4 s; (c) 0.8 s; (d) 1.2 s; (e) 1.6 s; (f) 2 s. The solid lines are tension distributions along the tube, and dotted lines are the corresponding sinusoidal wall shapes. In the calculation, $\epsilon/a = 0.523$, $Re=0.00457$.

3.7 Comparisons of Numerical Solution with Analytical Solution

In human body, propagating contraction waves often transport single boluses of physiological fluid from one place to another. We explore here the basic fluid dynamics of single wave peristaltic transport in tubes of finite length. In previous section, we calculated tension directly from the known bolus shape. Li and Brasseur [32] have obtained the pressure from the analytical solution of equation (3.9). For comparison, we calculated pressure distribution using Laplace equation.

In figure 3.6, the pressure distributions from the analytic and numerical method are plotted along the x direction. In figure, solid lines show pressure distributions of our numerical solution. Dashed lines represent pressure distributions of analytic solution (reproduced from Li and Brasseur [32]). Dotted lines are the corresponding sinusoidal wall shapes. In calculation, $L/\lambda = 1$ and $\varepsilon/a = 0.0523$. Note from figure that pressure distributions along the tube are similar tension distributions as in figure 3.4. Tube characteristics are exactly same in figure 3.6 with figure 3.4. But, we can see easily from the comparison two figures, locations of peak pressures are different than locations of peak tensions. Because of the low ε/a , pressure gradients are large near the points of maximum occlusion.

Results from numerical solution have excellent match with analytic solution as seen in figure 3.6. There are only very little difference in the some part of the pressure gradients. This difference in the pressure does not change with time. The peak pressure locations are not at the beginning and end of the tube (figure 3.6 (a)). The pressure at these point and center of tube are zero. So first half of the tube have positive pressure gradients and other half have negative pressure gradients. We applied periodic boundary conditions in numerical method. Li and Brasseur [32] has kept pressure zero at the beginning and end of tube. And they have obtained fluctuations on the pressure gradients. We obtained perfectly periodic pressure gradients in our solutions.

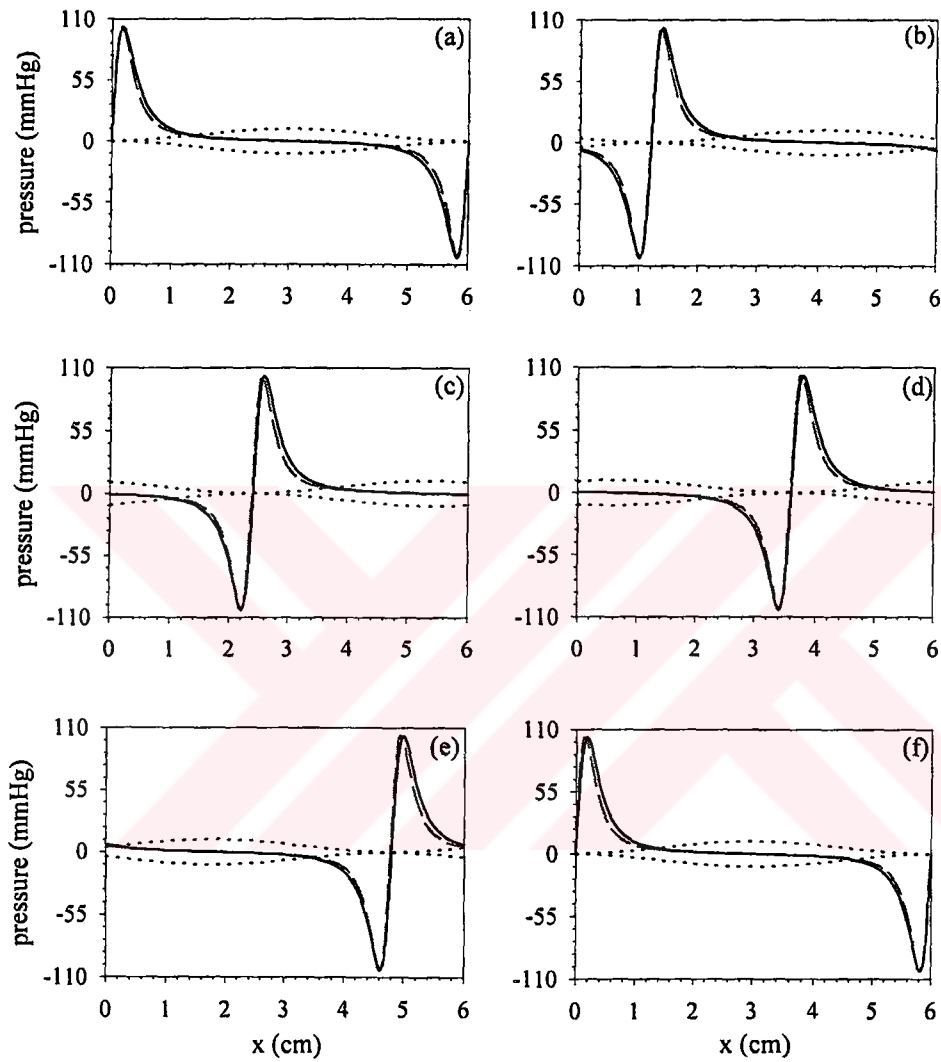


Figure 3.6. Comparison the pressures between the analytic and numerical solutions. Here, (a) $t=0$ s; (b) 0.4 s; (c) 0.8 s; (d) 1.2 s; (e) 1.6 s; (f) 2 s. The solid lines are pressure distributions from numerical solution, dashed lines are pressure distributions from analytic solution of [32], and dotted lines are the corresponding sinusoidal wall shapes. In the calculation, $\varepsilon/a = 0.0523$, $Re=0.00457$.

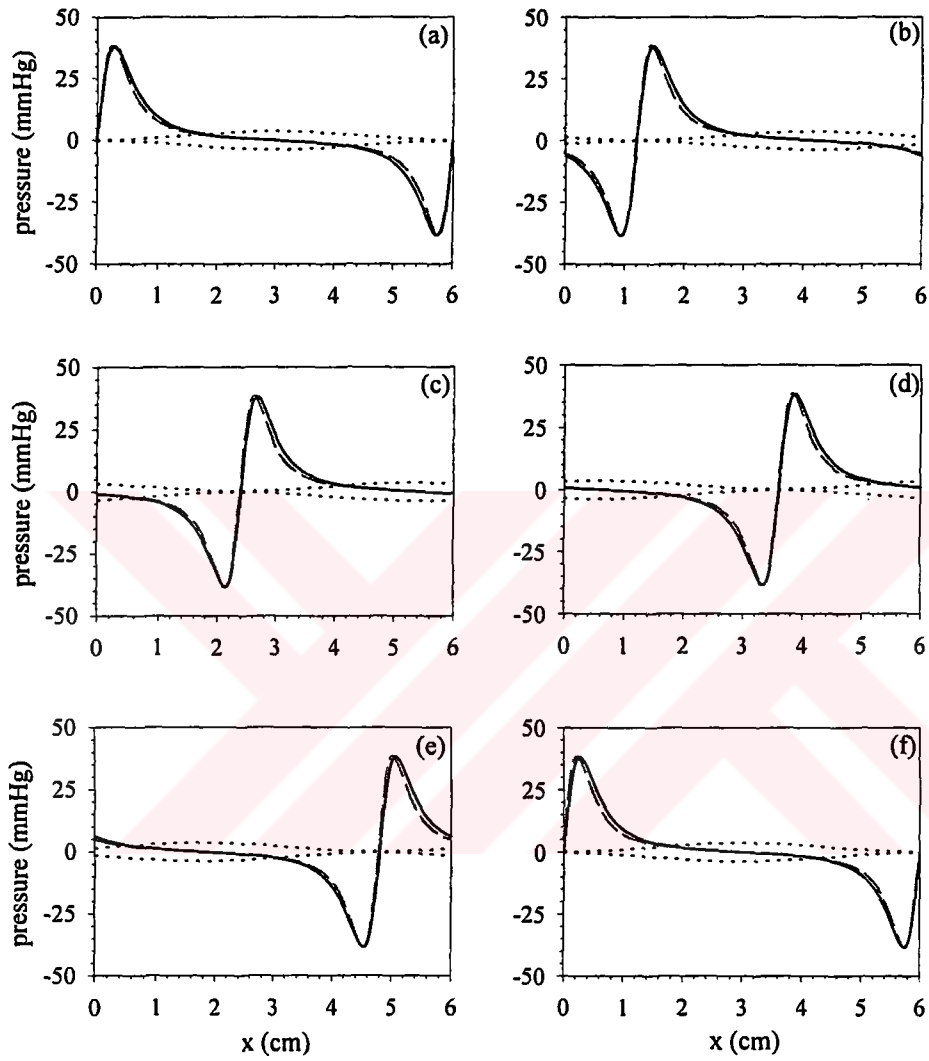


Figure 3.7. Same as figure 3.6, but different ε/a . Here, (a) $t=0$ s; (b) 0.4 s; (c) 0.8 s; (d) 1.2 s; (e) 1.6 s; (f) 2 s. The solid lines are pressure distributions from numerical solution, dashed lines are pressure distributions from analytic solution of [32], and dotted lines are the corresponding sinusoidal wall shapes. In the calculation, $\varepsilon/a = 0.103$, $Re=0.00473$.

Figure 3.7 shows pressure distributions along the tube for different ε/a . Pressure gradients change with tube occlusion as tension gradients, which is mentioned before. The little difference at pressure distributions along the tube between analytical and numerical solution still exists as seen in figure.

3.8 Effect of the Tube Occlusion on the Pressure Field

The limit of complete occlusion, where no bolus fluid is leaked, is of interest in esophageal transport. In this limit, it is of interest to determine the variations in pressure. The maximum pressure, P_{max} , is plotted against ε in figure 3.8. P_{max} becomes infinitely large as $\varepsilon \rightarrow 0$. This singularity in pressure is felt to be associated with the small slope approximation.

It is clear when the tube is totally occluded, as in figure 3.9a all fluid is trapped between the occluded points and moves to the right with the peristaltic wave. However, with partial occlusion (larger tube occlusion, ε as in figure 3.9b), some of the fluid within a wave can be expected to leak backward through the contracted region into the proximal wave. This is fluid left behind and is analogous to bolus fluid left behind an esophageal contraction wave. This situation causes bolus retention in the esophagus. Figure 1.5 shows concurrent manometric and videofluoroscopic data, in which the peristaltic stripping wave fails to progress after radiographically normal progression to the distal esophagus. The radiographic images indicate that most of the bolus fluid is retained in the distal esophagus after the contraction wave fails. The manometric pressure signatures indicate that the initial esophageal stripping action is associated with feeble peristaltic contraction. The contraction wave appears to increase in strength beyond the aortic arch before weakening and coming to rest as the LES opens, exposing the bolus to the higher, gastric, pressure and causing a simultaneous rise in intrabolus pressure at the distal three manometric ports. Because active contractile forces at the bolus tail have weakened considerably as the LES opens, when intrabolus pressure rises to sufficiently high values, the contraction wave fails completely and high intrabolus pressure forces the bolus fluid retrograde. When the LES closes, most of the original bolus fluid remains within the esophagus.

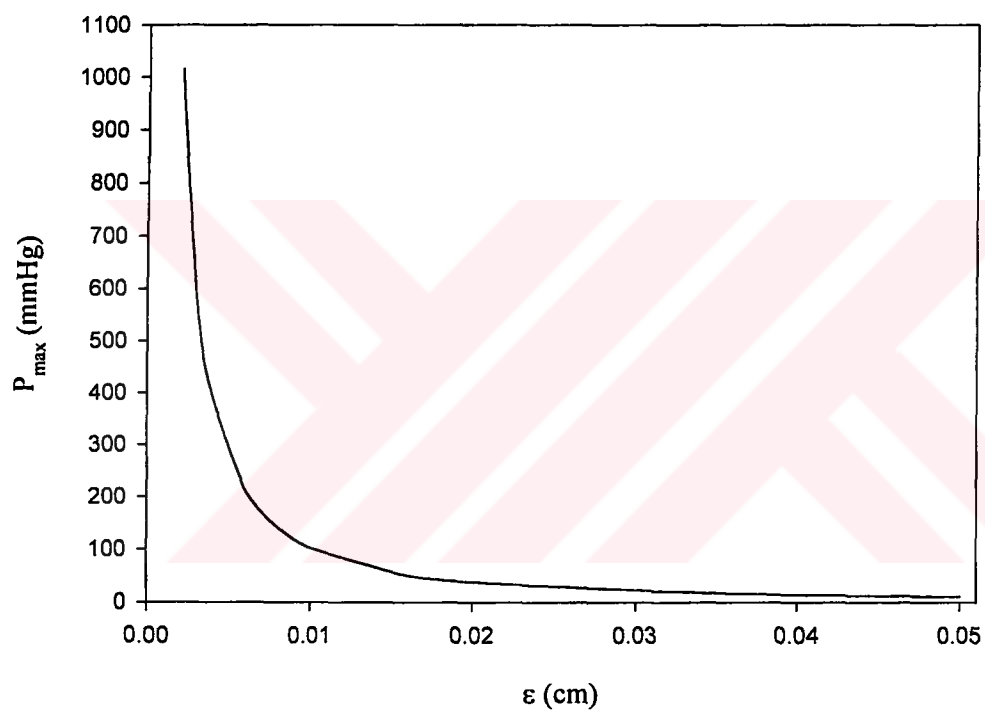


Figure 3.8. Maximum pressure in the flow domain (in the occlusion region) from numerical model as a function of the tube occlusion. As $\varepsilon \rightarrow 0$, the pressure in the occlusion region increases without bound.

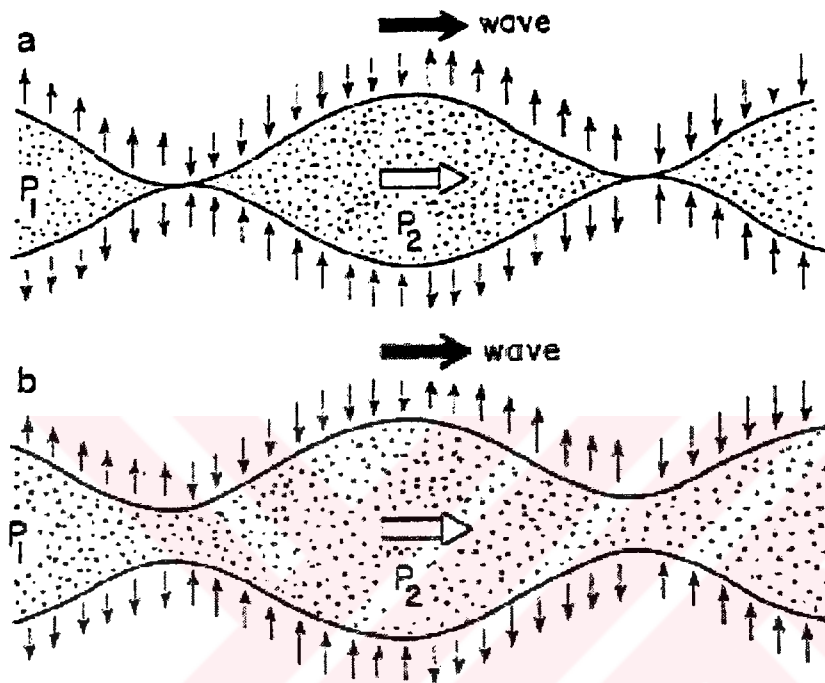


Figure 3.9. An infinite series of periodic sine waves, produced by the lateral motions of the wall. (a) The totally occluded tube transports the trapped fluid within the peristaltic wave. (b) Incomplete occlusion allows some fluid to leak proximally into trailing waves.

The extent to which fluid is lost from a peristaltic wave is expected to depend not only on the degree to which occlusion is incomplete but also on the difference in pressure between one wave and the next and on the viscosity of fluid. If the bolus pressure greater P_2 is greater than the proximal pressure P_1 , for example, more bolus fluid will likely be forced into the proximal wave than if the pressures were the same.

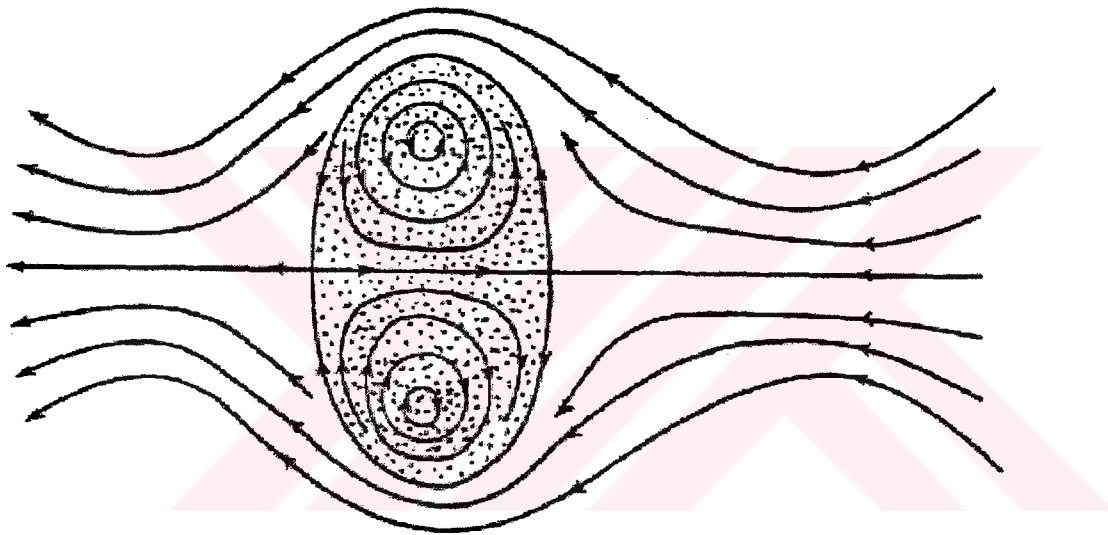


Figure 3.10. Fluid motions with incomplete occlusion. The observer is moving to the right with the traveling peristaltic waves. A region of fluid trapped relative to the moving wave is shown, surrounded by fluid that leaks proximally into the trailing wave.

The numerical model corroborates this line of reasoning. Figure 3.10 illustrates the fluid motions that occur with incomplete occlusion, depicted as if the observer were moving to the right along with the peristaltic wave. In this frame of reference the tube wall does not change in shape, in contrast with figure 3.9 where the peristaltic wave moves to the right past the observer. The fluid motions are therefore observed relative to the moving wave. What is calculated from the model is a central recirculating bolus in which the fluid is trapped and moves along with the peristaltic wave. Outside this trapped bolus, however, the fluid moves around and leaks into the proximal wave.

3.8.1 Effects of the number of grid points of the tube length

Calculations are obtained for different grid size along the tube length from both our numerical model and analytic solution of lubrication theory approximation. We calculated error between two solutions using following equation:

$$error = \sqrt{\frac{\sum(P_{lub} - P_{num})^2}{\sum P_{num}^2}}. \quad (3.23)$$

P_{lub} , P_{num} represent pressure from lubrication theory approximation and numerical model, respectively. Figure 3.11 shows error between two calculations. Expectation is that lower grid size gives more error than higher grid size. But calculations do not agree with expectation, and error shows interesting behavior. As seen in the figure, error is around 0.2 for grid sizes 100 and 200. It increases to 0.4 for grid size 300, and decreases 0.2 for grid size 400 and 500. And for grid size 600 and 700, error increases 0.65 and 0.8, respectively.

These calculations are performed for wavelength 6 cm, tube occlusion 0.01 cm, Reynolds number 0.00457.

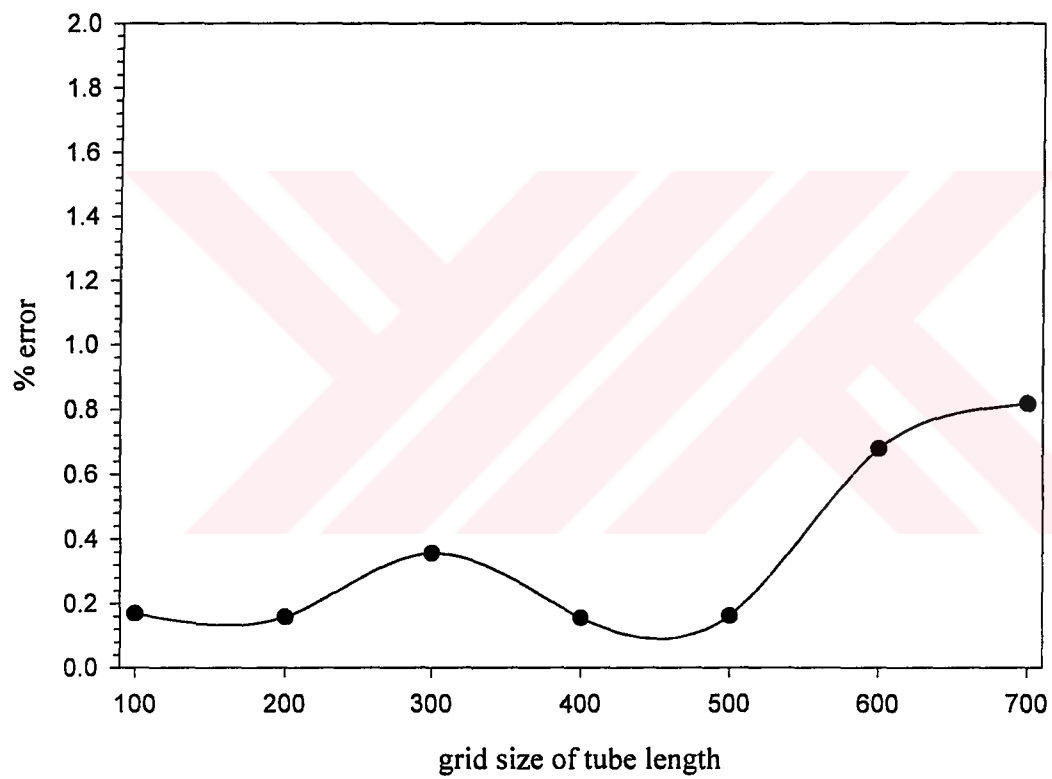


Figure 3.11. Error is plotted as a function of grid size. For same grid size pressure is calculated from our numerical method and analytic solution of lubrication theory approximation.

3.9 Peristaltic Pumping Performance

In the analysis of peristaltic transport as a mechanical pump, pumping performance is measured as the average pumping flow rate for given pressure head against which the pump operates. The relationship between the pressure difference $\Delta P = P_L - P_0$ and the flow rate averaged over one wave period, \bar{Q} , is linear in the infinite tube lubrication theory model [51], but nonlinear when a Newtonian peripheral layer exists adjacent to the tube wall [6]. In the finite tube homogenous lubrication theory model, the relationship ΔP and \bar{Q} is given below. When an integral number of waves exists in the tube, the pumping performance is that of the infinite tube model.

The trajectories of fluid particles are obtained by carefully integrating particle velocity in time using second-order quadrature. Local wall shear stress at $r = H$ is given as

$$\tau_w(x,t) = \frac{\partial U}{\partial r} = \frac{1}{2} \frac{\partial P}{\partial x} H \quad (3.24)$$

How volume flow rate, $Q(x,t)$, depends on the characteristics of the peristaltic pump. For a periodic train of peristaltic waves moving at a constant speed, flow rate is given by

$$Q(x,t) = 2 \int_0^H U r dr = -\frac{1}{8} \frac{\partial P}{\partial x} H^4. \quad (3.25)$$

Pumping performance is characterized by the relationship between a time-averaged volume flow rate,

$$\bar{Q} = \frac{1}{t_1} \int_{t_0}^{t_0+t_1} Q(x, t) dt,$$

and the pressure difference between the ends of the tube. With periodic train wave peristaltic pumps, the average volume flow rate \bar{Q} is defined over a single wave period, $t_1 = 1$. In this case, the average volume flow rate \bar{Q} is independent of t_0 and x . With single wave transport, however, the average is taken over the time that the wave travels the length of the tube, $t_1 = \frac{L}{\lambda}$, and $\bar{Q}(x)$ depends on the position in the

tube there the average is taken. The relationship between \bar{Q} and ΔP is obtained as follow

$$\bar{Q} = \bar{Q}_0 \left(1 - \frac{\Delta P}{\Delta P_0} \right), \quad (3.26)$$

where

$$\bar{Q}_0 = \frac{2}{t_1} \int_0^{t_1} \frac{\int_0^L H^{-4}(s_1, t) \left(\int_x^{s_1} H(s_2, t) \frac{\partial H(s_2, t)}{\partial t} ds_2 \right) ds_1}{\int_0^L H^{-4}(s, t) ds} dt \quad (3.27)$$

$$\Delta P_0 = 8 \bar{Q}_0 \left[\frac{1}{t_1} \int_0^{t_1} \frac{dt}{\int_0^L H^{-4} dx} \right]^{-1} \quad (3.28)$$

\bar{Q}_0 is the 'maximal' flow rate at x , the averaged flow rate when $\Delta P = 0$. ΔP_0 is the pressure difference required to maintain zero net flow rate at x .

In the infinite tube model \bar{Q} is invariant with the axial position where the time average is carried out. In the infinite model, the average volume flow rate \bar{Q} is, generally dependent on axial position x . However, if the peristaltic waves are periodic in $x(H(x,t) = H(x-t))$, the average volume flow rate may be shown to be independent of x regardless of L/λ .

3.10 Comparison of Single Peristaltic Waves with Train Waves

3.10.1 Particle trajectory and reflux

‘Reflux’ here refers to the presence of fluid particles that move, on average, in a direction opposite to that of the peristaltic wave. The phenomenon was first elucidated by Shapiro et al [51] where it was found, in the infinite tube model, that particle reflux occurs under conditions of partial occlusion and adverse net pressure difference across one wavelength. Brasseur et al [6] found that the existence of a peripheral layer of fluid with different viscosity strongly influences the extent and degree of particle reflux. Only periodic waves in infinitely long tubes were considered in these studies. The effect of wave shape, non-integral numbers of peristaltic waves in the tube, and the differences between single and train wave peristaltic transport in the backward migration of fluid particles are studied in this section.

The basic geometry of single wave peristaltic transport was illustrated in figure 3.1. To study the effects of wave shape, the sinusoidal wave shape of (3.16) is compared with the ‘tear-drop’ shape shown in figure 3.12, which is a more realistic model of bolus geometry in the esophagus and other physiological systems. Particle trajectories of the following four cases are compared in figure 3.13 when an adverse pressure head is placed across the tube: (a) a single sinusoidal peristaltic wave, (b) train waves with sinusoidal shape and (c) train waves with a tear-drop shape, where $L/\lambda = 5$ in all three cases; and (d) train waves with a sinusoidal shape but with a non-integral number of waves in the tube. All other conditions – fluid volume per wave, tube occlusion and length, wave speed, adverse pressure difference, fluid

viscosity, and the initial positions of the fluid particles – are the same in the four calculations. The single bolus case begins with the bolus centrally located in the tube. In all cases the trajectories of eight fluid particles are calculated, where the particles are initially placed on both sides of the peristaltic wave at the most highly occluded point as shown in figure 3.13. The fluid particle trajectories are shown in figure 3.13 over three wave periods. Note that the radial scale has been highly stretched relative to the axial scale in these figures to better observe the radial motions of the fluid particles.

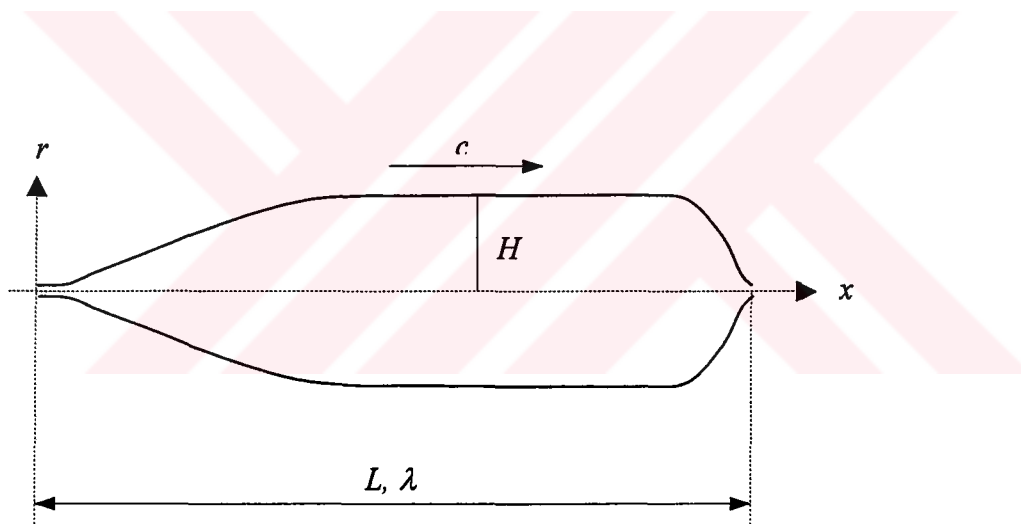


Figure 3.12. A single contraction wave which has 'tear drop' shape. Similar as in the figure 3.1, the fluid bolus is transported from left to right against a pressure difference by peristaltic contraction wave along the tube.

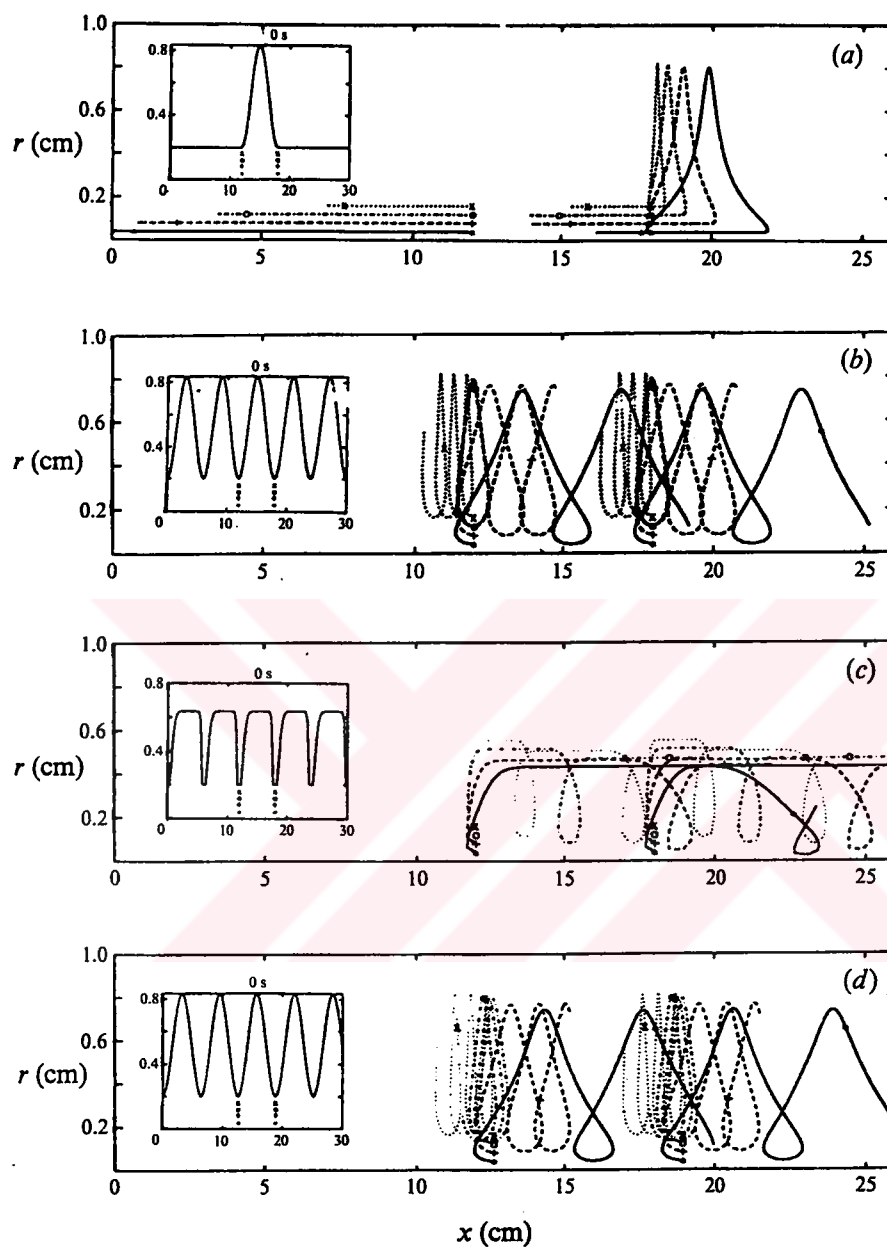


Figure 3.13. Trajectories of fluid particles for different cases of peristaltic transport: (a) a single sinusoidal wave ($L/\lambda = 5$); (b) train of sinusoidal waves with integral $L/\lambda = 5$; (c) train of sinusoidal waves with non-integral $L/\lambda = 4.76$. In all calculations a non-dimensional adverse pressure difference of 18.85 was applied across the tube. Initially the fluid particles are located at $x = 12$ and 18 cm. $\varepsilon/a = 0.354$ in all cases.

Figure 3.13(b) is the classical case of periodic sinusoidal wave contractions in an infinite tube with adverse pressure head. Whereas most of the fluid particles move, on average, in the direction of the peristaltic wave, the fluid particles nearest to the wall of the tube migrate in the opposite direction. Shapiro et al [51] found that the thickness of the region near the wall in which reflux occurs, and the relative flow rate in the reflux region, are strongly dependent on the degree of occlusion and the magnitude of the adverse pressure difference across the end of the pump. Comparison between figures 3.13(b) and 3.13(c) suggests that reflux is also strongly affected by the shape of the peristalsis wave. None of the fluid particles in figure 3.13(b) with 3.13(d) indicates that only minimal differences exist between non-integral and integral numbers of peristaltic waves in the tube.

The most interesting observation from figure 3.13 is in the comparison of particle motions between the single peristaltic wave of figure 3.13(a), and the train waves of figures 3.13(b) and 3.13(d). Whereas in figures 3.13(b) and 3.13(d) only the fluid particles closest to the tube wall move in a direction opposite to the peristaltic wave, in the single bolus case all fluid particles initially in the occlusion zone ultimately move to positions to the left of their starting point during the time that the wave has traveled through the tube outlet. It is found that, in general, significantly more fluid particle reflux occurs with single waves than with corresponding train wave peristaltic transport during the same time period, and that the distance over which the refluxed particles migrate is much greater with single waves.

The observations above are further quantified in figure 3.14 where the trajectories of 451 particles, initially distributed over 41 uniformly spaced cross-sectional areas within the tube, are shown. In each of these cross-sections 11 particles are evenly spaced from the wall to the tube centre at the initial time. In the single wave case, the peristaltic wave, initially located in the middle on the tube, passes the tube exit after three wave periods. The locations of each fluid particle relative to its starting point are recorded in all cases after three wave periods. Figure 3.14 shows the normalized distributions of relative particle motion for the four cases on figure 3.13.

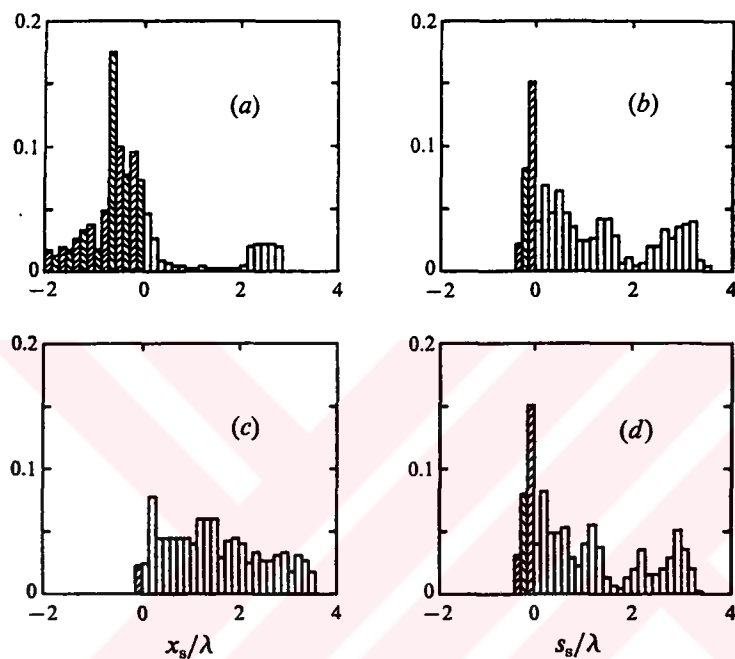


Figure 3.14. Distributions of the distance that fluid particles travel relative to their initial positions for the four cases of figure 3.13. The abscissa is the distance a particle has traveled, non-dimensionalized with the wavelength, after the three wave periods. The distributions are normalized to unity. In all cases, a non-dimensional adverse pressure difference of 18.85 was applied across the tube ends, and the trajectories of 451 particles are calculated. At the initial time, the 451 particles are distributed at 41 uniformly spaced cross sections, in each of which 11 particles are evenly placed from the wall to centre of the tube. The hatched bars correspond to refluxed particles. Single wave peristaltic transport leads to substantially greater reflux than train wave peristaltic transport. $\varepsilon/a = 0.354$ in all cases.

It is immediately apparent from figure 3.14 that single wave peristaltic transport (figure 3.14a) leads to substantially greater reflux than train wave peristaltic transport (figure 3.14b). In fact, 77% of the fluid particles migrated to a position to the left of where they started with single wave transport, whereas only 26% migrated to the left with periodic sinusoidal peristaltic waves over three wave periods. Consistent with the observations of figure 3.13, there is relatively little difference in the distributions of fluid particles between integral and non-integral numbers of peristaltic waves in the tube. On the other hand, tear-drop shaped peristaltic waves (figure 3.14c) are considerably more effective in resisting particle reflux and enhancing forward motion of fluid particles than sinusoidal peristaltic waves (figure 3.14b). Only 2% of the 451 fluid particles moved in a retrograde direction with the tear-drop wave shape, as compared with 26% with sinusoidal peristaltic waves.

It is interesting to note one fundamental difference between cases with integral and non-integral numbers of peristaltic waves. We observed in discussing figure 3.13(b) that particles near the wall tend to move against the peristaltic wave, whereas particles near the centre of the tube move with the peristaltic wave. Between these two regions lie fluid particles which do not move in either direction, but move around closed loops. For example, the particles indicated with symbol O in figure 3.13(b) are following such closed paths. No closed paths exist, however, when a non-integral number of waves occupy the tube. This is because the flow is inherently non-steady when L/λ is non-integral in all frames of reference, and periodic fluid motions do not occur. However, the global differences between integral and non-integral numbers of train waves are relatively minor, as observed by comparing 3.14(b) and 3.14(d).

3.10.2 Net loss of refluxed fluid from the tube inlet

In the classical train wave model, reflux can occur with an adverse pressure difference across the tube. Consequently, net retrograde flow is caused by a pressure-driven component induced by the net increase in pressure along the peristaltic pump. Fluid continually leaves the tube inlet during single wave peristaltic transport.

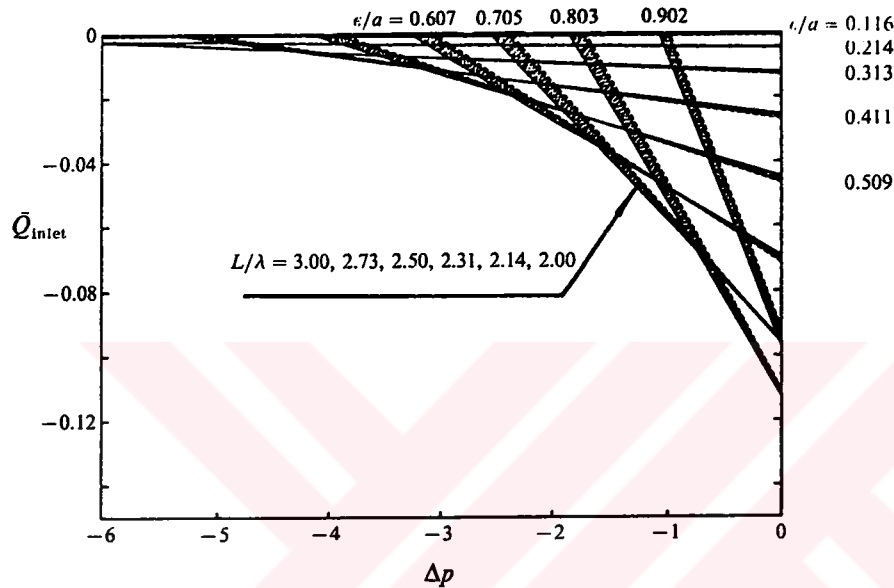


Figure 3.15. Pressure-volume flow rate characteristics of single wave peristaltic transport with different relative tube occlusion ϵ/a and different tube-to-wave lengths L/λ . The average volume flow rate at the tube inlet \bar{Q}_{inlet} is plotted against pressure difference $\Delta P = P_L - P_0$ in groups for different ϵ/a , where L/λ is varied within each group from 3 to 2 in the direction indicated by the arrow. A negative value of volume flow rate \bar{Q}_{inlet} implies fluid reflux from the tube inlet.

To quantify the net loss of fluid from the tube in single bolus peristaltic transport, we average the volume flow rate at the inlet of the tube over the time that the peristaltic wave travels from the inlet to the outlet of the tube. In figure 3.15 the average flow rate leaving the inlet, $\bar{Q}_{inlet} < 0$, is plotted against a favourable pressure difference between the outlet and inlet of the tube. Groups of curves with fixed ε/a but different L/λ are given, showing that the influence of L/λ on flow rate is much weaker than the influence of ε/a . A number of interesting observations can be made from figure 3.15. Net fluid reflux takes place in the presence of a favourable pressure gradient. Indeed, a favourable pressure gradient is required to prevent reflux from the inlet to the tube. This circumstance is very different from the classical train wave model where no reflux occurs unless an adverse pressure difference exists across the tube ends. Note from figure 3.15 that loss of fluid from the inlet of the pump cannot be prevented when $\Delta P = 0$.

Note that, as the level of occlusion increases, the magnitude of the favourable pressure difference required to prevent reflux from occurring increases, although the amount of the reflux at fixed ΔP eventually becomes small for small enough ε/a . An interesting observation from figure 3.15 is that, for fixed negative pressure difference ΔP , the level of refluxed fluid does not diminish monotonically with decreasing ε/a . In figure 3.16 \bar{Q}_{inlet} is plotted against ε/a for different fixed pressure difference ΔP . Observe that, at fixed ΔP , a critical occlusion exist at which the magnitude of refluxed fluid from the inlet to the tube is maximal. This critical occlusion shifts to smaller ε/a as the favourable pressure difference increases. Only as ε/a approaches 0 (complete occlusion) or 1 (no peristalsis) does reflux of fluid from the pump cease when $\Delta P = 0$.

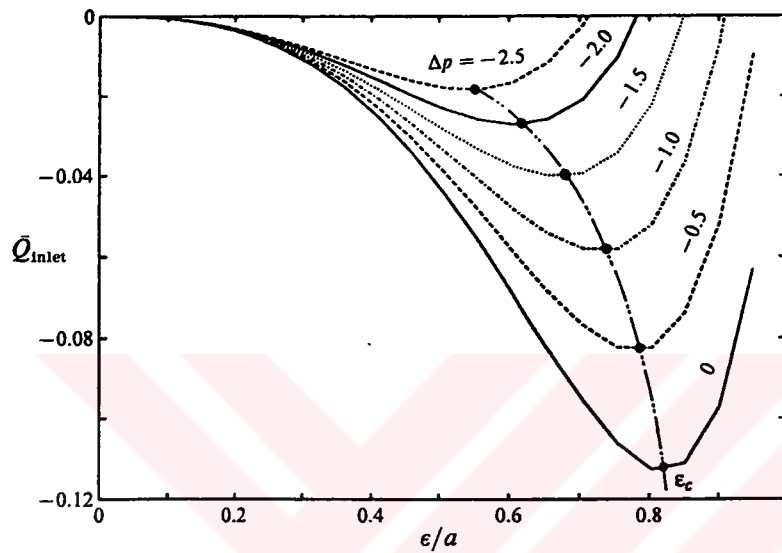


Figure 3.16. Average volume flow rate at the tube inlet \bar{Q}_{inlet} as a function of tube occlusion ε/a for fixed favourable pressure difference ΔP . A negative value of volume flow rate \bar{Q}_{inlet} implies fluid reflux at the inlet. At fixed ΔP a critical occlusion ε_c exists at which the amount of refluxed fluid from the inlet to the tube reaches a maximum. This critical occlusion shifts to smaller ε/a as the favourable pressure difference increases.

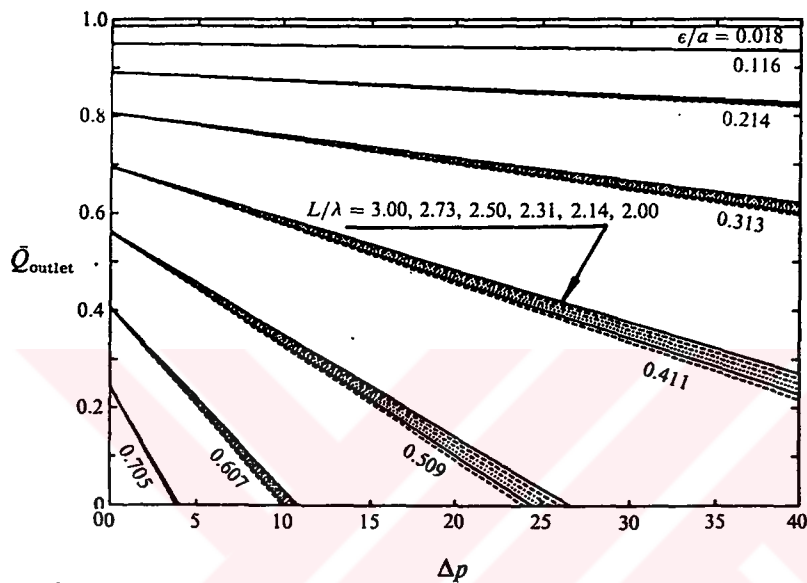


Figure 3.17. Pressure-volume flow rate characteristics of single wave peristaltic transport with different relative tube occlusions ϵ/a and different tube-to-wave lengths L/λ . The average volume flow rate at the tube outlet \bar{Q}_{outlet} is plotted against pressure difference $\Delta P = P_L - P_0$ in groups for different ϵ/a , where L/λ is varied within each group from 3 to 2 in the direction indicated by the arrow.

3.10.3 Pumping performance in single wave peristaltic transport

The pumping performance of single wave peristaltic transport is shown in figure 3.17, where ΔP is plotted against \bar{Q}_{outlet} in different groups of fixed ε/a , L/λ is varied between 2 and 3 within each group. Note that \bar{Q}_{outlet} and \bar{Q}_{inlet} are averages over the period that the wave travels from the tube inlet to the tube outlet, and that during this period the fluid volume in the tube changes.

Pumping performance with single waves is qualitatively similar to that with train waves. With single waves, however, the ‘maximal’ flow rate \bar{Q}_0 is slightly less than with train waves, whereas the pressure difference required to maintain zero net flow rate is significantly greater than with train-wave peristaltic transport. Note also that pumping performance continuously increases with increasing L/λ ; this is not the case in the train-wave peristaltic transport.

CHAPTER 4. PREDICTION OF THE WALL GEOMETRY

We developed a numerical model in previous chapter, which gives us ability to calculate muscle tension from known wall geometry. As mentioned earlier, two different data can be recorded in the human esophagus; manometry and radiography. Manometry provides information about pressure signature, however, radiography provides information about bolus shape (wall geometry). There are lots of difficulties to interpret esophageal functions by looking only one of the recorded data. Some information may be obtained from each data alone, but it is also difficult to decide if the interpreted data is true. The best method to obtain esophageal function is to combine manometry and radiography.

Because of esophageal bolus transport is inherently mechanical in nature, basic principles of mechanics underlie descriptions of the process by which a fluid bolus is transported from the pharynx to the stomach. These principles may be used to advantage in the analysis and characterization of esophageal function and esophageal dysfunction. Li et al [33] have studied the relationship between muscle squeeze, parameterized by axial variations in intraluminal pressure, and the deformation characteristics of the esophageal wall. Because manometric data are obtained at fixed spatial locations within the esophagus and videofluoroscopic data at fixed points in time, they have sought a methodology with sufficient spatial and temporal resolution to allow axial variations in pressure to be related in detail to axial variations in luminal geometry. The methodology involves combining mathematical modeling with biological data. The concept is to embed the essential dynamical principles required to properly characterize esophageal bolus transport into a mathematical model from which intraluminal geometry variations may be directly related to intraluminal pressure variations.



Figure 4.1. Raw radiographic image plotted along with the spatial distribution of intraluminal pressure. Pressure distribution is shown with the solid line. The scale is shown in the right corner of the image as mmHg. Horizontal dotted line represents bolus tail and corresponding intraluminal pressure.

Figure 4.1 illustrates raw radiographic image and intraluminal pressure distribution along the esophagus. Solid line represents intraluminal pressure distribution. Horizontal dotted lines corresponding of bolus tail and pressure value at this point.

Dodds et al [14] radiographically recorded the motion of tantalum wires inserted into feline esophageal longitudinal muscle in response to secondary peristalsis. Their results are shown in figure 4.2. Upon bolus injection in the proximal esophagus, markers first moved proximally as the bolus head passed over the marker, then distally just before the arrival of the circular muscle contraction wave, passing through their rest position near the time of peak intraluminal pressure. The marker continued to move distally before returning proximally to its rest position well after the passage of the tail.

Nicosia [40] has studied the estimation of active and passive components of human esophageal muscle tension during swallowing. For this purpose, the geometry of the deformed esophageal wall has computed to calculate stresses within the esophageal wall. Because the esophagus undergoes large deformations during swallowing, this calculation is non-trivial. Classical large deformation solutions exist for simple geometries, such as straight walled circular cylinder, a model which was recently extended by Humphrey and Yin [25] in a large deformation analysis of the heart. The geometry was still specified as a straight walled circular circular cylinder but the deformation included both radial variations in torsion and the influence of muscle fibers. Nicosia [40] has employed a relaxed Kirchhoff-type hypothesis in which normals to the undeformed reference surface remain on a straight line which is not necessarily normal to the deformed reference surface. The angle, which the deformed normal makes with the reference surface, has computed based on a balance of forces at the inner wall. Nicosia has also studied the affect of elastic strains have on the computed circular muscle tension. Although some of these elastic effects are absorbed into the parameterization of passive muscle elasticity, shear stress terms arising through curvature changes still remain.

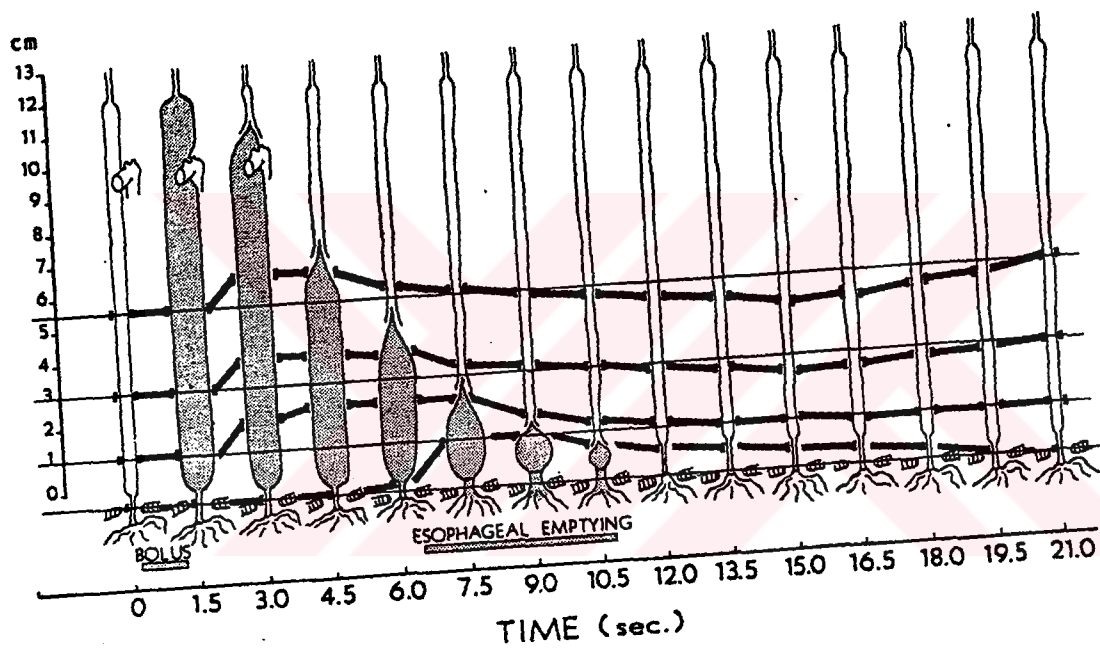


Figure 4.2. Schematic of the axial motion of tantalum markers attached to the feline esophageal wall in response to secondary peristalsis [14].

4.1 Numerical Method

To calculate bolus geometry along the esophagus from known tension in the muscle wall, we developed a fully explicit finite difference method based on numerical model, which is developed in chapter 3. The model was an application of finite difference scheme on the combined form of the lubrication theory approximations and Laplace equation.

The method is restricted to sinusoidal peristaltic deformations of the tube wall. The mathematics, however, can be applied more generally to arbitrary (but still periodic) peristaltic wave shapes. Because the motions of the wall are related directly to the tension within the fluid, the theory may be applied to study the relationship between the deformations of the esophageal wall as recorded radiographically and the intrabolus pressure as measured manometrically during bolus transport. Normal esophageal peristalsis involves a single wave of active muscle contraction preceded by a single wave of muscle relaxation. Because the theory requires periodic peristaltic waves, the bolus shall be isolated within a single peristaltic wave, with both extremities having the same degree of occlusion.

Finite difference schemes of first and second derivative terms were given in previous chapter. Equation (3.20) is changed as follow

$$H_i^{j+1} = H_i^j + \frac{\Delta t}{\mu} \left\{ \begin{array}{l} -\frac{A_0}{192\Delta x^2} H_i^j T_{i-2}^j + \frac{A_0}{12\Delta x^2} H_i^j T_{i-1}^j + \\ \frac{A_0}{96\Delta x^2} \left(H_{i-2}^j - 16H_{i-1}^j + 15H_i^j - 16H_{i+1}^j + H_{i+2}^j - \frac{(H_{i+1}^j - H_{i-1}^j)^2}{3H_i^j} \right) T_i^j + \\ \frac{A_0}{12\Delta x^2} H_i^j T_{i+1}^j - \frac{A_0}{192\Delta x^2} H_i^j T_{i+2}^j \end{array} \right\}$$

(4.1)

First derivative of H according to time includes $j+1$, when its finite difference scheme is written. We applied fully explicit finite difference method to calculate wall geometry for next time step when the proper initial conditions (boundary conditions) are given.

4.2 Results

Calculations are performed for different ε/a . Bolus volume is calculated for every time step. Following equation is applied to calculate bolus volume

$$V = \pi\lambda a^2. \quad (4.2)$$

In figures 4.3, 4.5, 4.7, 4.9 and 4.11, predicted wall geometries (bolus shapes) are shown and compared with analytic wall geometries. However, figures 4.4, 4.6, 4.8, 4.10 and 4.12 show volume change and comparison with original bolus volume. Because of time dependent solution is obtained in this section, small error at the beginning increase in next time steps. Therefore, final error is sum of the errors during calculation.

Convergence of the numerical solution to the analytic solution is very good at initial time steps. While time increases, error gets larger. Therefore, convergence gets worse a little. Figure 4.3 shows calculation for $\varepsilon/a = 0.1$, which is the largest occlusion rate in this section. Larger occlusion rate presumably gives better solution according with smaller occlusion rate. Our results confirm this hypothesis.

Figure 4.4 shows volume as a function of time. Volume from the numerical calculation should remain constant as dotted line. Because of the error in the calculation, there is some fluctuation on volume. As seen in figure, volume almost stays constant till $t=0.3$ s, then small fluctuation exists between $t=0.3 - 0.6$ s. After $t=0.6$ s, there is large error on volume.

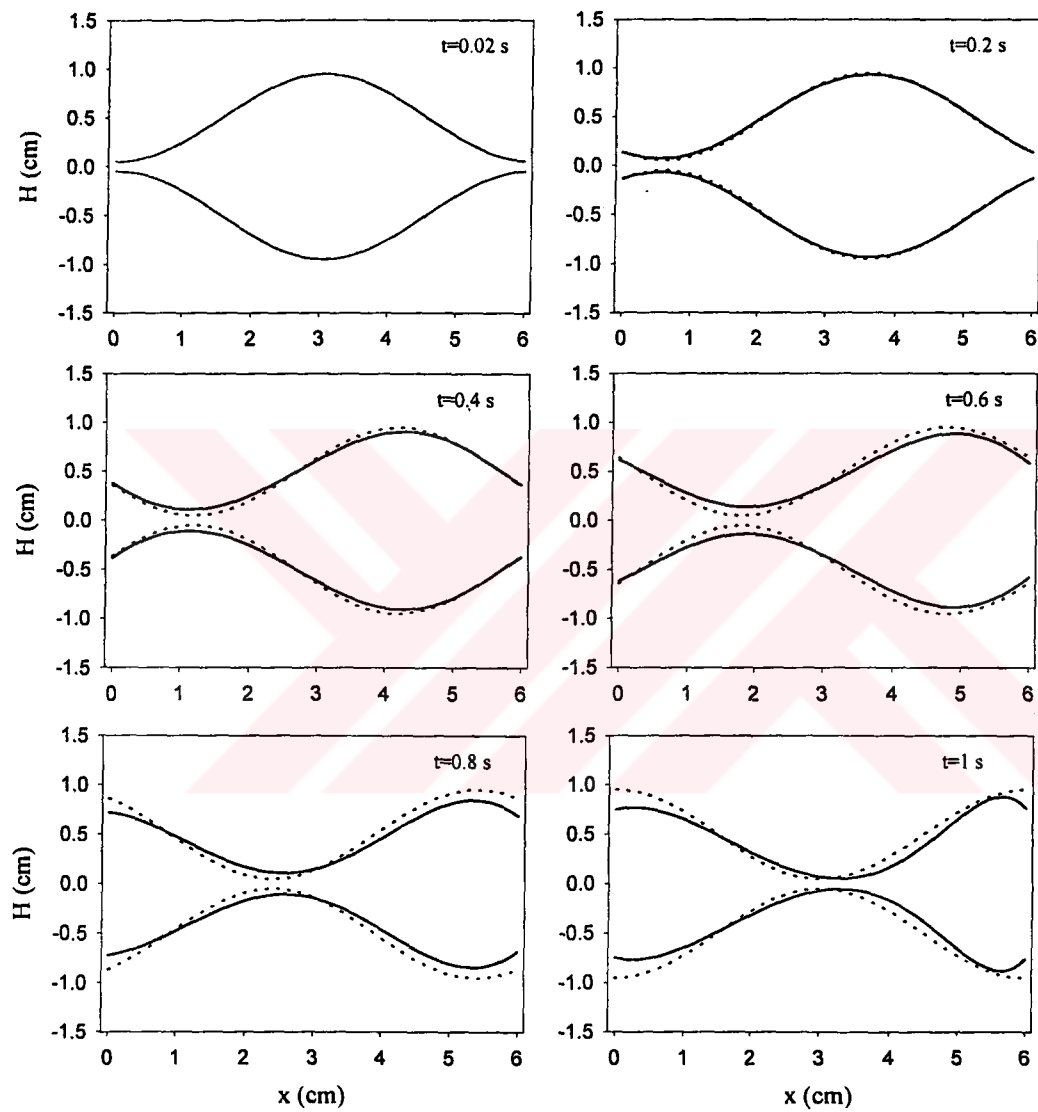


Figure 4.3. Comparison of predicted bolus shape with analytic bolus shape for different time steps. Solid and dotted lines represent predicted and analytic bolus shape, respectively. Here, $\varepsilon/a = 0.1$, $c=3$ cm/s and $\lambda = L = 6$ cm.

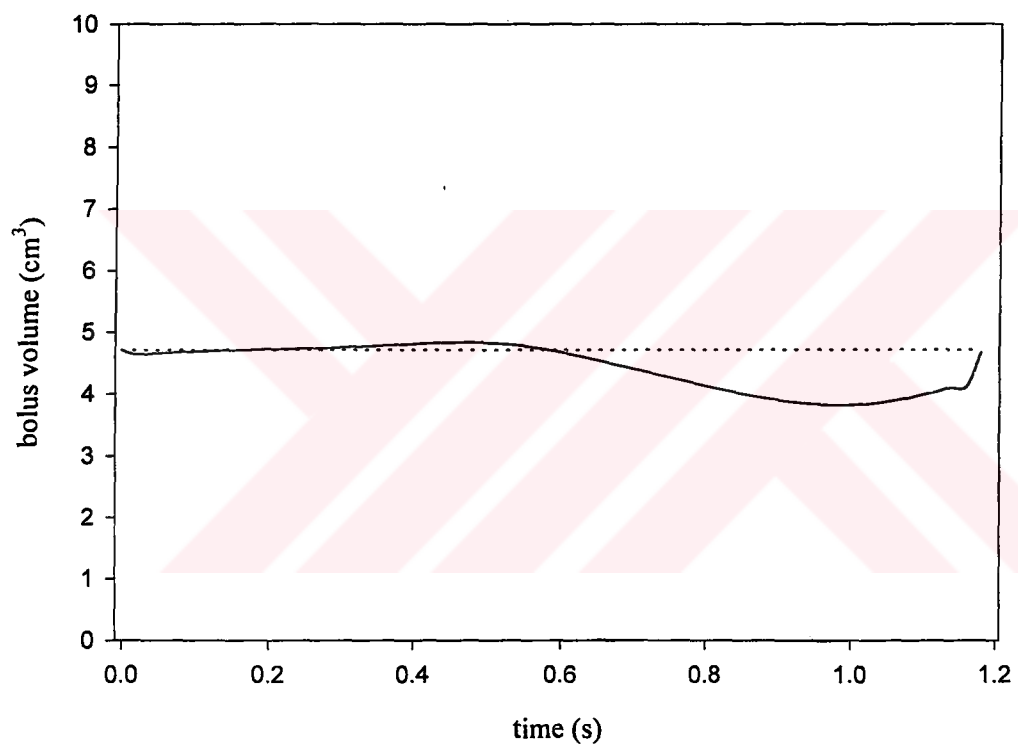


Figure 4.4. Variation of bolus volume, which is obtained from calculations as seen in figure 4.3, is shown in time. Dotted and solid lines represent calculated and analytic bolus volume.

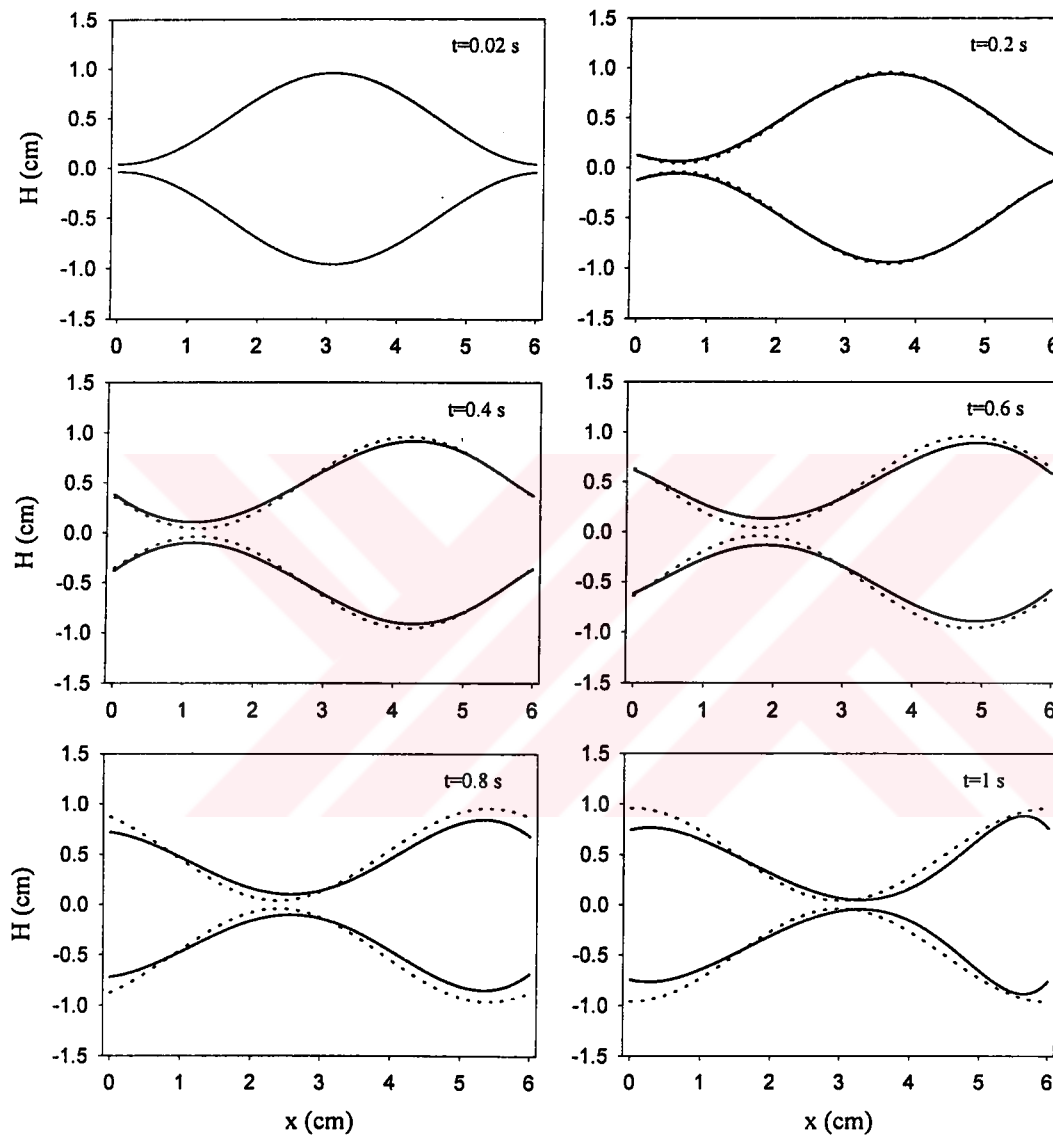


Figure 4.5. Similar to figure 4.3, comparison of predicted bolus shape with analytic bolus shape for different time steps. Solid and dotted lines represent predicted and analytic bolus shape, respectively. Here, $\varepsilon/a = 0.08$, $c=3$ cm/s and $\lambda = L = 6$ cm.

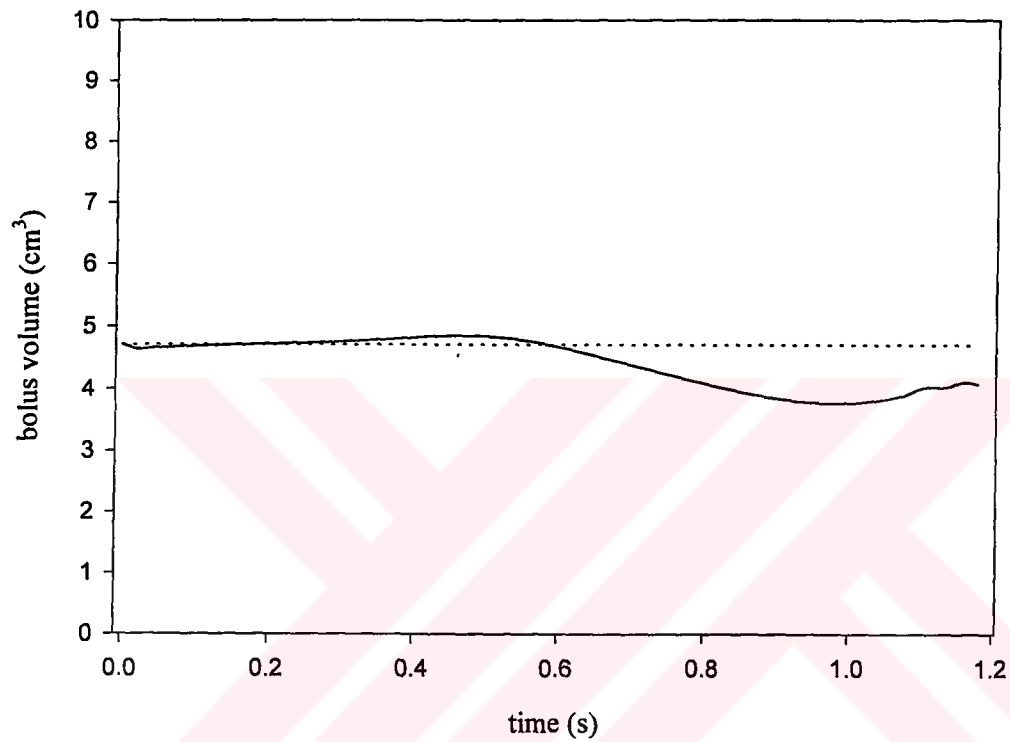


Figure 4.6. Similar to figure 4.4, variation of bolus volume, which is obtained from calculations as seen in figure 4.5, is shown in time. Dotted and solid lines represent calculated and analytic bolus volume.

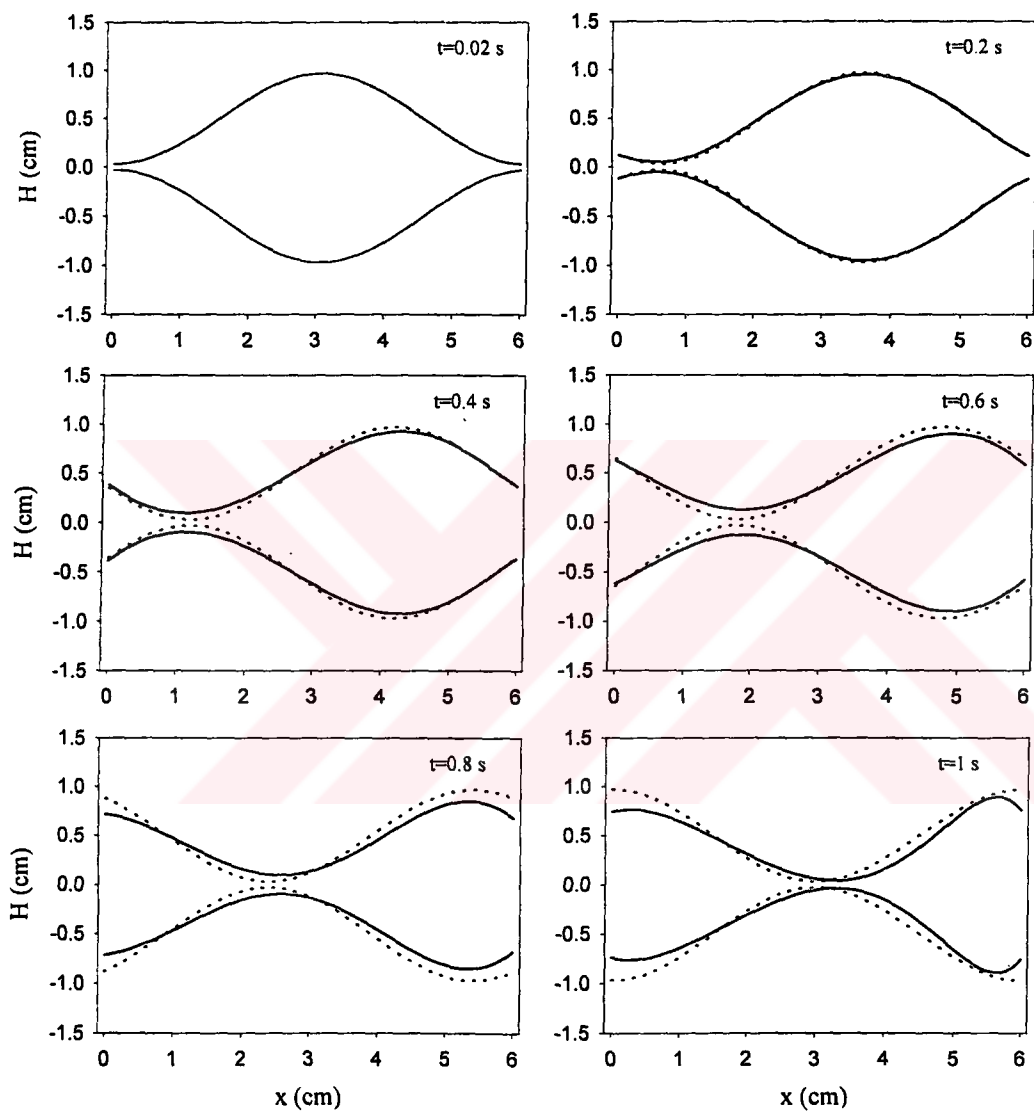


Figure 4.7. Similar to figure 4.3, comparison of predicted bolus shape with analytic bolus shape for different time steps. Solid and dotted lines represent predicted and analytic bolus shape, respectively. Here, $\varepsilon/a = 0.06$, $c=3$ cm/s and $\lambda = L = 6$ cm.

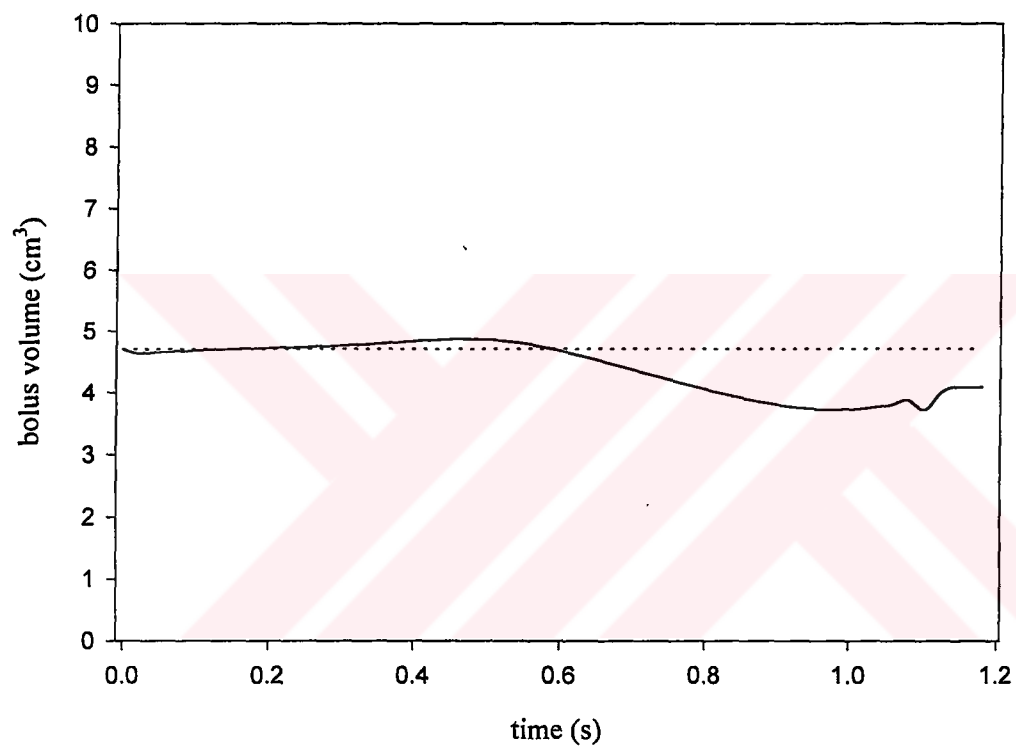


Figure 4.8. Similar to figure 4.4, variation of bolus volume, which is obtained from calculations as seen in figure 4.7, is shown in time. Dotted and solid lines represent calculated and analytic bolus volume.

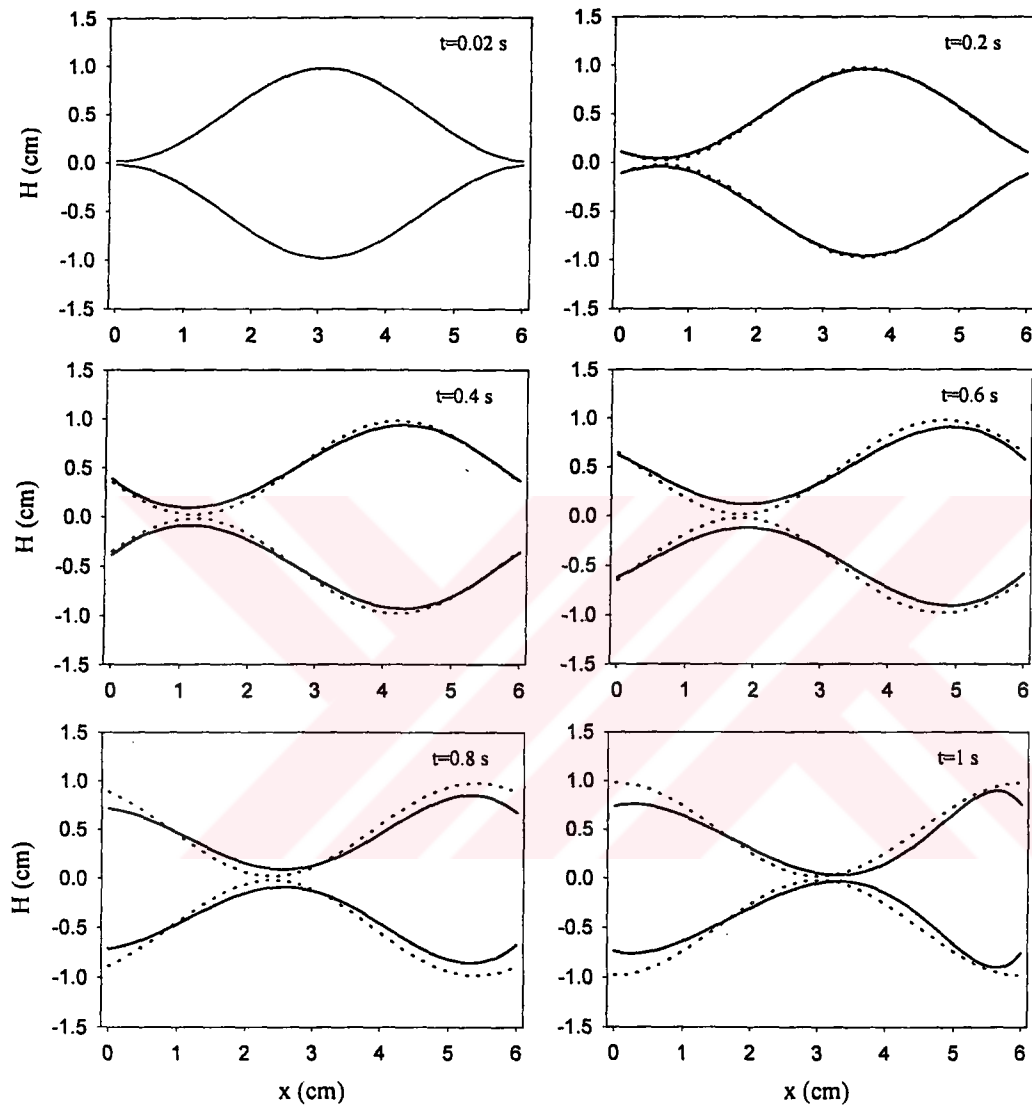


Figure 4.9. Similar to figure 4.3, comparison of predicted bolus shape with analytic bolus shape for different time steps. Solid and dotted lines represent predicted and analytic bolus shape, respectively. Here, $\varepsilon/a = 0.04$, $c=3$ cm/s and $\lambda = L = 6$ cm.

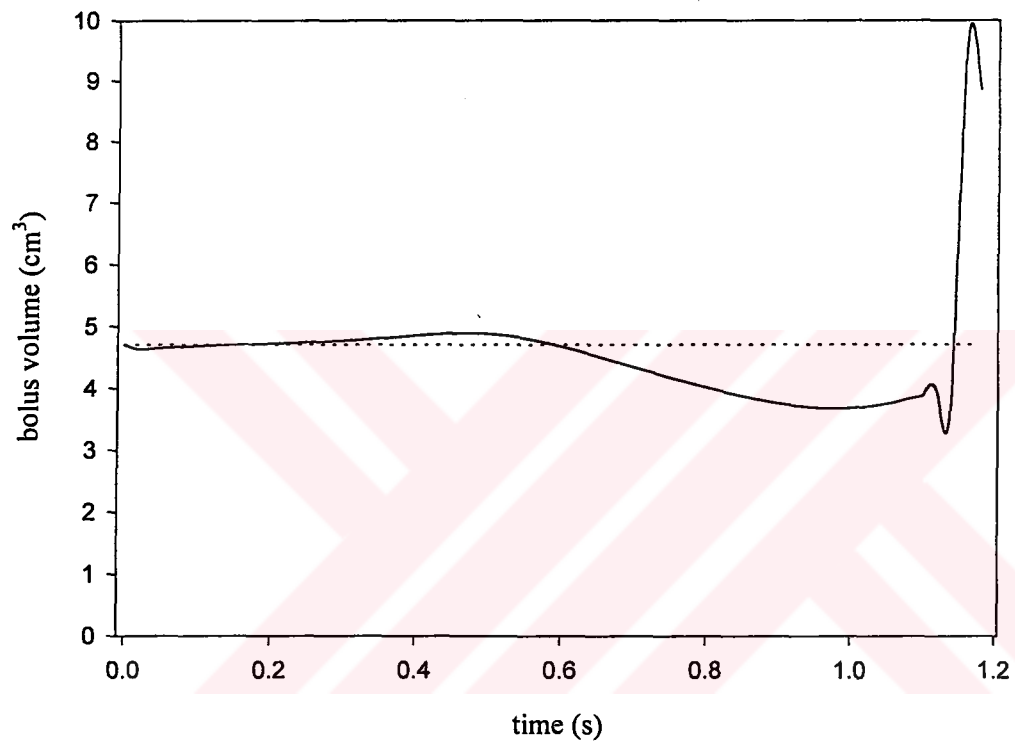


Figure 4.10. Similar to figure 4.4, variation of bolus volume, which is obtained from calculations as seen in figure 4.9, is shown in time. Dotted and solid lines represent calculated and analytic bolus volume.

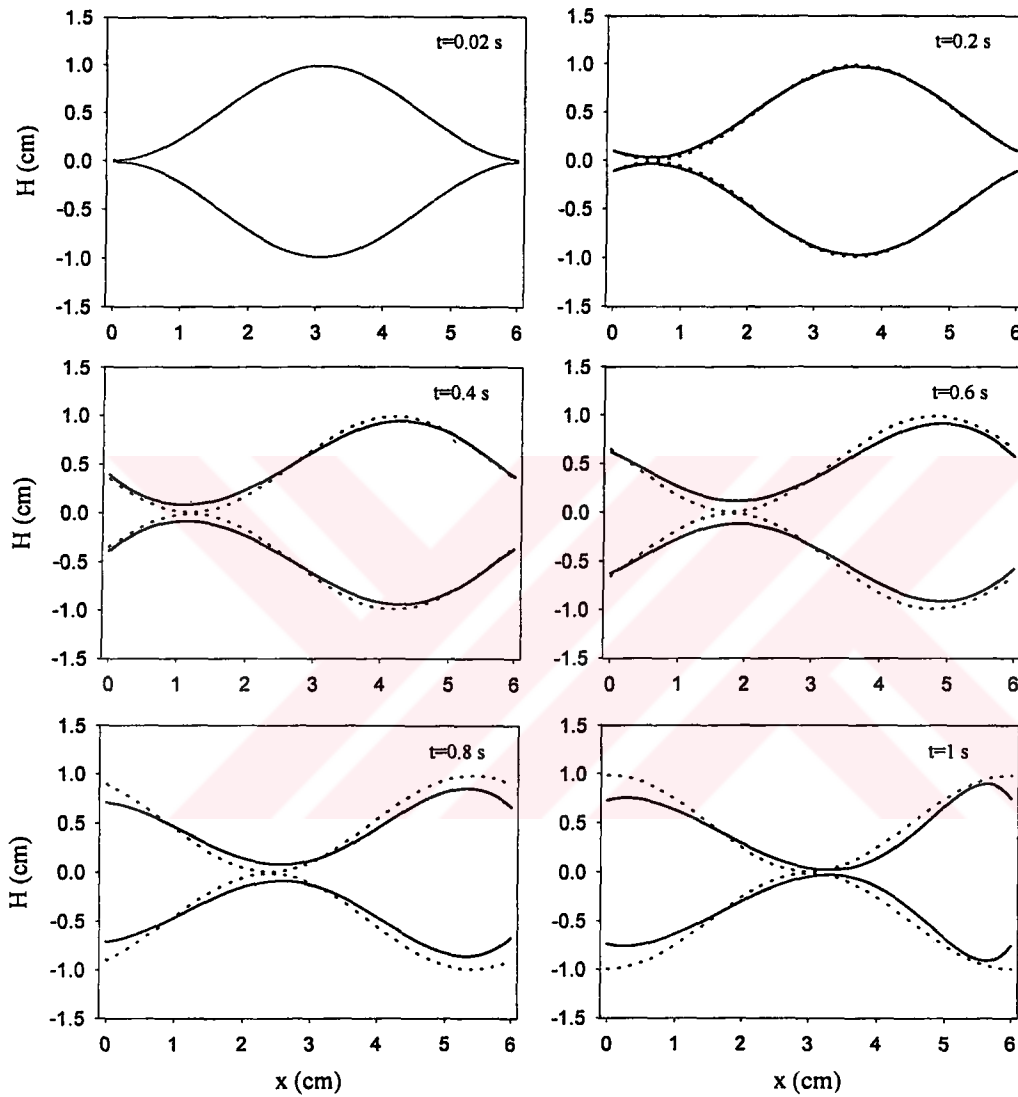


Figure 4.11. Similar to figure 4.3, comparison of predicted bolus shape with analytic bolus shape for different time steps. Solid and dotted lines represent predicted and analytic bolus shape, respectively. Here, $\varepsilon/a = 0.02$, $c=3$ cm/s and $\lambda = L = 6$ cm.

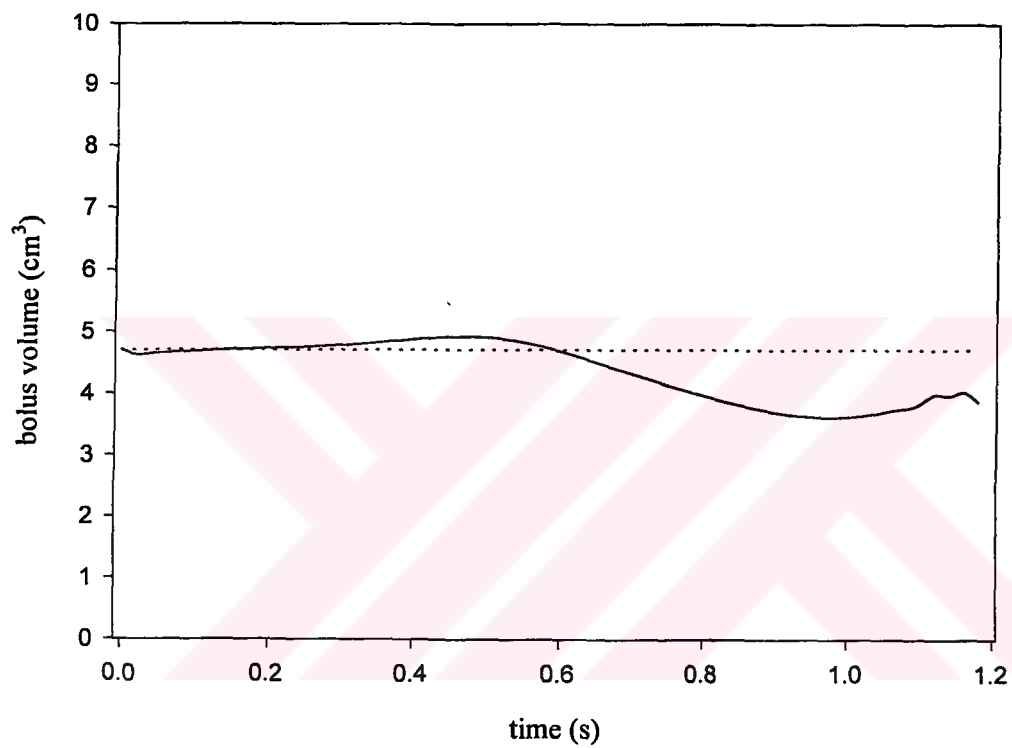


Figure 4.12. Similar to figure 4.4, variation of bolus volume, which is obtained from calculations as seen in figure 4.11, is shown in time. Dotted and solid lines represent calculated and analytic bolus volume.

Effects of ε/a on calculation and volume change are seen following figures. Variation on the wall geometries for different calculations are similar each other, but variation on the volumes are different from each other. The biggest difference appear in $\varepsilon/a = 0.04$.



CHAPTER 5. CONCLUSIONS

Underlying this thesis is the application of basic mechanical principles to the analysis of biological data in studying the physiology of human swallowing. Although swallowing is seemingly simple process, there are complex interactions between esophageal muscle, the nerves which signal them to contract and the resulting esophageal deformations which occur to successfully transport a bolus to stomach. We have utilized two different diagnostic modalities, which are used to study esophageal motility in both clinical and research settings; concurrent manometry and videofluoroscopy.

Temporal and spatial change of intraluminal pressure in the esophagus during normal human swallowing were recorded using a catheter. Intraluminal pressure alone gives some information about swallowing process. We analyzed intraluminal pressure to interpret esophageal functions in the absence of radiography. We found from these analyses that several sub-pressure waves and segments appear along the esophagus during swallowing. Locations and lengths of each sub-pressure waves and segments are almost same in the esophagus. Average magnitude of pressure along the each sub-pressure wave and segment show similar behavior. Location of the pressure trough is more-or-less same in the esophagus for different swallowing of each subject. Our findings confirm existing existing of more than one pressure through along the esophagus. We obtained 3 pressure troughs on a subject and 2 on other subjects.

We developed a numerical model to combine fluid mechanics with solid mechanics. Tension in the muscle wall of the esophagus can be calculated using this numerical model. Lubrication theory approximation and Laplace equation are combined to obtain the numerical model. The equation is solved using finite difference

approximation. It is found that we are able to calculate tension in the muscle wall from known wall geometry.

Prediction of the wall geometry from known tension is an important problem, which we solved in this study. To predict wall geometry in the absence of radiography helps us to interpret esophageal functions correctly. We applied a numerical method to calculate wall geometry, and wall geometry is calculated successfully.

In summary, this thesis has studied the physiology of human swallowing through an engineer's eyes. Only through the true marriage of basic engineering principles with physiology were these analyses possible.



REFERENCES

- [1] ABERG, A.K. and AXELSSON, J., "Some Mechanical Aspects of Intestinal Smooth Muscle", *Acta. Physiol. Scand.*, v. 64, pp. 15-27, 1965.
- [2] BIANCANI, P., ZABINSKI, M.P. and BEHAR, J., "Pressure, tension and force of closure of the Human Lower Esophageal Sphincter and Esophagus", *J. Clin. Invest.*, v. 56, pp. 476-483, 1975.
- [3] BIANCANI, P., ZABINSKI, M.P., KERSTEIN, M. and BEHAR, J., "Lower Esophageal Sphincter Mechanics: Anatomic and Physiologic Relationships of the esophagogastric Junction of Cat", *Gastroenterology*, v. 82, pp. 468-475, 1982.
- [4] BOHME, G.B. and FRIEDRICH, R., "Peristaltic Flow of Viscoelastic Liquids", *J. Fluid Mech.*, v. 128, pp. 109-122, 1983.
- [5] BRASSEUR, J.G., "Mechanical Studies of the Esophageal Function", *Dysphagia*, v. 8, pp. 384-386, 1993.
- [6] BRASSEUR, J.G., CORRSIN, S. and LU, N.Q., "The Influence of a Peripheral Layer of Different Viscosity on Peristaltic Pumping with Newtonian Fluid", *J. Fluid Mech.*, v. 174, pp. 495-519, 1987.
- [7] BRASSEUR, J.G. and DODDS, W.J., "Interpretation of Intraluminal Manometric Measurements in Terms of Swallowing Mechanics", *Dysphagia*, v. 6, pp. 100-119, 1991.

- [8] BROWN, T.D. and HUNG, T.K., "Computational and Experimental Investigations of Two-dimensional Nonlinear Peristaltic Flows", *J. Fluid Mech.*, v. 83, pp. 249-272, 1977.
- [9] BURNS, J.C. and PARKES, T., "Peristaltic Motion", *J. Fluid Mechanics*, v. 29, pp. 731-743, 1967.
- [10] CAREW, E.O. and PEDLEY, T.J., "An Active Membrane Model For Peristaltic Pumping: Part I – Periodic Activation Waves in an Infinite Tube", *J. Biomech. Engng.*, v. 119, pp. 66-76, 1997.
- [11] CLOUSE, R.E. and STANIO, A., "Topography of the Esophageal Peristaltic Pressure Wave", *The American J. of Physiol.*, v. 261 (Gastrointest. Liver Physiol. 24), pp. G677-G684, 1991.
- [12] CLOUSE, R.E. and STANIO, A., "Topography of Normal and High-Amplitude Esophageal Peristalsis", *The American J. of Physiol.*, v. 265 (Gastrointest. Liver Physiol. 28), pp. G1098-G1107, 1993.
- [13] CLOUSE, R.E., STANIO, A., BICKSTON, S.J. and COHN, S.M., "Characteristics of Propagating Pressure Wave in the Esophagus", *Digestive Diseases and Sciences.*, v. 41(12), pp. 2369-2376, 1996.
- [14] DODDS, W.J., SREWART, E.T., HODGES, D. and ZBORALSKE, F.F., "Movement of the Feline Esophagus Associated with Respiration and Peristalsis", *J. Clin. Invest.*, v. 52, pp. 1-13, 1972.
- [15] DODDS, W.J., "Current Concepts of Esophageal Motor Function: Clinical Implications For Radiology", *J. of Roentgenology*, v. 128, pp. 549-561, 1977.

- [16] DOOLEY, C.P., SCHLOSSMACHER, B. and JORGE, E.V., "Effect of Alterations in Bolus Viscosity on Esophageal Peristalsis in Humans", *American J. of Physiology*, v. 254, pp. G8-G11, 1988.
- [17] DUSEY, M.P., "Numerical Analysis of Lubrication Theory and Peristaltic Transport in the Esophagus", Ph.D. Thesis, Pennsylvania State University, 1993.
- [18] ECKARDT, V.F., ADAMI, B. and HUCKER, H.H., "The Esophagogastric Junction in Patients with Asymptotic Lower Esophageal Rings", *Gastroenterology*, v. 79, pp. 426-430, 1980.
- [19] EDMUNDOWICZ, S.A. and CLOUSE, R.E., "Shortening of the Esophagus in Response to Swallowing", *Am J Physiol*, v. 260, pp. G512-G516, 1991.
- [20] EKSTROM, J. and UVELIUS, B., "Length-Tension Relations of Smooth Muscle From Normal and Denervated Rat Urinary Bladders", *Acta. Physiol. Scand.*, v. 112, pp. 443-447, 1981.
- [21] FUNG, Y.C. and YIH, C.S., "Peristaltic Transport", *ASME E: J. Applied Mech.*, v. 35, pp. 731-743, 1968.
- [22] GABELLA, G., "The Force Generated by a Visceral Smooth Muscle", *J. of Physiology of London*, v. 263, pp. 199-213, 1976.
- [23] GUYTON, A.C., "Textbook of Medical Physiology", W. B. Saunders Company, Philadelphia, PA, 1991.
- [24] HELSTRAND, P. and JOHANNSSON, B., "The Force Velocity Relation in Phasic Contractions of Venous Smooth Muscle", *Acta. Physiol. Scand.*, v. 93, pp. 157-166, 1975.

- [25] HUMPREY, J.D. and YIN, F.C.P, "Constitutive Relations and Finite Deformations of Passive Cardiac Tissue II: Stress Analysis in the Left Ventricle", *Circ. Res.*, v. 65, pp. 805-817, 1989.
- [26] JAFFRIN, M.Y. and MEGINNISS, J.R., "The Hydrodynamics of Roller Pumps and Their Implication to Hemolysis", Fluid Mechanics Laboratory, Publication No. 71-1, Dept. of Mech. Eng., Massachusetts Institute of Technology, Cambridge, MA, 1971.
- [27] JAFFRIN, M.Y., "Inertia and Streamline Curvature Effects on Peristaltic Pumping", *Int. J. Engng. Sci.*, v. 11, pp. 681-699, 1973.
- [28] KAHRILAS, P.J., DODDS, W.J. and HOGAN, W.J., "Effect of Peristaltic Dysfunction on Esophageal Volume Clearance", *Gastroenterology*, v. 94, pp. 73-80, 1988.
- [29] KAHRILAS, P.J., "Esophageal Motility Disorders: Pathogenesis, Diagnosis, Treatment", In *Evolving Concepts in the Gastrointestinal Motility*, chapter 2, pp. 15-45, Blackwell Science Ltd., Oxford, UK, 1990.
- [30] KAHRILAS, P.J., "Functional Anatomy and Physiology of the Esophagus", In the *Esophagus*, chapter 1, p. 1-27, Little Brown and Co., Boston, MA, 1990.
- [31] LATHAM, T.W., "Fluid Motions in a Peristaltic Pump", MS Thesis, MIT, 1966.
- [32] LI, M. and BRASSEUR, J.G., "Non-steady Peristaltic Transport in Finite-Length Tubes", *J. Fluid Mech.*, v. 248, pp. 129-151, 1993.
- [33] LI, M., BRASEUR, J.G. and DODDS, W.J., "Analyses of Normal and Abnormal Esophageal Transport Using Computer Simulations", *Am J Physiol*, v. 266 (Gastrointest. Liver Physiol. 29), pp. G525-G543, 1994.

- [34] LIRON, N., "On Peristaltic Flow and Its Efficiency", *Bull. Math. Biol.*, v. 38, pp. 573-596, 1976.
- [35] LYKOUKIDIS, P.S. and ROOS, R., "The Fluid Mechanics of the Ureter From a Lubrication Theory Point of View", *J. Fluid Mech.*, v. 43, pp. 661-674, 1970.
- [36] MANTON, M.J., "Long Wavelength Peristaltic Pumping at Low Reynolds Number", *J. Fluid Mech.*, v. 68, pp. 467-476, 1975.
- [37] MEYER, G.W., AUSTIN, R.M., BRADY, C.E. and CASTELL, D.O., "Muscle Anatomy of the Human Esophagus", *J Clin Gastroenterol*, v. 8, pp. 131-134, 1986.
- [38] MITTRA, M.J. and PRASAD, S.N., "Interaction of Peristaltic Motion with Poiseuille Flow", *Bull. Math. Biol.*, v. 36, pp. 127-141, 1974.
- [39] NETTER, F.H., "Diseases of the Esophagus", v. 3 of *The Digestive Tract*. Ciba Pharmaceutical Products, Summit, NJ, 1972.
- [40] NICOSIA, M.A., "Muscle Mechanics and Modeling of the Esophagus During Swallowing", Ph.D. Thesis, Pennsylvania State University, 1997.
- [41] ORVAR, K.B., GREGERSEN, H. and CHRISTENSEN, J., "Biomechanical Characteristics of the Human Esophagus", *Dig. Dis. Sci.*, v. 38(2), pp. 197-205, 1993.
- [42] PAUL, R.J., "Smooth Muscle Mechanochemical Energy Conversion: Relations Between Metabolism and Contractility", In L. R. Johnson, editor, *Physiology of the Gastrointestinal Tract*, chapter 11, pp. 483-506, Raven Press, New York, NY, 1987.
- [43] POZRIKIDIS, C., "A Study of Peristaltic Flow", *J. Fluid Mech.*, v. 180, pp. 515-527, 1987.

- [44] RATH, H.J., "Ein Beitrag zur Berechnung einer Peristaltischen Stromung in Elastischen Leitungen", *Acta Mech.*, v. 31, pp. 1-12, 1978.
- [45] RATH, H.J., "Peristaltic Flow Through a Lobe-Shaped Tube", *Intl. J. Mech. Sci.*, v. 24, pp. 359-367, 1982.
- [46] REN, J., DODDS, W.J., MARTIN, C.J., DANTAS, R.O., MITTAL, R.K., HARRINGTON, S.S., KERN, M.K. and BRASSEUR, J.G., "Effect of Increased Intra-Abdominal Pressure on Peristalsis in Feline Esophagus", *Am Physiol Society*, p. G417-G425, 1993.
- [47] REN, J., MASSEY, B.T., DODDS, W.J., KERN, M.J., BRASSEUR, J.G., SHAKER, R., HARRINGTON, S.S., HOGAN, W.J. and ARNDORFER, R.C., "Determinants of Intrabolus Pressure During Esophageal Peristaltic Bolus Transport", *Am J Physiol*, v. 264 (Gastrointest. Liver Physiol. 27), pp. G407-G413, 1993.
- [48] ROOS, R. and LYKOURIS, P.S., "The Fluid Mechanics of the Ureter with an Inserted Catheter", *J. Fluid Mech.*, v. 46, pp. 625-630, 1971.
- [49] SCHATZKI, R., "The Lower Esophageal Ring: Long Term Follow-up of Symptomatic and Asymptomatic Rings", *American J of Roentgenology*, v. 90, pp. 805-810, 1963.
- [50] SHAPIRO, A.H., "Pumping and Retrograde Diffusion in Peristaltic Waves", *Proc. Workshop on Ureteral Reflux in Children*, *Natl. Acad. Sci. Washington DC*, 1967.
- [51] SHAPIRO, A.H., JAFFRIN, M.Y. and WEINBERG, S.L., "Peristaltic Pumping with Long Wavelengths at Low Reynolds Number", *J. Fluid Mech.*, v. 97, pp. 799-825, 1969.

- [52] SHUKLA, J.B., PARIHAR, R.S., RAO, B.R.P. and GUPTA, S.P., "Effects of Peripheral Layer Viscosity on Peristaltic Transport of Biofluid", *J. Fluid Mech.*, v. 97, pp. 225-237, 1980.
- [53] SHUKLA, J.B. and GUPTA, S.P., "Peristaltic Transport of a Power-law Fluid with Variable Consistency", *Trans. ASME K: J. Biomech. Engng.*, v. 104, pp. 182-186, 1982.
- [54] SPJUT, H.J. and NAVARRETE, A., "Pathology of the Esophagus", chapter 17, pp. 339-346, The C.V. Mosby Company, Chicago, IL, 1973.
- [55] SQUIRE, J.M., LUTHER, P.K. and MORRIS, E.P., "Organisation and Properties of the Striated Muscle Sarcomere", In J. M. Squire, editor, *Molecular Mechanisms in Muscular Contraction*, pp. 1-48, CRC Press, Boca Raton, FL, 1990.
- [56] STAVITSKY, D., MACAGNO, E.O. and CHRISTENSEN, J., "Finite-element Analysis of Flow Induced by Contractions Like Those of Intestine", *J. Biomech.*, v. 14, pp. 183-193, 1981.
- [57] TAKABATAKE, S. and AYUKAWA, K., "Numerical Study of Two-dimensional Peristaltic Flows", *J. Fluid Mech.*, v. 122, pp. 439-465, 1982.
- [58] TAKABATAKE, S., AYUKAWA, K. and MORI, A., "Peristaltic Pumping in Circular Cylindrical Tubes: a Numerical Study of Fluid Transport and Its Efficiency", *J. Fluid Mech.*, v. 193, pp. 267-283, 1988.
- [59] TONG, P. and VAWTER, D., "An Analysis of Peristaltic Pumping", *Trans. ASME E: J. Appl. Mech.*, v. 39, pp. 857-862, 1972.
- [60] VANTRAPPEN, G. and HELLEMANS, J., "Physiology", chapter 1, pp. 40-71, Springer-Verlag, New York, NY, 1974.

- [61] WEISBRODT, N.W., "Esophageal Motility", In *Gastrointestinal Physiology*, chapter 2, pp. 12-19, The C. V. Mosby Co., St. Louis, MO, 1977.
- [62] WINSHIP, D.H., ANDRADE, S.R.V. and ZBORALSKE, F.F., "Influence of Bolus Temperature on Human Esophageal Function", *The J of Clinical Investigation*, v. 49, pp. 243-250, 1970.
- [63] YIH, F. and FUNG, Y.C., "Peristaltic Waves in Circular Cylindrical Tubes", *ASME E: J. Applied Mech.* v. 36, pp. 579-587, 1969.
- [64] YIN, Y.C.P. and FUNG, Y.C., "Mechanical Properties of Isolated Mammalian Ureteral Segments", *American J. Physiology*, v. 221, pp. 1484-1493, 1971.
- [65] ZUPKAS, P.F. and FUNG, Y.C., "Active Contractions of Ureteral Segments", *Trans. Of the ASME*, v. 107, pp. 62-67, 1985.

VITA

Ethem Toklu was born on December 6, 1971 in Eynesil, Giresun. He was raised from the age of 13 in the small village of Kemerli, Eynesil, Giresun. He graduated from Trabzon Fatih High School in Trabzon in 1988. Ethem then enrolled at Yildiz University, Kocaeli Engineering Faculty in the Department of Mechanical Engineering. After finishing his B.S. degree in July 1992, he immediately began Master of Science work in Mechanical Engineering at Yildiz Technical University. He finished his Ms in 1994. Then he began his Doctorate study at Sakarya University in the Department of Mechanical Engineering with Prof. Dr. Ismail Calli. After completing his courses and other requirement at Sakarya University, he has been at Pennsylvania State University in the Department of Mechanical Engineering, USA to study his PhD thesis with Prof. Dr. James G. Brasseur between August 1996 and September 1998. He is the co-author of five publications in the field of his research interest.